

Copyright
by
Nathan William Johnson
2009

**The Dissertation Committee for Nathan William Johnson certifies that this is the
approved version of the following dissertation**

**MERCURY METHYLATION BENEATH AN
IN-SITU SEDIMENT CAP**

Committee:

Lynn E. Katz, Co-Supervisor

Danny D. Reible, Co-Supervisor

Kerry A. Kinney

David R. Maidment

G. Christopher Shank

**MERCURY METHYLATION BENEATH AN
IN-SITU SEDIMENT CAP**

by

Nathan William Johnson, B.S.E.; M.S.E.

Dissertation

Presented to the Faculty of the Graduate School of

The University of Texas at Austin

in Partial Fulfillment

of the Requirements

for the Degree of

Doctor of Philosophy

The University of Texas at Austin

August 2009

Dedication

...to my parents, whose love and support have been an invaluable source of
encouragement

... to my wife, whose gracious attitude during the journey that is a PhD has been
unswervingly consistent with the rest of her, pure gold

... and to Him who is able to do immeasurably more than all we ask or imagine

Acknowledgements

Acknowledgements are due to my advisors for their encouragement, support, and friendship over the past six years. To fellow EWRE students (past and present) and faculty for help with research and, more importantly, moral support. Special thanks are due to Tony, Mara, Susan, YS, and Dave. To George Luther (University of Delaware) and Don Nuzzio (Analytical Instrument Systems) for help with voltammetry, Eric Roden (University of Wisconsin) for initial help with diagenetic modeling, and Lisa Couret (Brooks Rand Labs) for help with methyl mercury analysis.

MERCURY METHYLATION BENEATH AN IN-SITU SEDIMENT CAP

Publication No. _____

Nathan William Johnson, Ph.D.

The University of Texas at Austin, 2009

Supervisors: Lynn E. Katz and Danny D. Reible

The production of methyl mercury, an acute neurotoxin which readily accumulates in the tissue of organisms, is a biologically mediated process facilitated by sulfate reducing bacteria in aquatic sediments. In-situ capping is a frequently considered risk management strategy for contaminated sediments. Since placement of an in-situ cap will induce anaerobic conditions that are known to be favorable for the growth of sulfate reducing bacteria, there is justifiable concern that capping could increase mercury methylation in underlying sediments. This research builds an understanding of the effects of in-situ capping on underlying biogeochemical processes and elucidates their importance in controlling methyl mercury production. Laboratory experiments and mathematical models were implemented to simulate mercury methylation in redox conditions likely to be induced by capping using sediment from different environments.

Mathematical descriptions of processes known to be involved in methylation were incorporated into the model to quantify the effects of these processes.

Observations in both well-mixed slurry conditions and intact sediment columns showed that methyl mercury concentrations are strongly dependent upon biogeochemical conditions. Results from experiments with sediment spanning a range of redox conditions and organic contents suggested that sulfate reduction rates, aqueous speciation, and solid phase partitioning are involved in limiting methylation depending on bulk geochemical characteristics. A model with a mechanistic basis that incorporates the effects of these processes provides a useful means of qualitatively and quantitatively considering their cumulative impact in limiting methyl mercury production. High methyl mercury concentrations observed in some lab experiments suggest that there is reason to be concerned about anoxic conditions induced by capping; however, not all anoxic conditions led to equivalent increases in methyl mercury. Experimental and modeling results suggest that in a high organic environment, in-situ capping may produce conditions which accelerate methylation in (formerly) surficial sediment while in a low organic environment, with an overall lower potential for methylation, capping can be expected to have a less dramatic effect. Over time, two processes will temper cap-induced increases in methyl mercury. Increases will only last until sulfide builds up to inhibitory levels in underlying sediment or until organic carbon is depleted and overall bacterial activity slows. By providing a more fundamental understanding of the effects of capping on mercury methylation, the results of this research will aid in identifying situations and conditions in which cap-induced increases in methyl mercury have the potential to limit the effectiveness of the management strategy.

Table of Contents

List of Tables	x
List of Figures	xii
Chapter 1: Introduction	1
1.1 Research Objectives.....	5
1.2 Research Outline.....	6
1.3 Document Structure	7
Chapter 2: Literature Review	9
2.1 Contaminated Sediments	9
2.2 Mercury in aquatic sediments	15
2.3 Sediment diagenesis.....	23
Chapter 3: Modeling Methyl mercury Production in a Range of Anaerobic Biogeochemical Conditions	28
3.1 Introduction.....	28
3.2 Materials and Methods.....	30
3.3 Speciation Calculations.....	38
3.4 Modeling Incubation Methyl Mercury.....	42
3.5 Results and Discussion	45
3.6 Conclusions and Implications	58
Chapter 4: Modeling Mercury-Related Geochemistry in Salt Marsh Sediment...	59
4.1 Introduction.....	59
4.2 Materials, Methods, and Modeling	60
4.3 Results and Discussion	67
Chapter 5: Biogeochemical Changes and Mercury Methylation beneath an In-Situ Sediment Cap	81
5.1 Introduction.....	81
5.2 Materials and Methods.....	83
5.3 Model Description	86

5.4 Results and Discussion	86
Chapter 6: Conclusions and Recommendations	98
6.1 Summary	98
6.2 Conclusions.....	98
6.3 Recommendations for Future Work.....	104
Appendix A: Supporting Information for Chapter 3.....	108
A.1 Radiolabeled Sulfate Reduction Rate Assay.....	108
A.2 Sulfate Reduction Rate Summary	110
A.3 Additional Spiked Mercury Results.....	112
Appendix B: Supporting Information for Chapter 4.....	116
B.1 Geochemical Profiles for Replicate Cores	116
B.2 Effect of pH on fraction uncharged (and consequently available).....	120
B.3 Simulation of diagenetic and methyl mercury impacts of capping.....	121
Appendix C: Supporting Information for Chapter 5.....	124
C.1 Microcosm Schematic	124
C.2 Laboratory QA/QC Results.....	124
C.3 Total Mercury Concentrations	125
C.4 Model Formulation.....	129
C.5 Reactions	130
References.....	134
Vita	142

List of Tables

Table 2.1	Stability constants for aqueous mercury partitioning to sulfide and DOM.	21
Table 3.1	Geochemical characteristics of Salt Marsh and Estuarine sediment. Standard deviation of replicate analysis is presented in parentheses.	31
Table 3.2	Nine geochemical conditions used to study methyl mercury production. Three different environments (range of organic matter) and three different geochemical conditions (redox zones).	32
Table 3.3	Expected effects of simulated geochemical conditions on mercury methylation	33
Table 3.4	Amendments in buffer added to encourage suboxic, mildly reduced, and fully reduced geochemical conditions.	35
Table 3.5	Stability constants for dissolved sulfide and organic mercury complexes	38
Table 3.6	Summary of geochemical and methyl mercury measurements used to calculate parameters for steady state methyl mercury model. Speciation models B and B' are as described in Section 3.3	52
Table 4.1	Mercury sulfide and organic complexes and stability constants used for equilibrium speciation modeling.....	62
Table 4.2	Linear regression parameters for steady state methyl mercury model developed in Chapter 3 for two different values of the HgS^0 stability constant.	65

Table A.1	Summary of sulfate reduction rates obtained using linear regression for observed sulfate concentrations, in uM/day. Comparison with rates obtained with $^{35}\text{SO}_4^{2-}$ assays.	110
Table A.2	Summary of regression parameters for alternative speciation models.	113

List of Figures

Figure 2.1	Mass transport processes affected by in-situ sediment capping	12
Figure 2.2	Illustration of mercury processes in the aquatic environment (adapted from Alpers et al., USGS, 2005-3014)	17
Figure 2.3	Predicted rates of microbial organic carbon degradation using alternative model formulations. (a) G-type model (Boudreau, 1997, VanCappellen and Wang 1995); (b) defined maximum rates for each population (Jaffe et al. 2001).	24
Figure 3.1	Phase diagram showing regions of predominance for two-sulfide mercury complex (upper left), single sulfide mercury complex (lower left), and organic complex (lower right) for pH 8 using (a) low stability constant for HgS^0 – Model B; and (b) high stability constant for HgS^0 – Model B'. Vertical dashed line represents organic complex concentration in each environment. Additional lines in (b) represent the effects of changing pH (shift right), and the stability constant for the organic complex (shift left).....	40
Figure 3.2	Mercury-related geochemistry and methyl mercury observations in low organic (LO) environment incubations. (a-c) suboxic conditions; (d-f) mildly reduced conditions; (g-i) fully reduced conditions.....	48
Figure 3.3	Mercury-related geochemistry and methyl mercury observations in high organic (HO) environment incubations. (a-c) suboxic conditions; (d-f) mildly reduced conditions; (g-i) fully reduced conditions.....	49

Figure 3.4	Mercury-related geochemistry and methyl mercury observations in middle organic (MO) environment incubations. (a-c) suboxic conditions; (d-f) mildly reduced conditions; (g-i) fully reduced conditions.....	50
Figure 3.5	Sulfate observations in 9 different incubations with linear regressions to calculate sulfate reduction rate. (a) LO environment, (b) HO environment, (c) MO environment	51
Figure 3.6	Model for % methyl mercury considering sulfate reduction rate, available aqueous fraction (Model B'), and partitioning to the solid phase, K_D	54
Figure 4.1	Phase diagram showing regions of predominance for two-sulfide mercury complex (upper left), single sulfide mercury complex (lower left), and organic complex (lower right) for pH 8 using (a) low formation constant for HgS^0 – Model B; and (b) high formation constant for HgS^0 – Model B'. Vertical dashed line represents organic complex concentration in the salt marsh sediment. Additional lines in (b) represent the effects of changing pH (shift right), and the stability constant for the organic complex (shift left).....	63
Figure 4.2	Workflow for combining physical measurements, speciation calculations, and parameters from laboratory conditions to predict in-situ % methyl mercury.....	66

Figure 4.3	Geochemical and methyl mercury observations in surficial sediment of salt marsh. (a) porewater sulfate, pH, and chloride (/20); (b) solid phase % methyl mercury (of total mercury), total mercury, and porewater total sulfide (sum of H ₂ S and HS ⁻). Zero depth represents sediment water interface.....	68
Figure 4.4	Diagenetic modeling results for surficial salt marsh sediment. (a) model fit to sulfate and sulfide concentrations. (b) simulated sulfate reduction rate, observed sulfate concentration, and sulfate concentration that would be present based on observed chloride concentration (seawater Cl:SO ₄ ratio = 19.1, molar basis).	70
Figure 4.5	Comparison of observations with methyl mercury model predictions using (a) speciation model B' and (b) speciation model B. Range of methyl mercury model predictions represent the effects of uncertainty in both chemical measurements and location of measurement.....	73
Figure 4.6	Speciation calculations for in-situ fraction available (a) uncertainty in sulfide observations associated with both concentration and measurement depth. Available fraction calculated with high stability constant for HgS ⁰ (logK=26.5), note reversed axis direction for available fraction (b) pH profile (symbols) and available fraction calculated with low stability constant for HgS ⁰ (logK=24.5), note reversed axis direction for available fraction.....	77

Figure 5.1.	Diagenetic model calibration (a – Baseline, 10umol/cm2 initial iron oxidized, $k_{FeOX}=1.6(106) \mu M\text{-}1\text{yr}^{-1}$) and sensitivity analysis of iron oxidation rates (b–Low rate, 5umol/cm2 or $k_{FeOX}=4.8(105) \mu M\text{-}1\text{yr}^{-1}$, and c–High rate 15umol/cm2 or $k_{FeOX}=1.6(107) \mu M\text{-}1\text{yr}^{-1}$) for control microcosm. Model predictions for capped and anoxic microcosms are shown in (d) and (g) respectively, with associated iron oxidation sensitivity analysis in (e,f) and (h,i) respectively.	90
Figure 5.2	Visual observations of biogeochemical zones in (a) control, (b) capped, and (c) anoxic microcosms at 3 months. Depth profiles of methyl mercury, oxygen (O ₂), dissolved iron (Fe ²⁺), and dissolved sulfide (HS-) in (d) control, (e) capped, and (f) anoxic microcosms at 120d. Error bars for HS- represent the standard deviation of triplicate electrodes spaced 2cm apart. The concentration range of duplicate electrode measurements is shown for Fe ²⁺ . Error shown for methyl mercury was calculated using the pooled variance of duplicate analytical analyses.	91
Figure 5.3	Simulated profiles of rates for biological organic carbon utilization by different electron accepting populations in (a) control, (b) capped, and (c) anoxic microcosms (iron oxidation rate =107 umol/cm3-year). Rates for iron and manganese reduction are orders of magnitude smaller and shown on a separate axis.....	95
Figure A.1	Summary of sulfate reduction rate measurements with radiolabeled sulfate. measured sulfate concentration (open symbols), detection limit for sulfate reduction rate (lines, based on minimum count of 250DPM), and sulfate reduction rate (closed symbols).....	111

Figure A.2	Model for % methyl mercury 48 hours after additional spike considering sulfate reduction rate, available aqueous fraction (Model B'), and partitioning to the solid phase.	112
Figure A.3	Alternative models considering speciation calculated with Model A and Model B (panels b,d). Regressions with only two of the geochemical parameters from the model of Equation 4.3. SRR & availability (panels a, c, e), and SRR & Kd (panel g).	114
Figure A.4	Alternative weighted regressions for minimizing the weight of the large methyl mercury point. (a) log-log regression (slope = 595, 560 without outlier), (b) weighted least squares regression (slope = 590, 520 without outlier) and 90% confidence intervals. Weights were calculated using the reciprocal of the power of the independent variable which minimized the error of the dependent variable.	115
Figure B.1	Geochemical profiles for replicate core in salt marsh	116
Figure B.2	Geochemical observations for full 30-cm of core described in Chapter 4.	117
Figure B.3	Diagenetic modeling results and predicted methyl mercury according to Equation 3.3 for high organic capping simulation in high organic environment. Zero represents interface between 20cm capping layer and underlying sediment. (a) bacterial carbon oxidation rates, (b) sulfate and organic substrate concentration, (c) dissolved sulfide, oxygen and dissolved ferrous iron, (d) available mercury, predicted methyl mercury, and sulfate reduction rate.	122

Figure B.4	Diagenetic modeling results and predicted methyl mercury according to Equation 3.3 for high organic capping simulation in low organic environment. Zero represents interface between 20cm capping layer and underlying sediment. (a) bacterial carbon oxidation rates, (b) sulfate and organic substrate concentration, (c) dissolved sulfide, oxygen and dissolved ferrous iron, (d) available mercury, predicted methyl mercury, and sulfate reduction rate.....	123
Figure C.1	Schematic of experimental microcosms. 7.5cm sediment depth with 3cm overlying water.	124
Figure C.2	Total mercury concentrations in control and capped microcosms..	125
Figure C3	Timeline of development of geochemical profiles in three microcosms	126
Figure C4	Visual observations of geochemical redox zones in microcosms at 3 and 22 days	127
Figure C.5	Depth profiles of SO ₄ ²⁻ and AVS concentrations in control, capped and anoxic microcosms at the close of experiments.....	128

Chapter 1: Introduction

Contaminated aquatic sediments comprise almost one third of the sites listed on the EPA's National Priority List (NPL). These sites have the potential of releasing toxic substances to an environment in which people or sensitive environments will be affected. (Agency 2008) Metals are contaminants of concern at over half of these sites, many of which include mercury contamination. Aquatic sediments are a complex environment, presenting a particularly challenging scenario for environmental management not only because a plethora of interacting biological, chemical, and transport processes affect contaminant speciation, mobility and bioavailability in these environments, but also because the relative rates of these processes can vary by orders of magnitude over small spatial scales.

One strategy that is currently being considered for managing the risk posed by contaminated sediments at many sites is in-situ capping. (Palermo et al. 1998) Several field-scale demonstrations and applications of in-situ capping are underway in the U.S. The primary objective of an in-situ cap is to reduce or eliminate the mobilization of contaminants by placing a clean layer of material on the contaminated sediment surface that physically isolates it from the overlying water and surficial organisms. In addition to physically isolating contaminants in underlying sediment, evidence suggests that an in-situ cap will alter the complex biogeochemical environment in underlying sediments and could significantly affect the mobility and bioavailability of contaminants. For example, upward translations of redox zones observed following the placement of in-situ caps have been attributed to the elimination of the oxidizing force provided by oxygen in the overlying water (Azcue et al. 1998; Liu et al. 2001; Himmelheber 2008). The promotion of anaerobic conditions in sediment underlying a cap has important implications for the

fate and transport of many contaminants, including mercury, an important environmental contaminant which exhibits redox sensitive speciation and undergoes redox sensitive transformations.

Mercury is highly toxic and exists widely in the environment, mostly as a result of anthropogenic activities. (Fitzgerald et al. 1998) The speciation of mercury, especially its transformation to methyl mercury, is critical in controlling exposure to humans. Methyl mercury, the most prevalent environmental organo-mercury complex, is an acute neurotoxin and readily accumulates in the tissue of organisms (Morel et al. 1998; Kraepiel et al. 2003). Biomagnification of methylmercury in fish tissue has led to at least one mercury fish consumption advisory in each state in the U.S. and statewide advisories in 23 states. Aquatic environments provide the most likely exposure pathways for mercury because they (1) are a sink for mercury, esp. sediments; (2) host bacterial communities that produce methyl mercury, and (3) are populated by game fish, a popular food for humans. (Fitzgerald et al. 2007). The predominant form of mercury in aquatic environments is inorganic mercury (Hg^{2+}), which partitions strongly to sediments. In sediments, inorganic mercury undergoes numerous biological and chemical reactions which control its speciation.

A growing body of laboratory and field-scale evidence has led to a widely accepted understanding that anaerobic bacteria in aquatic sediments, and sulfate reducing bacteria (SRB) in particular (Compeau and Bartha 1985, Gilmour and Henry 1991), play a dominant role in the production of methyl mercury in many water bodies. (Kerry et al. 1991, Gilmour et al. 1992, Harmon et al. 2004) The availability of energy-rich organic matter for driving the activity of methylating microbes has also been shown to be important for the efficient production of methyl mercury (Drott 2008; Hammerschmidt 2004; Lambertsson 2006). In-situ concentrations of methyl mercury in sediments

represent a balance between methylation and demethylation processes (Hinertmann et al. 2000) and it is believed that rates of demethylation are relatively constant regardless of dominant biological populations, but that methylation rates are strongly dependent upon the activity of sulfate reducing bacteria (Warner et al. 2003, King et al. 2001). Drott et al. 2008 explicitly demonstrated this by showing that variations in in-situ methyl mercury concentrations in surficial aquatic sediments are directly related to methylation rates.

Inorganic mercury forms aqueous complexes with a number of inorganic and organic ligands including hydroxide, chloride, sulfide, and thiol groups. The efficient production of methyl mercury in sediments is thought to be controlled by both aqueous speciation of inorganic mercury and partitioning to the solid phase. It is generally assumed that passive diffusion of uncharged, dissolved mercury complexes is the primary route of uptake into microorganisms and methylating bacteria in particular (Mason et al. 1996, Benoit et al. 2001). At concentrations greater than only 10^{-9} M, sulfide complexes dominate inorganic mercury speciation in anoxic systems. Previous research has suggested that increases in sulfide at low micromolar concentrations leads to a shift in speciation from the uncharged, bioavailable complex HgS^0 to the charged, and consequently not bioavailable, complex HgS_2H^- (Benoit et al. 1999). The competition between sulfide and organic ligands (mainly thiol functional groups) for complexing mercury, is still an area of active research (Drott et al. 2007). Because organic complexes are assumed to be unavailable to methylating bacteria (Drott et al. 2007), the thermodynamics for the formation of the uncharged mercury-sulfide species HgS^0 is critical to understanding the fraction of dissolved mercury available for methylation in many environments.

Association of contaminants with the solid phase is often quantified by a sediment-water partition coefficient, K_D , which gives the ratio of sediment concentration

to water concentration. For inorganic mercury, K_D values obtained in field-scale investigations range from 10^3 - 10^5 [L/kg] and $10^{1.5}$ - 10^3 [L/kg] for methylmercury (Fitzgerald and Lamborg 2007). In addition to the obvious significance of strong solid phase partitioning limiting transport through sediment porewater, a field study in Long Island Sound showed that the magnitude of the partitioning coefficient (K_D) was inversely related to the capacity of sediment to methylate mercury (Hammerschmidt and Fitzgerald 2004). This suggests that solid-phase partitioning is also important in controlling the availability of mercury to methylating microbes.

Methylating bacteria populate anaerobic environments in aquatic sediments, the very conditions encouraged by the placement of an in-situ cap. Consequently, there is justifiable concern that in-situ capping could increase methylation in underlying mercury-containing sediments. The physical sequestration provided by in-situ sediment capping has been studied in detail (Wang et al. 1991, Thoma et al. 1993, Liu et al. 2001, Liu et al. 2007), however, biogeochemical processes in underlying sediment and within capping material have received relatively little attention. Management decisions for aquatic sediments should be based on a site-specific assessment of the short and long-term risk reductions of potential management alternatives (EPA 2005). While some laboratory and field-scale studies have suggested that a cap may be effective in containing contamination in underlying sediment (Azcue et al. 1998, Liu et al. 2001, Himmelheber et al. 2007), a reliable long-term evaluation of the effectiveness of a cap must be based upon a fundamental understanding of the processes controlling contaminant fate and transport in the underlying sediment. The motivation for this research derives from previous research demonstrating that rates of mercury methylation changed followed geochemical alterations analogous to those expected during in-situ capping, (Harmon et al. 2004, Mehrotra and Sedlak 2005, Benoit et al. 2006), and the need for a fundamental

understanding of biogeochemical processes in making effective, long term management decisions.

The dependence of methyl mercury production on sulfate reduction, mercury-sulfide speciation, and solid phase partitioning, suggests that redox conditions in aquatic sediment, especially the transition between oxic and anoxic conditions (Sunderland, Gobas et al. 2004) are important in controlling in-situ methyl mercury concentrations. Previous research attempting to elucidate the specific conditions required for increased methylation have studied sediment from different environments and geochemical conditions and suggested relationships between methyl mercury production and sulfate reduction rate, energetic organic carbon (Drott et al. 2007, Drott et al. 2008, Lambertsson and Nilsson 2006), availability of inorganic mercury for methylation (Han et al. 2008, Benoit 1999), and solid-phase partitioning (Hammerschmidt and Fitzgerald 2004, Miller 2006).

1.1 RESEARCH OBJECTIVES

The current research explores these relationships through experimental and mathematical modeling at the laboratory and field scale in order to:

- (1) characterize methyl mercury production in a range of geochemical conditions and verify that efficient methylation is confined to a narrow geochemical redox zone.
- (2) Combine the effects of sulfate reduction, aqueous availability, and solid phase partitioning to quantify the cumulative effects of these processes in controlling methyl mercury

- (3) verify that geochemical influences on methylation characterized in the laboratory are consistent with field observations.
- (4) evaluate the biogeochemical impacts of in-situ capping, a commonly selected sediment remediation strategy, on mercury methylation

These objectives were accomplished using laboratory experiments designed to reproduce the geochemical conditions expected to occur following the placement of an in-situ cap (reduced conditions) in sediment with a range of organic content. Mathematical descriptions of biological processes affecting methylation, aqueous speciation, and solid-phase partitioning are incorporated into a steady state model to describe methyl mercury and quantify the effects of biogeochemical processes and parameters that affect methylation.

1.2 RESEARCH OUTLINE

Three experimental tasks were used answer the questions posed above and each task was coupled with mathematical modeling of relevant processes.

The first task involved monitoring the production of methyl mercury in well-mixed sediment incubations under different redox conditions. Biological (sulfate reduction) and geochemical (solid-phase partitioning and aqueous speciation) factors known to be important in controlling mercury methylation were monitored. A steady-state mathematical model with a basis in these fundamental processes was applied to explain the variability in methyl mercury observed under different geochemical conditions.

The second experimental task first involved obtaining depth profiles of in-situ biogeochemical conditions and methyl mercury concentrations in a salt marsh sediment. The steady state model employed during Task 1 was applied to in-situ methyl mercury observations to assess its ability to describe field observations.

The third task involved the placement of an in-situ cap on laboratory-scale river simulator microcosms. Cap-induced transitions in underlying redox zones and methyl mercury concentrations were monitored and compared to control microcosms (without caps) to determine whether the placement of the cap induced concomitant increases in sulfate reduction and methyl mercury production at shallower depths

By providing a more fundamental understanding of the effects of capping on mercury methylation, the results of this research will aid in identifying situations and conditions in which cap-induced increases in methyl mercury have the potential to limit the effectiveness of the management strategy. Consideration of the key parameters important for controlling methyl mercury production will help managers make informed, appropriate, site-specific decisions related to capping sediment containing mercury contamination.

1.3 DOCUMENT STRUCTURE

A review of relevant literature and background on important concepts is presented in Chapter 2. Chapter 3 presents the conceptual model and results for the laboratory experiments used to measure methyl mercury production in a range of geochemical conditions. The steady state model used to explain the effects of these conditions on mercury methylation is also presented in Chapter 3. Chapter 4 describes an application of this model to in-situ observations at a salt marsh site. Chapter 5 outlines the procedures and results from a laboratory-scale simulation of the mercury-related

biogeochemical effects of in-situ capping. Chapter 6 contains a discussion of the results and conclusions from this work as well as recommendations for future research building on the present studies.

Chapter 2: Literature Review

2.1 CONTAMINATED SEDIMENTS

2.1.1 Overview of Contaminated Sediments

In 1997, the US Environmental Protection Agency (EPA) published a report entitled “The Incidence and Severity of Sediment Contamination in Surface Waters of the United States,” (EPA 1997) containing sediment quality data collected between 1980 and 1993. It was estimated that 10% of the approximately 12 billion cubic yards of sediment in the surface waters of the US are contaminated enough to present significant risk to wildlife or humans who consume them. In response to the understanding of the severity of sediment contamination, a management strategy was released that outlined the policy framework for how the EPA would pursue a reduction in the risks posed by sediment contamination (EPA 1998). The strategy contained four explicit objectives:

- 1) Prevent the volume of contaminated sediment from increasing
- 2) Reduce the volume of existing contaminated sediment
- 3) Ensure dredged material is managed in an environmentally sound manner
- 4) Develop scientifically sound management tools for use in pollution prevention, source control, remediation, and dredged material management

In the years since, decreases in surficial sediment concentrations of DDT (dichlorodiphenyltrichloroethane) and Pb (lead) have been observed following elimination or reduction in their use. This trend suggests that source control is controlling the volume of contaminated sediment for some contaminants. However, for other contaminants that have urban or non-point sources such as PAHs (polycyclic aromatic hydrocarbons), chlorinated organics, and some metals such as mercury,

substantial increases or negligible changes have been observed following urbanization (EPA 2004). Many anthropogenic contaminants of concern in sediment, including pesticides, chlorinated organics, cyclic or aromatic hydrocarbons, and metals, are sufficiently recalcitrant that source control alone is ineffective in controlling their risk, and contaminated areas become, in the absence of effective management, a source of contamination to the surrounding environment.

At many sites, it has been found that reducing the volume of contaminated sediment is either infeasible due to cost or logistical considerations or ineffective in reducing risk due to the presence of residual material after removal. In these situations, sediment managers have turned to the fourth goal of the Management Strategy: the development of sound management tools for remediation. A remedy has been selected under the EPA's Superfund program for 150 contaminated sediment sites, eleven of which are 'Mega Sites' costing more than \$50M for sediment remediation. Almost all of the remedies contain a management strategy in addition to or in place of sediment removal. Remediation of nearly 20% of these sites is driven by risk from mercury contamination (EPA 2005).

2.1.2 In-situ Management Strategies

In addition to dredging and excavation, the EPA's 2005 Contaminated Sediment Remediation Guidance document (EPA 2005) outlines three broad in-situ management approaches for managing risk from contaminated sediment:

- 1) In-situ capping
- 2) Monitored natural recovery (MNR)
- 3) Institutional controls

In addition to these three approaches, hybrid approaches that involve multiple management strategies are suggested as well as active in-situ treatment variations on capping or natural recovery including reactive caps and enhanced biodegradation (EPA 2005). Institutional controls are not recommended to be used alone, and the guidance document explicitly states that “institutional controls shall not be substituted for active response measures” (p. 7-15) and that they are intended to supplement engineering controls to control both short and long term exposure. Monitored natural recovery (MNR) takes advantage of natural processes to reduce the risk posed by contaminants. In cases where natural processes including degradation to a less toxic form, sorption to sediment material, burial, and dilution through mixing or dispersion are expected to reduce risk over an acceptable time period, careful monitoring of site conditions may provide a suitable solution. MNR processes are typically considered in tandem with other remedial measures when evaluating the potential effectiveness of a management alternative.

2.1.3 In-situ Sediment Capping

In situ capping has the primary objective of reducing or eliminating the mobilization of contaminants by placing a clean layer of material on the contaminated sediment surface that physically isolates it from the overlying water and surficial organisms. Figure 2.1 illustrates some of the mass transfer processes which mobilize sediment contaminants to the overlying water and subsequent exposure pathways. An isolation cap layer moves these processes, which formerly occurred in contaminated material, upwards into clean capping material, and the transport of contaminants from the underlying sediment can be substantially reduced or eliminated.

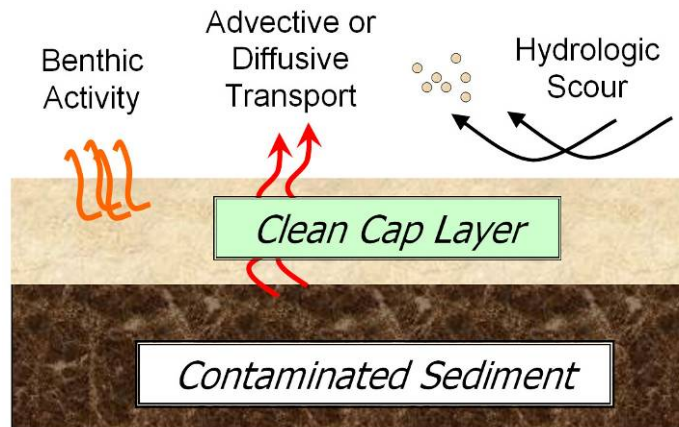


Figure 2.1 Mass transport processes affected by in-situ sediment capping

Isolation capping layers can be structurally complex with both a physical isolation component designed to reduce risk by separating contaminants from exposure pathways and, in cases where erosion presents a risk to the physical integrity of a cap, a stabilization component composed of larger particles or engineering materials designed to withstand large bed shear stresses (EPA 2005). Sediment contaminants tend to associate very strongly with the solid phase, and a chemical isolation component is sometimes considered when the material in the physical isolation layer will not sufficiently sequester contaminants transported by diffusion or advective flow.

Another strategy that is frequently considered as a part of management strategies at contaminated sediment sites is termed ‘thin layer capping.’ While a containment capping layer may have a thickness of up to 2-3 feet, a thin layer cap may consist of only a few inches of material. Although thin layer caps are not designed to completely isolate benthic organisms from contaminants like an isolation cap, they can reduce risk in combination with MNR or dredging by diluting contaminated surficial material with clean material. This type of thin layer cap falls in the category of ‘enhanced natural recovery’ and is not considered in-situ capping (EPA 2005).

By providing an immediate isolation layer between contaminants and the overlying water, in-situ capping has the advantage of an immediate reduction in risk posed by underlying contamination and typically involves the handling of far less handling of contaminated material. Additionally the material used in the surficial layer of a cap can be designed to encourage the recolonization of a natural ecosystem. The most evident disadvantage of in-situ capping is that contaminated material remains in place, indefinitely in the absence of degradation or transport mechanisms that reduce concentrations, and could present future risk in the event of cap failure.

Biodegradation, the microbially mediated conversion of a contaminant to a less toxic form, has been observed for many common sediment contaminants including PAHs, chlorinated organics, and nitroaromatics (Hollinger 97). The potential for biodegradation during MNR and capping are considered during remedy selection for sediment sites, but the effectiveness of these processes in attenuating risk are more difficult to characterize and less well understood than physical containment processes. Additionally, the strong association of contaminants to the solid phase can limit their availability to microbes that could degrade them. For sediments contaminated with metals, bioremediation is not generally considered a viable option as biodegradation of metals may alter speciation but does not remove overall risk. Metals including mercury drive the risk at over 1/2 of Superfund sediment sites (EPA 2005). For these sites, the best possible outcome from an in-situ management strategy is complete immobilization.

2.1.4 Biogeochemical Effects of Capping

In addition to physically isolating contaminants in underlying sediment, evidence suggests that an in-situ cap will alter the complex biogeochemical environment in underlying sediments that could significantly affect the mobility and bioavailability of

contaminants. Redox zones have been monitored following the placement of an in-situ cap have shown upward translations due to the elimination of the oxidizing force provided by oxygen in the overlying water. (Liu et al. 2001, Himmelheber et al. 2008) Some short-term laboratory and field-scale capping studies have attributed reductions in contaminant flux to both the physical separation provided by a cap and cap-induced changes in the biogeochemistry of the underlying sediment; e.g. immobilization of metals by metal-sulfide precipitation and biodegradation of chlorinated organics (Simpson et al. 2002, Himmelheber et al. 2007, Eek et al. 2008, Liu et al. 2007, Azcue et al. 1998).

Himmelheber et al. (2008) explicitly measured biogeochemical changes beneath a sediment cap in freshwater sediment columns in both stagnant and upflow conditions. Formerly surficial, oxic sediment was driven anaerobic, and redox zones experienced a clear upward shift as a result of cap placement. Iron reducing conditions were observed within a cap placed over sediment from a freshwater system. It was hypothesized that these shifts in biogeochemistry, and redox profiles in particular, will influence the speciation and fate of reactive contaminants.

The major biogeochemical change expected to be induced by a thick isolation layer, an active geotextile layer, or a thin-layer cap is the same, namely the elimination of the oxidizing force from the overlying water and an upward translation of redox zones. Since the fate of contaminants in underlying sediment will be changed as a result of cap placement, evaluation of contaminant fate beneath and within capping material and potential exposure to underlying sediment cannot be based on pre-capping conditions.

2.2 MERCURY IN AQUATIC SEDIMENTS

2.2.1 Sources

Mercury is highly toxic and exists widely in the environment, mostly as a result of anthropogenic activities. (Fitzgerald et al. 1998) Nearly 20% of the contaminated sediment sites on the EPA's Superfund program are driven by risk from mercury contamination (EPA 2005). Sources of mercury to the atmosphere are primarily coal fired power plants and incinerators. Atmospheric releases of mercury are transported long distances due to mercury's long residence time in the atmosphere (Mason, Fitzgerald, Morel, 1994). Elevated fish tissue mercury concentrations in remote areas with no known local sources of mercury have been attributed to the atmospheric transport and subsequent terrestrial deposition of mercury (Fitzgerald et al. 1998). Mercury has also been released to the environment from industrial and manufacturing sources, primarily from chlor-alkali, cement, and paper/pulp facilities. Prior to the implementation of federal regulations in the early 1990s, mercury was also widely used and released to the environment as a result of the use of mercury in paint, batteries, and pesticides (EPA report to congress, 1997).

2.2.2 Toxicology and Exposure Pathways

Although the toxicity of mercury has been thoroughly investigated for carcinogenic, genetic, reproductive, and cardiovascular effects, the neurological effects of mercury are most notable. Exposure to elemental (Hg^0) mercury occurs primarily through inhalation and is mostly limited to occupational exposure as ambient atmospheric concentrations are extremely low (NRC 2000). Effects of exposure to elemental mercury have included autoimmune, reproductive, and renal toxicity. Human exposure to divalent mercury (Hg^{2+}) results from the ingestion of mercury containing food. The preferential

absorption of organic forms of mercury, of which mono methyl mercury (CH_3Hg^+) is the most common in the environment, over inorganic forms is attributed to the lipid solubility of methyl mercury which allows it to be retained in the fatty tissue of animals. Mercury is accumulated as it moves up the food chain and the structure of the food web is critical in determining the magnitude of accumulation in an ecosystem (Cabana 1994).

The toxicity of methyl mercury on the central nervous system has been well documented in two short-term poisoning events (Japan, 1950s and Iraq, 1970s) as well as many low-level chronic exposure studies (NRC 2000). Exposure to elevated concentrations of methyl mercury during pregnancy have resulted in adverse effects in children including mental retardation, cerebellar ataxia, limb deformities, hyperkenesis, cerebral palsy and seizures. Several long-term studies have detected increases in the frequency of abnormal findings on standardized neurological examinations amongst populations with chronic exposure to methyl mercury; however, the results are less conclusive than the acute exposure cases (NRC 2000).

For the general population, aquatic environments provide the most likely exposure pathways for mercury because they (1) are a sink for mercury, esp. sediments; (2) host bacterial communities that produce bioaccumulative methyl mercury, and (3) are populated by game fish, a popular food for humans. (Fitzgerald et al. 2007). As shown in Figure 2.1, mercury enters aquatic environments either through direct discharge from industrial processes or via exchange with mercury in the atmosphere.

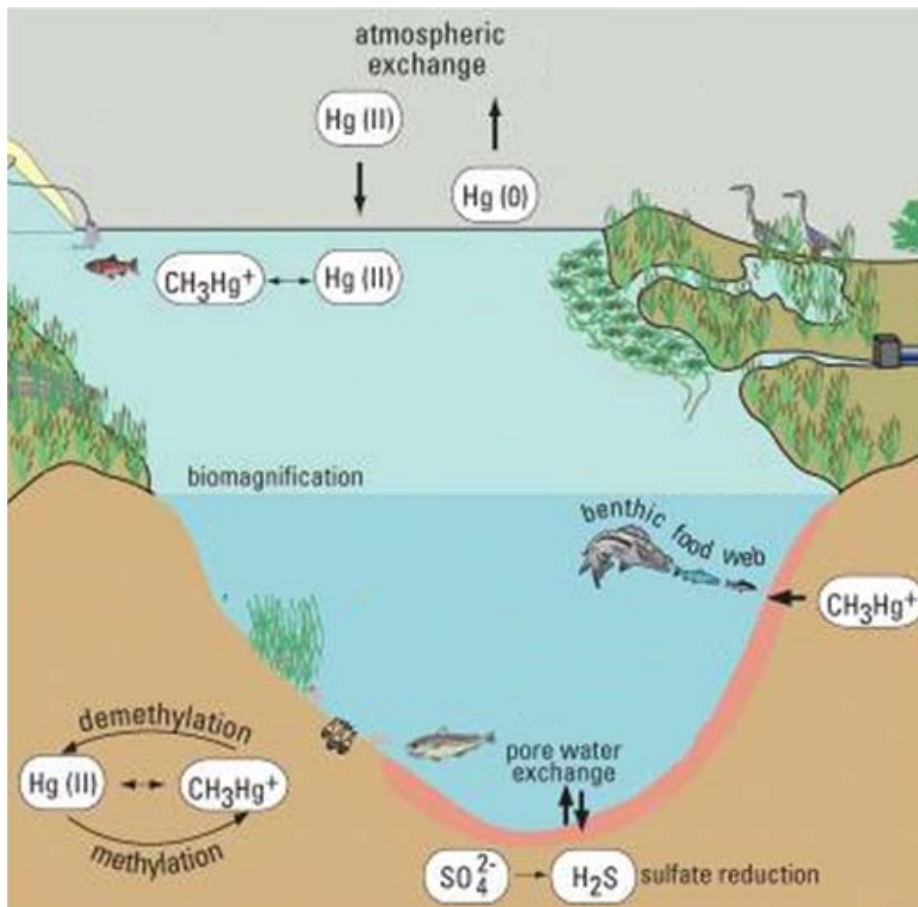


Figure 2.2 Illustration of mercury processes in the aquatic environment (adapted from Alpers et al., USGS, 2005-3014)

2.2.3 Mercury Chemistry in the Environment

Mercury exists in two oxidation states in the environment: Hg^0 (volatile gas or metallic liquid); and Hg^{2+} (soluble in water and forms complexes with inorganic and organic ligands). Both forms are strongly associated with particulate matter in the gaseous and aqueous environments. Elemental mercury (Hg^0) comprises over 95% of the mercury in the atmosphere, while the predominant form of mercury in aquatic environments is inorganic mercury (Hg^{2+}), which forms complexes with a variety of

organic and inorganic ligands. The other form of mercury which has been widely documented in the environment is methyl mercury, which is unstable in the gaseous phase and also forms organic and inorganic complexes in the aqueous phase (Morel et al. 1998).

Once in the terrestrial and aquatic environment, all three forms of mercury (elemental, inorganic, and methyl mercury) undergo various transport and transformation processes. Although inorganic mercury is theoretically extremely soluble (>7 g/L for mercuric chloride) strong associations with the solid phase limit its mobility in the environment. Association of mercury with the solid phase is often quantified by a sediment-water partition coefficient, K_D , which gives the ratio of sediment concentration to water concentration. K_D values obtained for sediment-water partitioning in field-scale investigations range from 10^3 - 10^5 [L/kg] for inorganic mercury and $10^{1.5}$ - $10^{3.5}$ [L/kg] for methyl mercury. The difference in partitioning strength of inorganic and methyl mercury results in methyl mercury comprising between 10 and 80% of total mercury in the pore water as opposed to typically less than 5% in the solid phase. Partitioning to suspended particulate matter in oxic waters are consistently 10-100 times greater than partitioning in sediments (Fitzgerald et al. 2007). In addition to the obvious significance of solid phase partitioning limiting transport, a field study in Long Island Sound showed that the magnitude of the partitioning coefficient (K_D) was directly related to the capacity of sediment to methylate mercury (Hammerschmidt and Fitzgerald 2004). This suggests that solid-phase partitioning is important in controlling the availability of mercury to methylating microbes.

Mercury associations with organic matter are very important in most environments (Lambertsson and Nilsson 2006) and K_D values for both inorganic and methylmercury have shown correlation with organic content (Bloom et al. 1999,

Hammerschmidt et al. 2004). XAS (X-ray absorption spectroscopy) evaluations have shown that thiol (reduced sulfur) groups play a dominant role in mercury associations with organic matter (Xia et al. 1999) and it is assumed that mercury association with dissolved organic carbon (DOC) is responsible for maintaining dissolved mercury concentrations below the solubility of cinnabar (HgS(s)) even in sulfidic environments (Benoit et al. 1999). Miller 2006, measured the partitioning of mercury and methylmercury to freshly precipitated hydrous ferrous oxide and amorphous iron-sulfide. Results showed that both forms of mercury partitioned more strongly to iron-sulfide phases than iron oxide phases. K_D values for both inorganic and methylmercury have been correlated with acid volatile sulfides (AVS), a proxy for iron-sulfides, in environmental systems (Hammerschmidt and Fitzgerald 2004).

The transformation of inorganic mercury to the more volatile elemental mercury results in the loss of mercury from the aquatic or terrestrial system to the atmosphere. Elemental mercury production has been observed to be mediated by both humic substances and light. Thus, a complete picture of mercury biogeochemistry must include cycling between air/water and sediment/water media and transformations within each of these media. The transformation processes that affect the production of methyl mercury have been most widely studied since this form poses the greatest risk to the general population, and will be reviewed in detail in the sections below.

2.2.4 Mercury Methylation

A growing body of laboratory and field-scale evidence has led to a widely accepted understanding that anaerobic bacteria in aquatic sediments, and sulfate reducing bacteria (SRB) in particular, play a dominant role in the production of methyl mercury.

(Compeau and Bartha 1985; Gilmour and Henry 1991) Though it has recently been suggested that other anaerobic bacteria are involved in mercury methylation, including iron reducing bacteria and methanogens (Pak and Bartha 1998, Warner et al. 2003), a host of studies have shown that additions of sulfate stimulate the biological production of methyl mercury. (Kerry et al. 1991, Gilmour et al. 1992, Harmon et al. 2004)

In-situ concentrations of methyl mercury represent a balance between methylation and demethylation processes (Hinertmann et al. 2000, Drott et al. 2008) and it is believed that rates of demethylation are relatively constant regardless of dominant biological populations, but that methylation rates are strongly dependent upon the activity of sulfate reducing bacteria (Warner et al. 2003, King et al. 2001). Recent research has shown that variations in in-situ methyl mercury concentrations are more dependent upon methylation rates than demethylation rates (Drott et al. 2008, Warner et al. 2005).

Photodegradation of methyl mercury has been observed in surface waters (Sellers et al. 1996), however, biologically mediated demethylation is believed to be dominant in dark environments. Oxidative demethylation, defined by the production of CO_2 as an end product, is hypothesized to be a metabolic process, while reductive demethylation (production of CH_4) is likely a detoxification mechanism (Marvin-DiPasquale et al. 2000).

2.2.5 Aqueous Mercury Speciation

In aerobic aquatic environments, dominant inorganic ligands for mercury are chloride and hydroxide. In anoxic environments, the inorganic speciation of mercury is dominated by mercury-sulfur species when sulfide is present at even nanomolar levels (Morel et al. 1998, Drott et al. 2007), and it has been hypothesized that uncharged dissolved mercury-sulfide complexes play an important role in controlling the

bioavailability of inorganic mercury to methylating bacteria in sulfidic sediments (Benoit, Gilmour et al. 1999, Benoit et al. 2003, Drott et al. 2007). The efficiency of uptake of uncharged mercury and methyl mercury chloride complexes in phytoplankton was explicitly demonstrated by Mason et al. 1996, and the same is assumed to be true for neutral mercury-sulfide complexes in anoxic environments.

Stability constants for mercury-sulfide complexes have been the subject of much research. The speciation model proposed by Benoit et al. 1999 and variations thereof have been routinely used in interpreting methyl mercury observations by estimating the uncharged, and assumedly bioavailable, fraction of the dissolved mercury pool. The model was developed to explain observations that seemed to show that the concentration of dissolved mercury species available for methylation by bacteria decreased with increasing sulfide concentrations. The original model uses the complexation constants given in Table 2.1.

Table 2.1 Stability constants for aqueous mercury partitioning to sulfide and DOM.

1	$\text{Hg}^{2+} + 2\text{HS}^- = \text{Hg}(\text{SH})_2^0$	37.5	Benoit et al. 1999
2	$\text{Hg}^{2+} + 2\text{HS}^- = \text{HgS}_2\text{H}^+ + \text{H}^+$	32.0	Benoit et al. 1999
3	$\text{Hg}^{2+} + 2\text{HS}^- = \text{HgS}_2^{2-} + 2\text{H}^+$	23.5	Benoit et al. 1999
4	$\text{Hg}^{2+} + \text{HS}^- = \text{HgSH}^+$	30.5	Benoit et al. 1999
5	$\text{Hg}^{2+} + \text{HS}^- + \text{H}_2\text{O} = \text{HOHgSH}^0 + \text{H}^+$	27.0	Benoit et al. 1999
6	$\text{Hg}^{2+} + \text{RS}^- = \text{HgRS}^-$	calibrated	Benoit et al. 2001
7	$\text{Hg}^{2+} + (\text{RS}^-)_2 = \text{Hg}(\text{RS})_2$	calibrated	

The stability constant for reaction number 5 in Table 2.1 is calculated by combining the inherent solubility of cinnabar ($\text{HgS}_{(s)} + \text{H}^+ = \text{Hg}^{2+} + \text{HS}^-$; $\log K_{\text{sp}} \sim -37$ to -39) with the so-called intrinsic solubility of cinnabar ($\text{HgS}_{(s)} = \text{HgS}^0$; $\log K_{\text{sl}} \sim -10$). This intrinsic solubility was estimated by Schwarzenbach and Widmer 1963 through extrapolation of experimentally determined solubilities of zinc and cadmium sulfides and

the fact that an uncharged mercury-sulfide-hydroxide complex ($\text{Hg-HS}^-\text{-OH}^-$) would be experimentally indistinguishable from HgS^0 (Schwarzenbach and Widmer 1963). Although the value for the stability constant for this reaction (Reaction 5 in Table 2.1), and the likelihood of its formation with or without the presence of pure phase cinnabar is a matter of some speculation (Drott and Skyllberg 07), the model has been used in various forms to explain methylmercury observations in a variety of marine and freshwater systems (Hammerschmidt et al. 2004, Drott et al. 2007).

The final reactions in Table 2.1 (6 and 7) were included in Benoit et al. 1999's original model as a simplification of several processes including associations with reduced thiol groups on organic matter, sorption to the solid phase involving one or two thiol groups, and associations with other solid phases. Dissolved organic matter is known to be involved in mercury complexation in both aerobic and anaerobic environments, and it is assumed that mercury association with dissolved organic carbon (DOC) is responsible for maintaining dissolved mercury concentrations below the solubility of cinnabar ($\text{HgS}_{(s)}$) even in sulfidic environments (Benoit et al. 1999). Stability constants for mercury interactions with dissolved organic matter (DOM) have been measured in several environments (Hintelmann et al. 1997, Benoit et al. 2001, Drexel et al. 2002), and it is assumed that mercury interactions with reduced-sulfur groups play a dominant role in mercury binding to dissolved organic matter. (Drott et al. 2007) Though it has been suggested that mercury-sulfide or mercury-organic complexes dominate dissolved speciation in anoxic environments, recent research has shown that interactions amongst mercury, DOM, and sulfide may all be important in understanding anoxic speciation (Miller 2006).

2.3 SEDIMENT DIAGENESIS

The collection of complex, interrelated biological and geochemical processes that occur in surficial aquatic sediments is termed diagenesis. Stratified biogeochemical zones in surficial sediments arise as a result of a delicate balance amongst biological and chemical processes. Ubiquitous bacteria utilize the familiar sequence of electron acceptors (O_2 , Mn^{4+} , Fe^{3+} , and SO_4^{2-} , and CO_2) to release energy stored in labile organic matter (Boudreau 1997). The byproducts of these bacterial reactions participate in a host of acid-base, oxidation-reduction, precipitation-dissolution, and sorption-desorption reactions. Countless formulations of these reactions into numerical models have been developed and applied to a variety of aquatic environments to study everything from nutrient and metal cycling to gas generation and release. Some well-known model applications include Boudreau 1997, VanCappellen and Wang 1995, and DiToro 2001.

Although many implementations of diagenetic models have been presented, almost all of them contain the same basic reactions or types of reactions:

- (1) Primary Redox Reactions – biologically driven reduction of carbon in organic matter by bacterial respiration
- (2) Secondary Oxidation/reduction Reactions – oxidation of byproducts of bacterial respiration by more oxidized species
- (3) Precipitation / Dissolution – precipitation of reduced byproducts as insoluble solids
- (4) Sorption / Desorption – association of species with the solid phase

Most diagenetic models are implemented to study one specific process in detail and a more rigorous treatment of the factors affecting this process is implemented. For

processes peripheral to the objective of the model, a simplified treatment may be sufficient.

Models for the primary reactions noted above, the degradation of labile organic matter by biological activity, are formulated in different ways. Common G-type formulations (Boudreau 97, VanCappellen and Wang 96) are applied in continual deposition environments use an assumed maximum carbon utilization rate defined as a function of depth. This rate is assigned to whichever bacterial population is presently active. A second type of model formulation assigns a maximum rate of carbon degradation for each electron accepting substrate (Jaffe et al. 2001). The resulting differences in these model formulations are depicted in Figure 2.3.

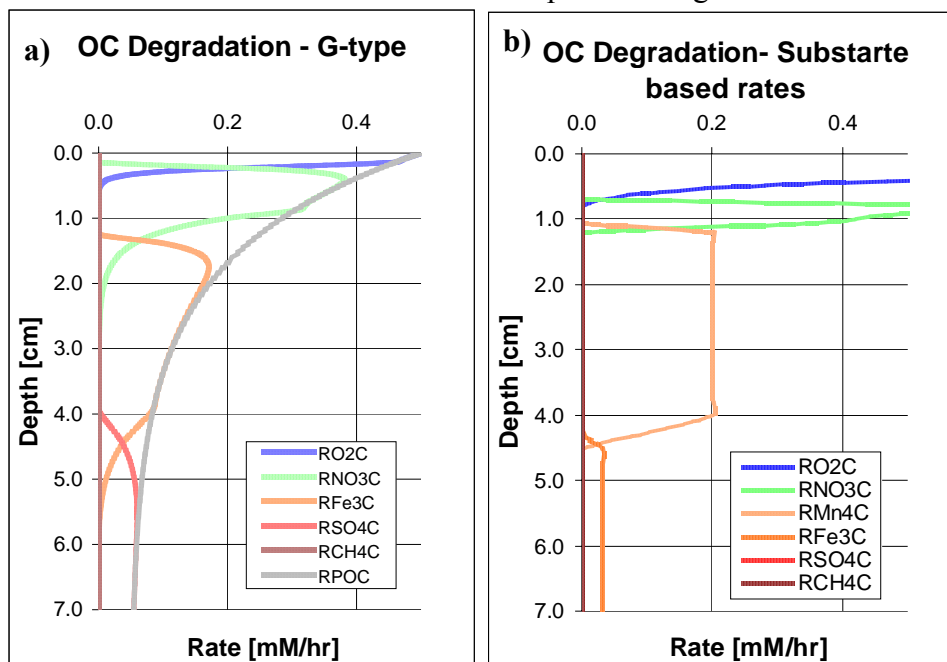


Figure 2.3 Predicted rates of microbial organic carbon degradation using alternative model formulations. (a) G-type model (Boudreau, 1997, VanCappellen and Wang 1995); (b) defined maximum rates for each population (Jaffe et al. 2001).

Both the G-type and substrate rate-based model formulations are capable of producing similar, realistic profiles for the stratified activity of different bacterial populations as shown in Figure 2.3. The justification for using G-type models in continuous deposition environments is that material at depth has been subject to biological degradation for a longer time than material near the surface and, consequently, deeper sediments have less energetic organic matter to drive bacterial processes (VanCappellen 96). The G-type model for organic carbon degradation is limited in its ability to simulate a system with discontinuous organic matter content, such as an in-situ capping layer. The alternative model for organic matter degradation defines rates of organic matter degradation in a more versatile way, but includes additional parameters for the maximum rate of carbon utilization for each bacterial population.

2.3.1 Diagenesis and In-situ Capping

The primary short-term effect of an in-situ cap on diagenetic processes in sediment will be the elimination of an oxygen flux to (formerly) surficial sediment. It is expected that biologically-driven redox zones will shift upwards in search of more favorable electron accepting conditions (Himmelheber et al. 2008). The magnitude of this shift and timescale over which it occurs will depend on the thickness of the cap and the bulk geochemical characteristics of the sediment and cap material. For example, high concentrations of sulfate in saline environments expand the depth over which SRB are active, while low sulfate freshwater environments contain a very limited zone of sulfate reduction if any at all. A thick cap with a substantial amount of organic matter in a low salinity environment will likely shift most early diagenetic processes into cap material, leaving the underlying sediment very reduced. However, a thin-layer cap with little labile organic matter in a highly saline environment may not shift biological processes as significantly, leaving the predominantly sulfate reducing conditions in underlying

sediment unchanged. Due to the typically high oxygen demand in sediments and strong reducing power provided by active microbial communities, oxidizing conditions in surficial sediment will likely be reduced on timescales of weeks to months.

A cap will also cut off the supply of organic material from the overlying water. In many depositional environments, labile organic carbon is decomposed in the top 10-20cm of the sediment and biological processes are inhibited in deeper sediment due to organic carbon limitations. A cap will eliminate the driving force for heterotrophic microbial activity to underlying sediment, however, biological communities will repopulate freshly deposited material on top of a cap. The timescale of the degradation of organic matter is on the order of years to decades in most environments.

2.3.2 Diagenesis and Mercury Methylation

The transition of surficial sediments underlying a cap from aerobic to anaerobic will cause iron-oxides to be replaced by iron-sulfides, potentially altering the solid phase partitioning and mobility of mercury. The diagenetic relationship amongst sulfate, organic carbon, and methyl mercury production is complex. While sulfate and energy rich organic matter drive the biological processes that produce methyl mercury (Lambertsson et al. 2006), sulfide, the reduced byproduct of sulfate reduction, has been shown to inhibit methylation at high concentrations (Benoit et al. 2003) and organic content has been found to correlate with the strength of partitioning to the solid phase (Hammerschmidt et al. 2004).

Evidence from both large, ecosystem-level gradients in geochemistry (Gilmour et al. 1998) as well as depth profiles at individual locations (Benoit et al. 2003, Merritt et al. 2008) have suggested that mildly reducing conditions, where sulfate reduction has begun, but sulfide has not yet built up to inhibitory levels, provide the most conducive

environments for mercury methylation. On the large, ecosystem-scale, this means that lower methyl mercury production is observed in systems where high organic matter and sufficient sulfate drives dissolved sulfide concentrations to millimolar levels. On a depth profile scale, this means that the depth corresponding to maximum methyl mercury production is concurrent with the onset of sulfate reduction.

Chapter 3: Modeling Methyl mercury Production in a Range of Anaerobic Biogeochemical Conditions

3.1 INTRODUCTION

Numerous studies have shown that the production of methyl mercury by bacterial processes in sediments represents a major source of mercury contamination for higher aquatic trophic levels and humans (Hammerschmidt et al. 2004, Benoit et al. 2003). The speciation of mercury, especially transformation to methyl mercury, is sensitive to local biogeochemical conditions and critical to defining transport and availability (Benoit et al. 1999). The sensitivity of methyl mercury production to local biogeochemical conditions may dictate the feasibility of engineering management tools for natural systems such as engineered wetlands (Mehrota and Sedlak 2005), water management structures in the FL everglades (Hurley et al. 1998), and in-situ management options for contaminated sediments (Liu et al. 2001, Liu et al. 2007, Chapter 5). The motivation for this research is the widespread consideration of in-situ sediment capping as a management option for contaminated sediment. Research has shown that biogeochemical changes induced by the placement of a sediment cap will encourage anaerobic conditions known to enhance methyl mercury production. This research quantifies methyl mercury production and the processes and parameters that control it over a range of biogeochemical conditions likely to be found beneath an in-situ sediment cap.

In-situ sediment methyl mercury concentrations represent a balance between methylation and demethylation processes (Hintelmann et al. 2000). Vertical variability in the in-situ methyl mercury concentration has been observed in several estuarine conditions (Merritt et al. 2008, Bloom et al. 1999, Langer et al. 2001, Hammerschmidt et al. 2004, Benoit et al. 2006). The causes of this vertical variability can be attributed to

interrelated biological and geochemical processes including the activity of methylating and demethylating bacteria as well as the availability of inorganic mercury (Hammerschmidt et al. 2007). Recent research has shown that variations in in-situ concentrations are more dependent upon methylation rates than demethylation rates (Drott et al. 2008). Demethylation appears to occur efficiently regardless of dominant bacterial population (Warner et al. 2003); however, sulfate reducing bacteria (SRB) methylate mercury more efficiently than other anaerobic populations (Gilmour et al. 1992, Harmon et al. 2004, Warner et al. 2003). Vertical profiles of in-situ methyl mercury have consistently shown maximum concentrations near the oxic-anoxic transition (Benoit et al. 2006, Hammerschmidt et al. 2004, Merritt et al. 2008). Rates of methylation appear to be limited by the complexation of dissolved inorganic mercury with organic and inorganic ligands, which can reduce the availability of mercury to methylating microbes (Drott et al. 2007). It is assumed that passive diffusion of uncharged, dissolved mercury complexes is the primary route of uptake into methylating bacteria (Mason et al. 1996), and previous research has suggested that aqueous speciation shifts with increasing sulfide concentration from the uncharged, bioavailable complex HgS^0 , to the charged and consequently unavailable complex HgS_2H^- at low micromolar sulfide concentrations (Benoit et al. 1999, 2001). Although the exact sulfide concentration which leads to this shift is not well characterized (Drott et al. 2007) it has been estimated to be near the solubility of sulfide in the presence of iron sulfides in environmentally relevant conditions (1-20 μM). The presence of both iron and sulfide in sediment environments leads to the precipitation of iron sulfides, which maintains low dissolved sulfide concentrations if a stoichiometric excess of iron is present.

The above observations have led to the theory that a geochemical zone of maximum methylation exists where the activity of sulfate reducing bacteria is high, but

sulfide has not yet build up to a level that would limit the availability of inorganic mercury by shifting speciation away from an uncharged mercury-sulfide complex (Merritt et al. 2007, Benoit et al. 2003). The objective of this study is to evaluate methyl mercury production over a range of biogeochemical conditions likely to occur following the placement of an in-situ sediment cap and determine whether efficient methylation is confined to a narrow geochemical redox zone. Sediment from different environments with a range of organic content was incubated under different well-mixed anaerobic conditions to characterize in-situ methyl mercury production and the biogeochemical factors that affect methylation. A model for steady state methyl mercury concentration that incorporates the effects of sulfate reduction, aqueous availability, and solid-phase partitioning is developed and applied to observations in order to quantify the cumulative impact of these processes in controlling methylation

3.2 MATERIALS AND METHODS

3.2.1 Sediment Environments, Collection, and Treatment

Sediment was collected from two sites with a range of organic content in the Gulf of Mexico. Sediment from a mercury contaminated estuarine site in Lavaca Bay (Bloom et al. 1999, near site OR-3) was collected in August 2007 and had a low organic content (3% loss on ignition – LOI). Sediment from an un-impacted salt marsh in the ship channel of Corpus Christi Bay near Port Aransas (27°50', -97°05') was collected in August 2008 and contained much higher organic content (27% LOI). Bulk sediment was collected from approximately the top 12 inches at both sites and stored at 4°C until the initiation of experiments.

The geochemical differences amongst the two sediments were obvious from visual observations as well as chemical analysis. The salt marsh sediment (HO-High Organic) had a very dark color and a strong smell of sulfide. The sandy estuarine sediment (LO-Low Organic) was much lighter color, did not exhibit any sulfide odor, and settled very quickly in a slurry. Table 3.1 presents some characteristic differences between the two environments.

Table 3.1 Geochemical characteristics of Salt Marsh and Estuarine sediment. Standard deviation of replicate analysis is presented in parentheses.

	Salt Marsh Environment (HO)	Estuarine Environment (LO)
Organic content [% LOI]	27 (± 2.8)	3.1 (± 0.4)
DOC [mM]	16.6 (± 5.4)	0.63 (± 0.24)
Total Fe [$\mu\text{mol/g}$]	80	100
Surficial sediment sulfide concentrations [mM]	>1-2	<0.050
Depth to active sulfate reduction [cm]	0.2-1.0	5-10

Sediment from each site was sieved through a 1mm mesh under an N₂ atmosphere, spiked to a solid phase concentration of $\sim 1\mu\text{g/g}$ total mercury with HgCl₂ (Alfa Aesar), and homogenized for 48 hours. Because of the extreme differences between the environments, aliquots from each environment were mixed to produce a sediment environment with a moderate organic content of $\sim 10\%$ LOI (20% salt marsh solids +80% sandy estuarine) for comparison. This mixture is referred to in the following discussions as MO (Medium Organic).

3.2.2 Sediment Incubation Experiments

Batch sediment incubations spanning a range of redox conditions were prepared for each of three sediment environments as outlined in Table 3.2.

Table 3.2 Nine geochemical conditions used to study methyl mercury production. Three different environments (range of organic matter) and three different geochemical conditions (redox zones).

	Salt Marsh Environment (High Organic-HO)	Mixture Environment (Medium Organic-MO)	Estuarine Environment (Low Organic-LO)
Suboxic	25-30% OC ^a Pre-Aerated	5-10% OC Pre-Aerated	2-5% OC Pre-Aerated
Mildly reduced	25-30% OC Fe ²⁺ spike – (15mM) Low sulfide	5-10% OC Fe ²⁺ spike – (5mM) Low sulfide	2-5% OC Fe ²⁺ spike – (0.5mM) Low sulfide
Fully reduced	25-30% OC SO ₄ spike High sulfide	5-10% OC SO ₄ spike High sulfide	2-5% OC SO ₄ spike High sulfide
^a Organic Carbon, characterized by loss on ignition, combustion at 550 C			

Aliquots from each environment (HO, MO, LO), were sealed in well-mixed anoxic test tubes in order to facilitate three different redox conditions:

- (1) Suboxic condition – representative of surficial sediment following the elimination of oxygen.
- (2) Mildly reduced condition – representative of the transition to sulfate reduction and characterized by active sulfate reduction but low dissolved sulfide

- (3) Fully reduced condition – representative of deep sediment and characterized by sulfate reduction and a buildup of dissolved sulfide, $>100\mu\text{M}$

The three geochemical conditions described above were simulated for each of the three environments (HO, MO, LO) by varying oxygen, sulfate and Fe^{+2} concentrations in at the start of the experiments. These geochemical conditions were chosen to represent different, stratified zones in the sediment column. Additionally, the conditions were chosen because of characteristic differences in the factors controlling the production of methyl mercury. Based on the theory that a maximum zone of methylation should occur in the mildly reduced zone, Table 3.4 outlines the mercury-related biological and geochemical factors expected to occur in each simulated geochemical condition.

Table 3.3 Expected effects of simulated geochemical conditions on mercury methylation

Simulated Geochemical Condition	<i>Sulfate Reduction?</i>	<i>Uncharged mercury-sulfide speciation?</i>
Suboxic	NO	NO
Mildly reduced	YES	YES
Fully reduced (Sulfate reducing)	YES	NO

The geochemical conditions in Table 3.2 can be thought of as an abstraction of redox zones at increasing depth in the sediment although the actual depth at which they occur is dependent upon bulk geochemical conditions. The onset of sulfate reduction and accumulation of sulfide has been observed at ~5-10cm depths in the sandy estuarine

environment, LO, (Bloom et al. 1999, Chapter 5) and is typically 1-2cm below the surface in salt marsh sediment, (HO, Langer et al. 2001, Chapter 4).

The conditions outlined in Table 3.2 were facilitated in the following way: Prior to initiation of the experiments, an aliquot from each of the three environments (HO, MO, LO, post-mercury spike) was separated, mixed with 5 parts (by volume) water and bubbled with filtered ambient air (HEPA, 0.2um) for 3 weeks to oxidize reduced solid phases. The liquid phase was replaced periodically to remove SO_4^{2-} produced by oxidized sulfur minerals. This condition will be referred to as the ‘Suboxic Condition.’ During the same time, a second aliquot of each sediment environment was not oxidized, but sealed and incubated at 25°C for three weeks. Sulfate was added periodically to maintain $>2\text{mM SO}_4^{2-}$. This second aliquot was divided into two parts, one of which was amended with Fe^{2+} to maintain low sulfide concentrations (Mildly Reduced Condition) and the other which was amended with seawater (Fully Reduced Condition). At the end of this initial incubation time, ~500mL of wet sediment was mixed with ~400mL of deoxygenated buffer solution, as outlined in Table 3.4, to encourage the different geochemical conditions (Table 3.2). Sodium chloride was added to maintain a similar ionic strength in all solutions, and ferrous iron (as FeSO_4) was added to the mildly reduced condition to maintain low sulfide concentrations. The pH was adjusted to approximately 8.0 using HCl or NaOH.

Table 3.4 Amendments in buffer added to encourage suboxic, mildly reduced, and fully reduced geochemical conditions.

Simulated condition	HEPES^d buffer	Initial pH^a	NaCl	% seawater^c	FeSO₄
Suboxic	50mM	8.1	440mM	5%	0mM 15mM ^b
Mildly reduced	50mM	8.2	150mM	30%	5mM ^b 0.5mM ^b
Fully reduced	50mM	8.1	0mM	100%	0Mm

^a – negative log of activity of hydrogen ion; ^b – added 15mM for HO incubation, 5mM for MO, and 0.5mM for LO incubations; ^c – 100% seawater had 35ppt salinity; ^d HEPES – Goods biological buffer, pK_a=7.55

Forty five milliliter aliquots of homogenized sediment-buffer mixture were sealed in 50mL borosilicate glass centrifuge tubes, sealed with PTFE-lined caps, and placed on a tumbler in the dark at ~50RPM. All incubation preparations were performed in an N₂ atmosphere with deoxygenated water and reagents. Duplicate or triplicate centrifuge tubes from each of the nine conditions were sacrificed at regular intervals as independent replicates in order to measure solid-phase methyl mercury and dissolved total mercury as well as relevant geochemical parameters including pH, dissolved sulfide, ferrous iron, sulfate, and acid volatile sulfides (AVS).

Observations of sulfide, dissolved mercury, and solid phase methyl mercury between 20 and 40 days of incubation suggested that the biogeochemical conditions had

stabilized from the effects of initial conditions. At this point, an additional spike of mercury (HgCl_2 , to 20ppm, solid phase) was added after 60 days to increase the mercury available for methylation. Dissolved mercury, solid phase methyl mercury, as well as the above suite of geochemical parameters was measured 48 hours after the additional mercury spike.

3.2.3 Analytical Methods

During a sampling event, replicate centrifuge tubes were removed from the tumbler and sacrificed for analysis. Under an N_2 atmosphere, aliquots of homogenized sediment incubation were removed for AVS determination (1.0-1.5mL), ferrous iron extraction (1.0-1.5mL), methyl mercury (4mL), and sulfate reduction rate (4mL). AVS was measured by a diffusion method (Hsieh et al. 2002), and the detection limit was determined to be $<0.1 \text{ umol/g}$ dry sediment based on the mass of sediment and the detection limit of the sulfide electrode. Ferrous iron was extracted from the solid phase using oxalic acid (Phillips and Lovely 1987) and quantified spectrophotometrically using phenanthroline. An aliquot of slurry was removed for methyl mercury samples, placed in borosilicate glass vials with PTFE lined caps, and immediately frozen at -20°C until extraction and quantification as described below. Assays using $^{35}\text{SO}_4^{2-}$ gave variable results and were not used to quantify SRR. A thorough discussion of the method is included in Appendix A. Following 30 minutes of centrifugation at 2500 RPM, pH was measured in the supernatant of centrifuge tubes using an electrode (VWR) calibrated in ionic-strength adjusted pH buffers. Sulfide anti-oxidant buffer was mixed 1:1 with incubation porewater (1.5mL) and sulfide was quantified with an ion-specific electrode (VWR) calibrated in a similar matrix (pH 8, seawater + 50mM HEPES). Aliquots of incubation porewater were filtered ($0.45\mu\text{m}$ polypropylene syringe) and analyzed for

chloride and sulfate (1mL) using ion chromatography on a MetroOhm IC system (700 Series, 15cm Metrosep A Supp 5 column) and dissolved ferrous iron (2.5mL) using the phenanthroline method. Fresh stock solutions for Fe^{2+} and SO_4^{2-} were prepared monthly, although checks with older stocks showed no evidence of degradation.

Loss on ignition (LOI) was measured gravimetrically by overnight combustion at 550(degrees) C as a surrogate for organic matter content in the solid phase. Total solid phase iron and mercury were measured by microwave digestion in concentrated nitric acid (20min, 50psi) and quantified on graphite furnace AA (PerkinElmer, AAnalyst600). DOC in each environment was quantified following 0.45 μm filtration (polypropylene) and prior to the addition of HEPES buffer using a TOC analyzer (Dhormann).

3.2.4 Mercury and Methyl mercury Analysis

To determine dissolved mercury, centrifuged incubation water was filtered using 0.45 μm polyethersulfone membrane filters (Pall Life Sciences–Supor®) and digested overnight at room temperature with 2% bromine monochloride. Samples were stored at 4°C until analysis of total mercury by stannous chloride reduction, dual stage gold preconcentration, and quantification using CVAFS (Tekran 2600, EPA method 1631). Speciation modeling was used to calculate the distribution of this dissolved mercury (defined as mercury passing a 0.45 μm filter) amongst organic and inorganic ligands. This total filtered concentration will be referred to as dissolved mercury throughout the discussion that follows.

Methyl mercury samples were thawed and immediately extracted (within 30 minutes) and analyzed using using USGS method 5A-7 (organic extraction, aqueous ethylation, purge and trap, GC separation, and CVAFS) (USGS 2004). An aliquot of estuarine reference material (ERM-CC580, RTC Analytical) was extracted with every 10

samples, and matrix spikes and duplicates at 1-5 times the sample concentration were used to verify the efficiency of the extraction procedure. Ongoing calibration checks fell within the limits specified in EPA Method 1630. Replicate analyses of aliquots from the same digestion were within 10% (n=15) and typically less than 5%. Recovery of reference material (ERM CC580, 75ng/g +/- 2ng/g MeHg) averaged 102% (n=12). Recovery of matrix averaged 95% (n=8) and RPD for duplicate matrix spikes was 10% (n=4). Duplicate digestions of homogenized sediment aliquots had a relative percent difference averaging 14% (n=9).

3.3 SPECIATION CALCULATIONS

In order to estimate the relative distribution of dissolved mercury amongst organic and inorganic ligands, speciation calculations were performed using published thermodynamic constants. It was assumed that sulfide and an organic ligand dominate speciation in anoxic environments (Morel et al. 1998, Drott et al. 2007). The stability constants used for speciation calculations in this research are based on those applied by Drott et al. 2007, and presented in Table 3.5.

Table 3.5 Stability constants for dissolved sulfide and organic mercury complexes

Reaction	Complex stoichiometry	Log K	Source
1	$\text{Hg}^{2+} + 2\text{HS}^- = \text{Hg}(\text{SH})_2^0$	37.5	Benoit et al. 1999
2	$\text{Hg}^{2+} + 2\text{HS}^- = \text{HgS}_2\text{H}^+ + \text{H}^+$	31.3	Benoit et al. 1999
3	$\text{Hg}^{2+} + 2\text{HS}^- = \text{HgS}_2^{2-} + 2\text{H}^+$	23.0	Benoit et al. 1999
4 ^b	$\text{Hg}^{2+} + \text{HS}^- = \text{HgSH}^+$	20.0	Drott et al. 2007
5 ^a	$\text{Hg}^{2+} + \text{HS}^- = \text{HgS}^0 + \text{H}^+$	24.5-26.5	Drott et al. 2007, Benoit et al. 1999
6	$\text{Hg}^{2+} + 2\text{RSH} = \text{Hg}(\text{RS})_2 + 2\text{H}^+$	22.1	Skyllberg et al. 2001

^aModel B – $\log K_5 = 24.5$, for model B' – $\log K_5 = 26.5$. ^bthe complex from Reaction 4 was not significant (<1%) under all conditions simulated with a log stability constant of either 20 or 30

Sulfide concentrations were measured directly, and the concentration of organic ligands was defined by thiol groups on DOC. The concentration of these thiol groups (RSH) was calculated after the method outlined in Skjellberg et al. 2006, assuming 1% by mass reduced sulfur (S:C = 0.01), and 15% mol thiol groups of reduced sulfur, based on results from other organic soils (Drott et al. 2007, Skjellberg et al. 2006). Measurements for DOC in each environment (HO, MO, LO) were converted to molar concentrations of organic ligands based on the above assumptions and resulted in 9.5 μ M for the HO environment, 2.3 μ M for the MO environment, and 0.23 μ M for the LO environment. Total sulfide concentrations measured in sediment incubations were adjusted to the bisulfide ligand (HS⁻) using measured pH and a pK_a for sulfide of 7.0 (Stumm and Morgan 1996).

Calculations of equilibrium speciation resulted in an estimate of the relative distribution of each of the mercury complexes listed in Table 3.5. The value of the stability constant for Reaction 5, and the likelihood of its formation in the absence of pure phase cinnabar has been questioned (Drott et al. 2007); however, models including this complex have been routinely used to interpret methyl mercury observations (Hammerschmidt et al. 2004, Merritt et al. 2007). Two constants were used for Reaction 5 in order to investigate the importance of the single sulfide mercury complex HgS⁰ in defining inorganic mercury availability to methylating microbes. Model B included a stability constant of 24.5 for HgS⁰ from Skjellberg et al. 2007 and model B' used a higher constant of 26.5 from Benoit et al. 1999.

The log concentration diagrams shown in Figure 3.1 highlight the differences in speciation resulting from the two different stability constants for HgS⁰ as a function of sulfide and organic ligand concentrations at pH 8.0. The concentration of bisulfide (HS⁻) is plotted on the vertical axes. In Figure 3.1b, lines are also plotted to show the effect of

a change in pH (to pH 6), and a change in the stability constant for the organic complex $\text{Hg}(\text{SR})_2$ to 24.1. Analogous shifts in speciation for changes in pH and $\log K_{\text{Hg}(\text{SR})_2}$ would be observed for Model B in Figure 3.1a. Vertical dashed lines show the approximate concentrations of the RSH ligands in each of the three environments (HO, MO, LO).

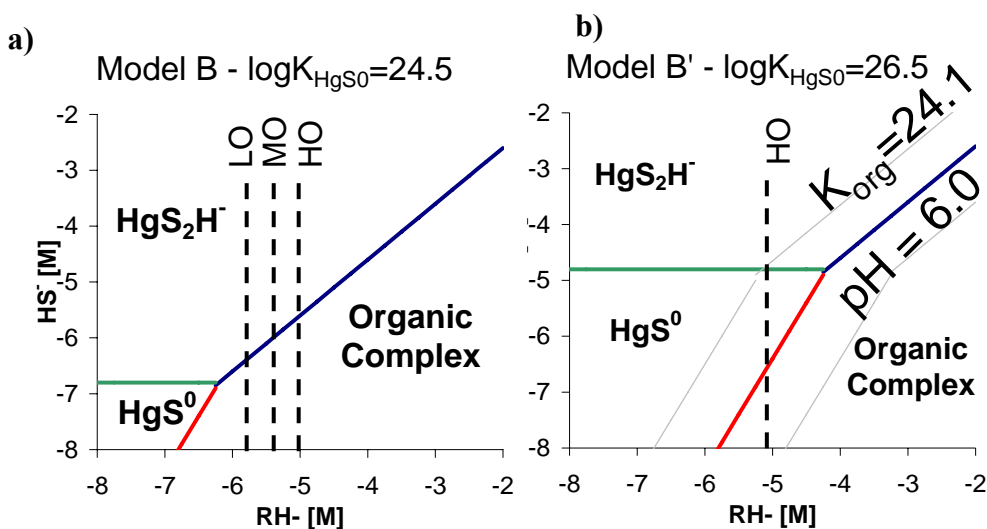


Figure 3.1 Phase diagram showing regions of predominance for two-sulfide mercury complex (upper left), single sulfide mercury complex (lower left), and organic complex (lower right) for pH 8 using (a) low stability constant for HgS^0 – Model B; and (b) high stability constant for HgS^0 – Model B'. Vertical dashed line represents organic complex concentration in each environment. Additional lines in (b) represent the effects of changing pH (shift right), and the stability constant for the organic complex (shift left).

For both systems, three mercury species dominate within the envelope of environmentally relevant sulfide and organic ligand concentrations. In both cases, at low organic ligand concentration the dominant species is either the neutral species HgS^0 or the negatively charged species HgS_2H^- . The particular sulfide concentration at which speciation shifts from HgS^0 (Reaction 5) to HgS_2H^- (Reaction 2) is defined by the difference between the stability constants ($\log K_2 - \log K_5$) and this concentration was 10^{-7}

^{6.8} for Model B and $10^{-4.8}$ for Model B'. Model B (Figure 3.1a) predicts a small window at very low sulfide (<150nM) and thiol ligand (<200nM) concentrations where the uncharged single sulfide complex HgS^0 dominates speciation. In contrast, the larger log stability constant for HgS^0 of 26.5 for Model B' (Figure 3.1b) yields results which suggest that HgS^0 dominates for sulfide concentrations less than ~15uM and thiol ligand concentrations less than ~10uM. This larger range of dominance for HgS^0 brings the uncharged, single sulfide species into relevance for many anoxic sediments that have sulfide concentrations in the low micromolar range and DOC in the 1-50mg/L range (0.2-10uM thiol ligand).

Unfortunately, the phase diagrams of Figure 3.1, provide only a partial representation of the speciation of uncharged mercury-sulfide complexes because other mercury-sulfide species, including the uncharged and consequently bioavailable species $\text{Hg}(\text{SH})_2^0$, are present as minor components in the HgS_2H^- dominated region. For example, at sulfide concentrations above the shift from HgS^0 to HgS_2H^- , ($10^{-4.8}$ for Model B') about 2% of dissolved mercury is predicted to be present as the two-sulfide neutral complex $\text{Hg}(\text{SH})_2^0$ at pH 8. Since sulfide concentrations were never below 10^{-6}M in the sediment incubations from this experiment (and are rarely below 10^{-7}M in anoxic sediment porewater), the main difference between Models B and B' is the following: for Model B' the uncharged fraction is dominated by HgS^0 at low sulfide and $\text{Hg}(\text{HS})_2^0$ at high sulfide, while for Model B, the only relevant uncharged species is $\text{Hg}(\text{HS})_2^0$. Throughout the following text, the term “available fraction” will be used to refer to the fraction of dissolved mercury (passing 0.45μM filter) calculated to be present as HgS^0 and $\text{Hg}(\text{HS})_2^0$ using speciation model B and B'.

While sulfide inhibits methylation at high concentrations by shifting speciation away from uncharged, bioavailable mercury-sulfide complexes, at very low sulfide

concentrations, increases in sulfide shifts speciation away from organic complexes and towards the uncharged, single sulfide HgS^0 . This can be seen in Figure 3.1b by following the vertical line corresponding to the high organic environment. At sulfide concentrations less than 10^{-7}M , speciation is dominated by organic complex, while increasing sulfide up to 10^{-6}M , leads to a shift towards HgS^0 , and an increase in mercury availability to methylating microbes. This means that while high sulfide concentrations are inhibitory to availability, some sulfide is necessary to out-compete organic ligands and produce uncharged mercury-sulfide complexes.

3.4 MODELING INCUBATION METHYL MERCURY

A conceptual model incorporating descriptions of fundamental processes known to be involved mercury methylation was used to quantify the effects of biogeochemical processes on in-situ methyl mercury concentrations. The assumptions of the model were: (1) biological mercury methylation and demethylation take place primarily in the aqueous phase; (2) only a fraction of the aqueous mercury is available for methylation and demethylation reactions; and (3) the rates of methylation and demethylation are proportional to aqueous concentrations of inorganic and methyl mercury, respectively. Subject to these assumptions, Equation 3.1 describes the balance amongst methylation and demethylation in sediment (Sunderland et al. 2006):

$$\frac{d\text{MeHg}_{(T)}}{dt} = (k_{m\text{-SRB}} + k_{m\text{-other}})\phi_{\text{Hg}}\text{Hg}_{(aq)} - k_d\phi_{\text{MeHg}}\text{MeHg}_{(aq)} \quad \text{Equation 3.1}$$

where: $\text{MeHg}_{(T)}$ is the total concentration of methyl mercury in the sediment [ug/cm^3]; $\text{Hg}_{(aq)}$ is the dissolved inorganic mercury [ng/L]; $\text{MeHg}_{(aq)}$ is the dissolved methyl mercury [ng/L]; $k_{m\text{-SRB}}$ is the methylation rate due to sulfate reduction [$/\text{day}$]; $k_{m\text{-other}}$ is the methylation rate due to other biotic or abiotic processes [$/\text{day}$]; k_d is the

demethylation rate [/day]; ϕ_{Hg} is the fraction of dissolved mercury available for methylation [dimensionless]; and ϕ_{MeHg} is the fraction of dissolved methyl mercury available for demethylation [dimensionless]. Research has shown that bacterial populations other than sulfate reducing bacteria as well as abiotic processes are capable of producing methyl mercury, and the effects of these processes are incorporated into the constant $k_{\text{m-other}}$.

Hintelmann et al. 2000 estimated a methyl mercury turnover time of ~2 days using ambient-level spikes of radiolabeled mercury species suggesting that methylation and demethylation processes occur relatively quickly. With the assumption that methylation and demethylation reactions happen relatively quickly compared to transport, in situ concentrations represent an effective equilibrium between methylation and demethylation (Sunderland et al. 2006). Applied to the well-mixed sediment incubations described here, this assumption means that methylation – demethylation reactions happen on a timescale smaller than geochemical changes. Although there was some variability in geochemical measurements over time in the incubations, the major temporal (Figures 3.2-3.4) occurred at timescale of ~10 days.

If the dissolved inorganic and methyl mercury are expressed in terms of the solid concentration (assuming linear partitioning, $\text{Hg}_{(\text{aq})} = \text{Hg}_{(\text{s})} / K_{\text{D-Hg}}$), the methyl mercury concentration represented as a fraction of the total mercury in the sediment at steady state can be written as Equation 3.2:

$$\begin{aligned} \% \text{MeHg} &= \frac{\text{MeHg}_{(\text{s})}}{\text{Hg}_{(\text{s})}} = \frac{k_{\text{m-SRB}}}{k_d} \frac{\phi_{\text{Hg}}}{\phi_{\text{MeHg}}} \frac{K_{\text{D-MeHg}}}{K_{\text{D-Hg}}} + \% \text{MeHg}_0 \\ \% \text{MeHg}_0 &= \frac{k_{\text{m-other}}}{k_d} \frac{\phi_{\text{Hg}}}{\phi_{\text{MeHg}}} \frac{K_{\text{D-MeHg}}}{K_{\text{D-Hg}}} \end{aligned} \quad \text{Equation 3.2}$$

where %MeHg₀ is the percent methyl mercury expected in the absence of active sulfate reduction. The relationship in Equation 3.2 shows that the steady state % methyl mercury in sediment is related to (1) methylation and demethylation rates, (2) the available fraction of inorganic and methyl mercury in the aqueous phase, and (3) the strength of partitioning to the solid phase.

Previous studies that have used large cold spikes (Warner et al. 2003, King and Kostka 2001) or radiolabeled isotopes (Hintlemann 2000, Drott et al. 2007) to measure rates of methylation and demethylation have expressed rates on a whole sediment basis, so that the availability and solid-phase partitioning (from Equation 3.2) are effectively lumped into a single parameter ($k_m' = k_m \phi_{Hg} / K_{D-Hg}$). However, since the data collected in the current study provide estimates for processes known to control methylation, the parameters representing these processes can be taken out of the lumped parameter k' and used to describe methylation in more detail. The processes measured in the experiment include: (1) activity of methylating microbes (sulfate reduction), (2) available dissolved fraction (ligands and speciation calculations), and (3) solid phase partitioning (dissolved and solid phase mercury).

In order to quantify the simultaneous influence of these three processes in limiting mercury methylation (according to Equation 3.2), the fraction of methyl mercury can be plotted against quantities measured during the incubations. In Equation 3.3, the fraction of uncharged aqueous mercury calculated with thermodynamic data (Section 3.3) is assumed to represent the fraction available for methylation, and it is assumed that methylation above background levels is proportional to the rate of sulfate reduction $k_{m-SRB} = k_{meth-SRR} * SRR$. K_D was defined as the ratio of solid phase to total dissolved mercury.

$$\%MeHg = \frac{k_{meth-SRR}}{k_d'} SRR \frac{\phi_{Hg}}{K_D} + \%MeHg_0 \quad \text{Equation 3.3}$$

Equation 3.3 presents a simple linear relationship between steady state % methyl mercury and commonly quantified geochemical measurements known to affect methylation: sulfate reduction rate, dissolved sulfide and organic carbon (to calculate ϕ_{Hg}), and solid phase partitioning (K_D). The parameters describing the process of demethylation (k_d , ϕ_{MeHg} , and $K_{D-\text{MeHg}}$) were not explicitly measured during the incubations because demethylation rates are thought to be less variable than rates of methylation, and research has shown that methylation rates are more important than demethylation rates and transport in defining in-situ methyl mercury concentrations (Skylberg et al. 2008). Active demethylation has been observed in a variety of microbial communities (Warner et al. 2003), and the uptake of methyl mercury to bacterial cells is thought to be an active detoxification mechanism, rather than passive diffusion of inorganic mercury for methylation (DiPasquale et al. 2000). Demethylation parameters therefore, are lumped into a single, whole sediment parameter ($k_d' = k_d \phi_{\text{MeHg}} / K_{D-\text{MeHg}}$) in Equation 3.3.

3.5 RESULTS AND DISCUSSION

Geochemical observations showed that the incubations were successful in producing the nine targeted biogeochemical conditions presented in Tables 3.2 (Figures 3.2-3.4). All three suboxic conditions (LO, HO, MO) initially showed very low AVS concentrations ($<0.1 \mu\text{mol/g}$), suggesting that reduced metal and sulfur phases were effectively oxidized (Figures 3.2b, 3.3b, 3.4b). The mildly reduced conditions for HO and MO had low sulfide concentrations ($<25 \mu\text{M}$) throughout the experiment (Figures 3.3e, 3.4e), while high sulfide ($>1 \text{mM}$) was observed in both fully reduced incubations (Figures 3.3h, 3.4h). Decreases in dissolved ferrous iron in all three mildly reduced

conditions are consistent with the production of sulfide and precipitation as insoluble FeS (Figure 3.2d, 3.3d, 3.4d). Within each environment, similar rates of sulfate reduction, calculated from sulfate observations (Figure 3.5), occurred in mildly and fully reduced incubations, consistent with expectations outlined in Table 3.3. However, iron reduction was expected to persist in suboxic incubations due to the presence of oxidized metals, and this was clearly not the case for HO and MO incubations (Figure 3.5).

In the suboxic conditions for HO and MO environments, it appeared that there was insufficient oxidized iron to sustain iron reducing conditions. This was apparent because sulfate concentrations decreased quickly to near zero between 1 and 22 days in the suboxic HO incubation and AVS increased stoichiometrically ($3\text{mM SO}_4^{2-} \sim 10\text{ug/g}$ at 300g/L solids) (Figure 3.3b). In the MO suboxic incubation, the onset of sulfate reduction may have been slightly delayed (Figure 3.4c), but after approximately 5 days of incubation, sulfate depletion began and a stoichiometric increase in AVS was observed as sulfate went to zero by 40 days. In the suboxic HO and MO incubations, dissolved ferrous iron and sulfide remained low ($<20\text{uM}$) in the oxidized MO incubation (Figure 3.4d-e). Since sulfate reduction began very quickly and dissolved sulfide remained low in the suboxic HO and MO incubations, the mercury-related biogeochemistry in them was similar to the expectations for the mildly reduced conditions outlined in Table 3.3 (zone of efficient methylation: active sulfate reduction, low dissolved sulfide).

For the LO environment (Figure 3.2), sulfate reduction rates in the suboxic incubation remained low throughout the experiment. Sulfate reduction rates in mildly reduced and fully reduced LO incubations were lower than in MO and HO environments ($20\text{-}30\text{uM/day}$, Figure 3.5b-c) assumedly due to lower organic substrate. The buildup of sulfide in the pore water of the LO fully reduced incubation occurred more slowly and was much less dramatic than in the HO and MO systems (Figure 3.2h). Sulfide

concentrations also increased in the mildly reduced LO incubation (Figure 3.2e) after ~20 days, as the added ferrous iron (0.5mM) was apparently not sufficient to hold down sulfide concentrations.

Consistent with the theory that high sulfide inhibits methyl mercury production, methyl mercury concentrations remained lower in the fully-reduced conditions for all environments (especially those with high sulfide), despite higher dissolved mercury (Figures 3.2-3.4, panel i) and similar sulfate reduction rates. This suggests that not all dissolved mercury is available for methylation under these conditions and that high sulfide concentration altered the available mercury pool.

The highest methyl mercury production, was observed in the suboxic HO incubation (Figure 3.3c), where concentration increased from 5.7 to 31 ng/g (0.5% to 3% of total mercury) between 5 and 13 days. This high concentration was maintained until the end of the experiments. A parallel increase was observed for the suboxic incubation in the MO environment (Figure 3.4c), though the increase and final concentration was not as dramatic (6ng/g to 10ng/g). Although lower rates of sulfate reduction were observed in the LO mildly reduced and fully reduced incubations (Figure 3.5a), methyl mercury concentrations were similar to or higher than in MO and HO environments (Figure 3.2 f, i). A slight decrease in methyl mercury over time was seen in LO mildly reduced and fully reduced incubations as sulfide concentrations increased (Figure 3.2f and i). Dissolved mercury was consistently higher in the incubations that had elevated sulfide levels, (fully reduced MO and HO, Figure 3.3h-i, 3.4h-i), and an increase in dissolved mercury was also observed in the LO fully reduced condition as sulfide concentrations increased (Figure 3.2, h-i).

LO Observations

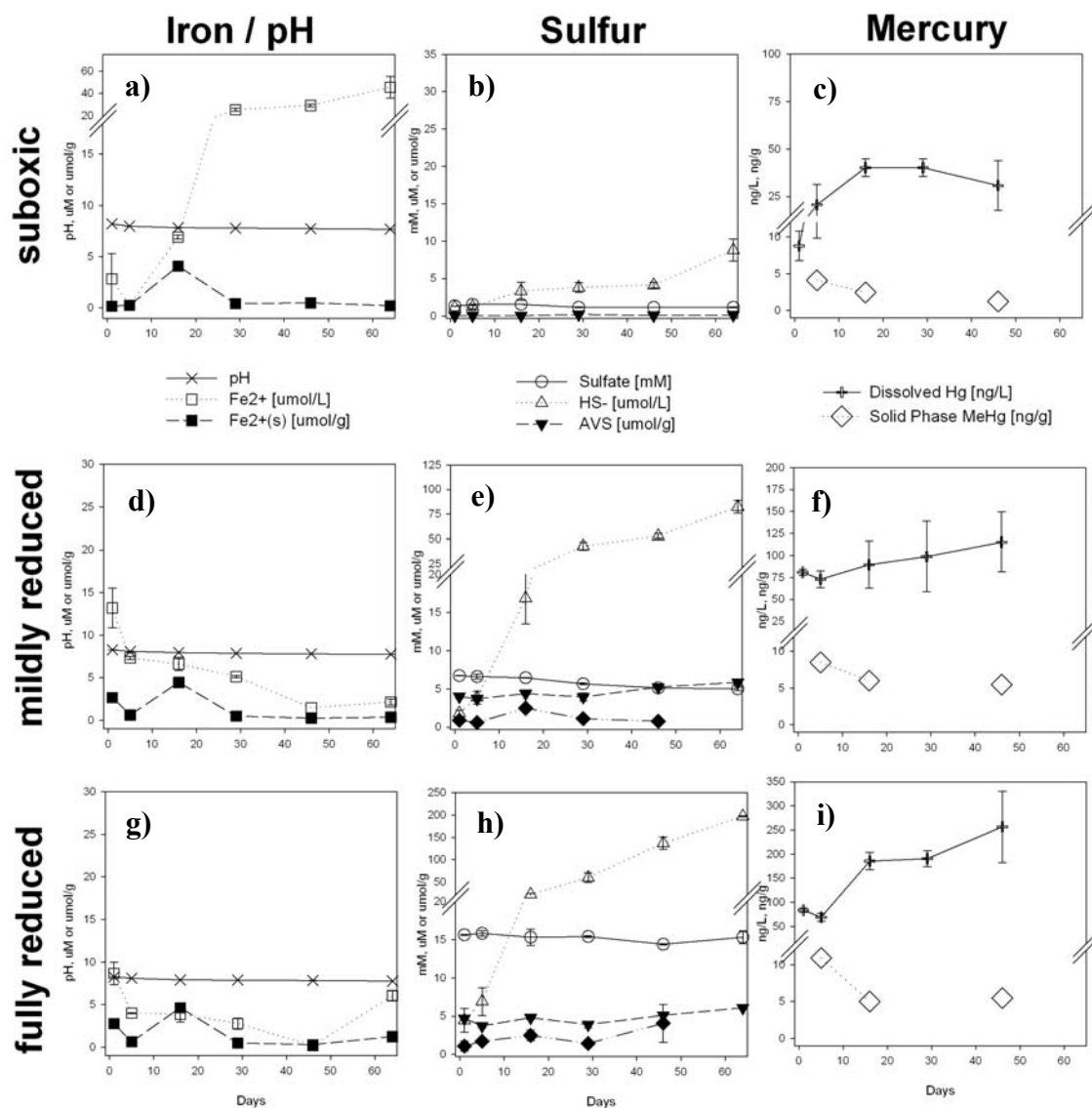


Figure 3.2 Mercury-related geochemistry and methyl mercury observations in low organic (LO) environment incubations. (a-c) suboxic conditions; (d-f) mildly reduced conditions; (g-i) fully reduced conditions.

HO Observations

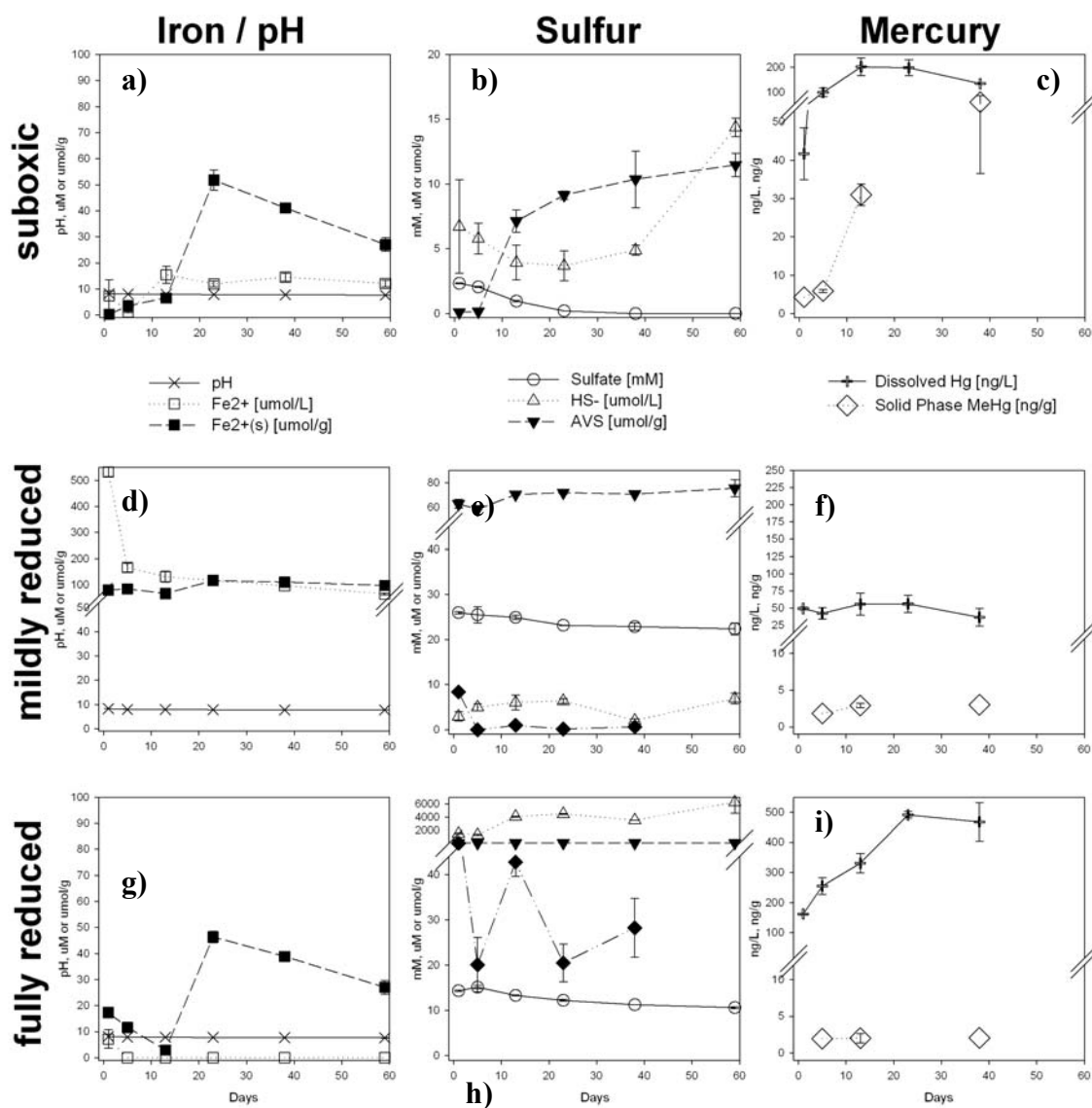


Figure 3.3 Mercury-related geochemistry and methyl mercury observations in high organic (HO) environment incubations. (a-c) suboxic conditions; (d-f) mildly reduced conditions; (g-i) fully reduced conditions.

MO Observations

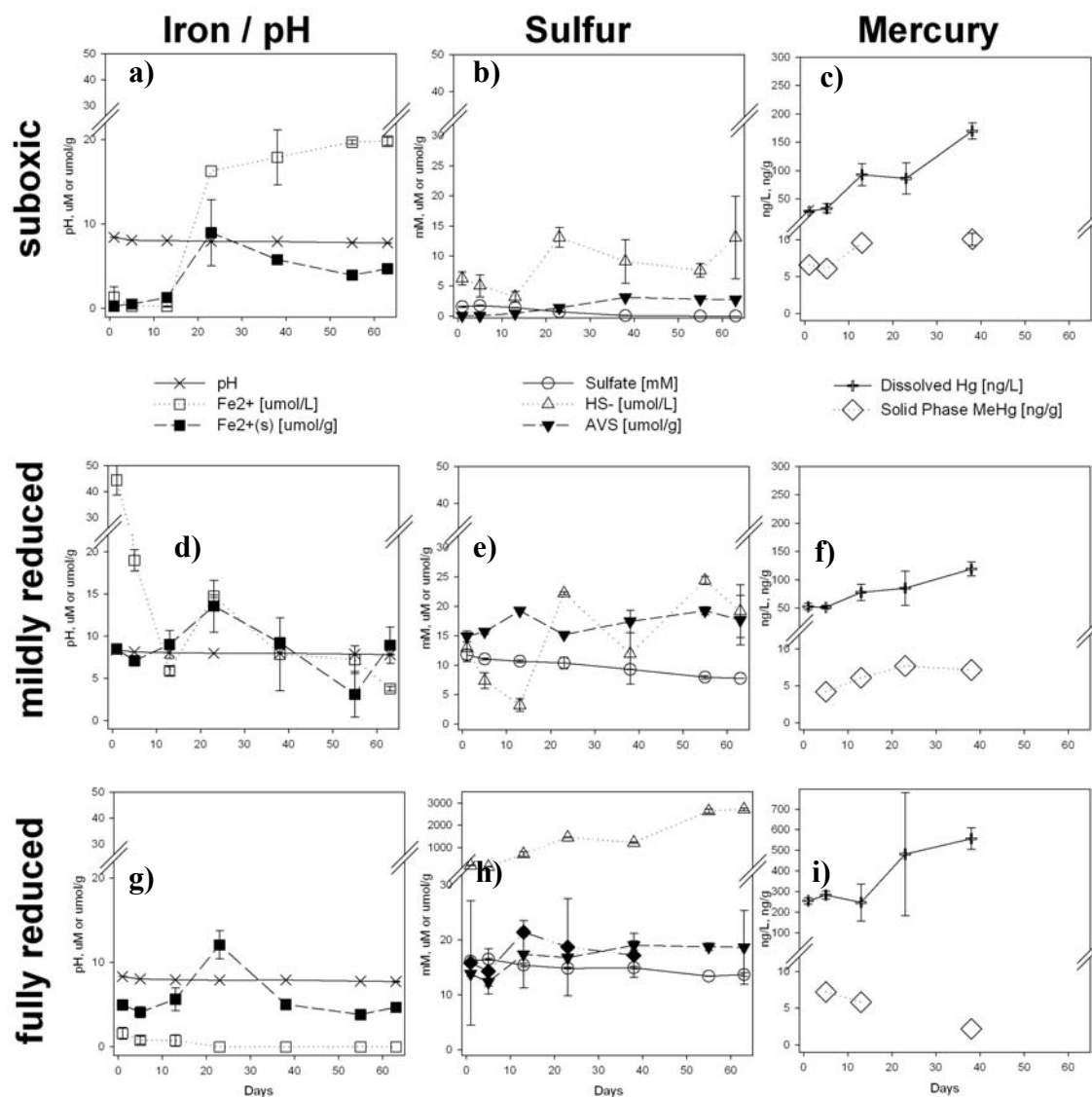


Figure 3.4 Mercury-related geochemistry and methyl mercury observations in middle organic (MO) environment incubations. (a-c) suboxic conditions; (d-f) mildly reduced conditions; (g-i) fully reduced conditions.

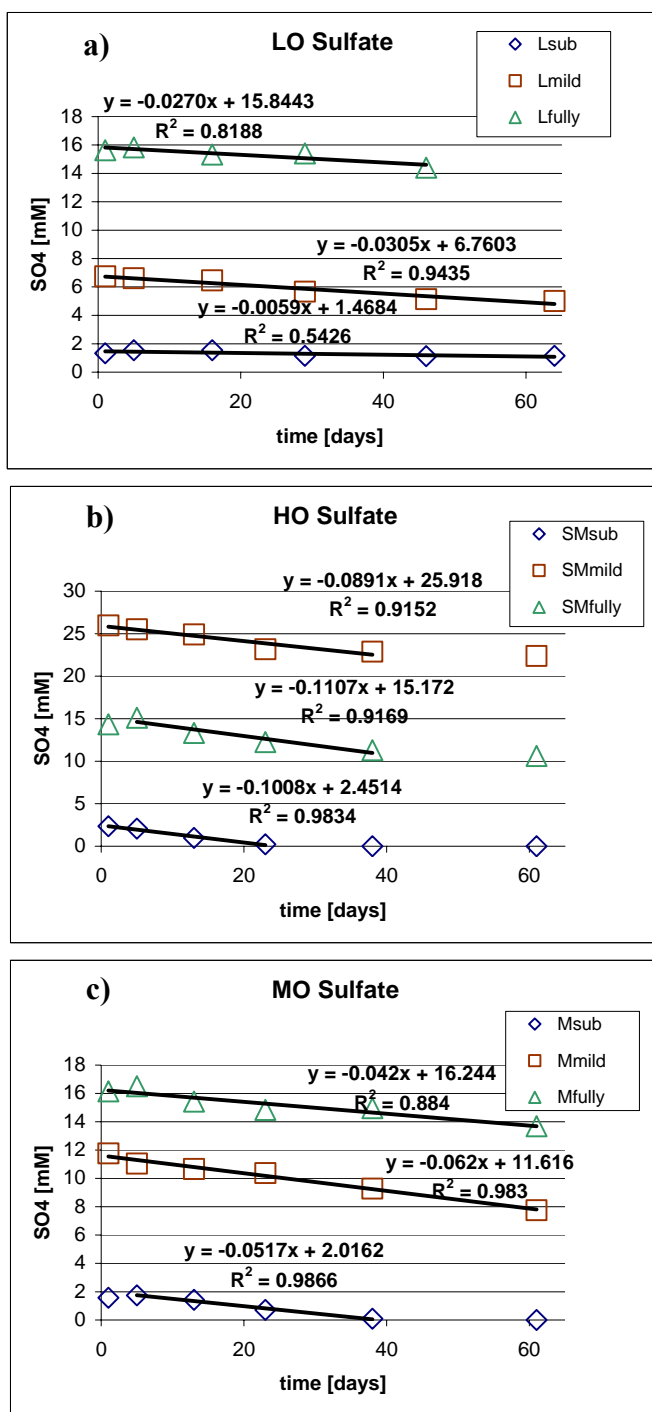


Figure 3.5 Sulfate observations in 9 different incubations with linear regressions to calculate sulfate reduction rate. (a) LO environment, (b) HO environment, (c) MO environment

In order to quantify the simultaneous effects of sulfate reduction, aqueous availability, and solid-phase partitioning according to Equation 3.2, the average of data collected in the incubations between 10 and 50 days (Figures 3.2-3.4) was used to calculate the parameters for the steady state methyl mercury model. Beginning with the mechanistic basis outlined in Equations 3.1-3.3, the model uses the variability biogeochemical processes amongst the nine incubation environments to describe the variability in methyl mercury. Table 3.6 outlines the measurements made during the incubations related to estimating the parameters in Equation 3.3. Averages and standard deviations (range for duplicates) are reported.

Table 3.6 Summary of geochemical and methyl mercury measurements used to calculate parameters for steady state methyl mercury model. Speciation models B and B' are as described in Section 3.3

	SRR [uM/day]	Hg-diss [ng/L]	Sulfide [uM]	Available Fraction		% MeHg	Spike Hg-diss [ng/L]	Spike % MeHg
				B	B'			
LO-suboxic	6±3 ^a	37±5.4 ^b	3.8±0.40 ^b	0.029	0.710 ^c	0.18±0.09 ^b	2200	0.005
LO-mildly reduced	30±4	100±13	38±19	0.012	0.187	0.57±0.04	450	0.05
LO-fully reduced	27±7	210±40	73±58	0.011	0.118	0.52±0.03	850	0.03
MO-suboxic	52±4	120±47	8.5±5.0	0.022	0.596	0.99±0.04	1300	0.10
MO-mildly reduced	62±4	94±22	13±9.5	0.017	0.461	0.70±0.08	320	0.06
MO-fully reduced	42±8	430±160	1130±380	0.011	0.028	0.40±0.26	1800	0.01
HO-suboxic	101±9	180±37	4.2±0.6	0.026	0.689	4.0±1.3	800	0.25
HO-mildly reduced	89±16	50±11	4.8±2.4	0.026	0.689	0.30±0.01	800	0.10
HO-fully reduced	111±24	430±87	4000±470	0.010	0.024	0.2±0.0	3000	0.02

^aaverage ± standard error of regression slope for observed sulfate; ^baverage ± standard deviation of data between 10 and 50 days;

^ccalculated fraction from mean values

The first input to the model, sulfate reduction rate (Table 3.6, Figure 3.4), was used directly in Equation 3.3. The second input, K_D , was calculated from the dissolved

mercury concentration (0.45 μ m filtered) and the spiked total mercury concentration in the sediment 0.93 (\pm 0.05, n=6). The final input was calculated using two different stability constants for HgS⁰ (logK=24.5 for Model B and logK=26.5 for Model B'). The calculated values for both speciation models are reported in Table 3.6.

In the incubations with high sulfide conditions (HO and MO, fully reduced), 20-30 times lower available mercury was predicted using Model B' and this is consistent with low % methyl mercury in these conditions. This was different than results from Model B, where high sulfide environments had only 2-3 times lower available mercury. For Model B', the higher stability constant for HgS⁰ allowed it to out-compete organic ligands at low sulfide and resulted in higher predictions for uncharged, available mercury at low sulfide.

The data from Table 3.6 is plotted in Figure 3.6 according to Equation 3.3 using the available fraction calculated with Model B'. Different shapes represent the different environments (HO, MO, LO) and the mildly reduced HO incubation is noted specifically. A trend of increased % methyl mercury is seen with an increase in the geochemical factors known to increase methylation as described in Equation 3.3. This trend is true for the incubations collectively, but also consistent within each environment (LO, MO, HO). In addition to quantifying the cumulative effects of biogeochemical processes controlling methyl mercury, the plot in Figure 3.6 and underlying model in Equation 3.3 provides a useful way of qualitatively interpreting the effects of different biogeochemical processes.

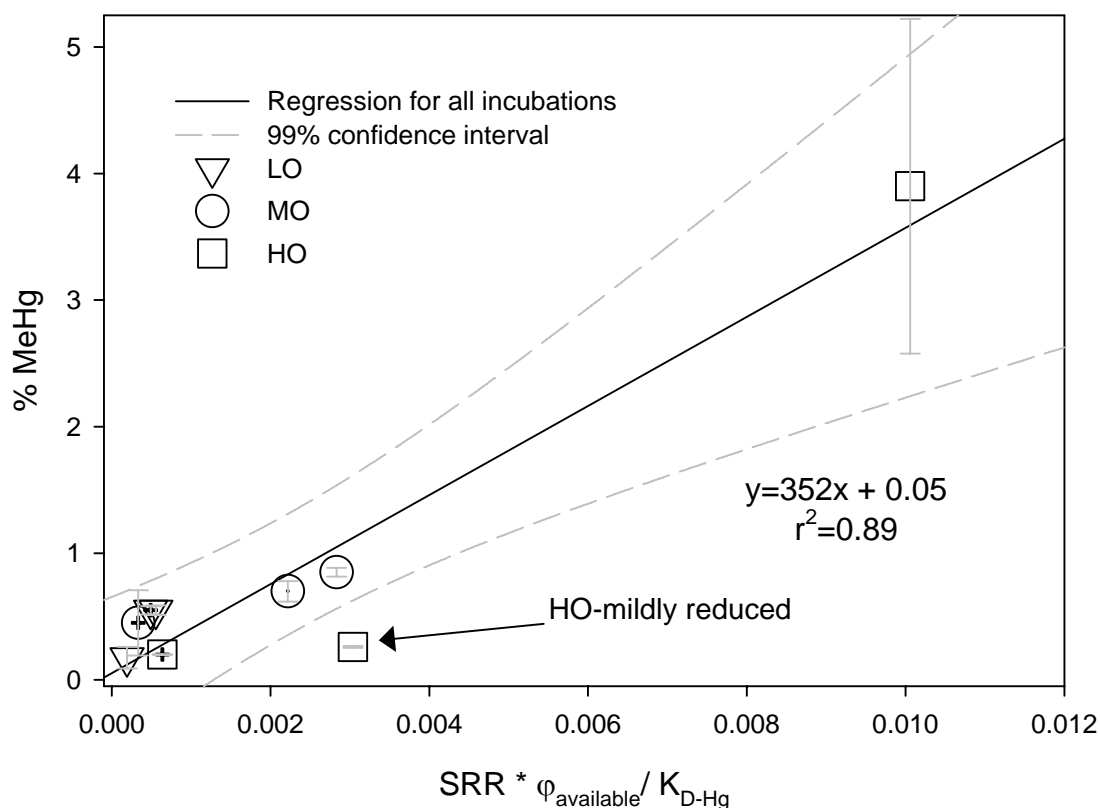


Figure 3.6 Model for % methyl mercury considering sulfate reduction rate, available aqueous fraction (Model B'), and partitioning to the solid phase, K_D .

Within the LO environment, the very low % methyl mercury in the oxic incubation can be attributed to low SRR and low dissolved mercury. Higher methyl mercury concentrations in mildly reduced and fully reduced incubations are due to increased SRR and dissolved mercury despite a smaller available fraction (Table 3.6). For MO incubations, similar SRR was observed in all incubations; however, % methyl mercury in the suboxic and mildly reduced incubations were higher than the fully reduced incubation despite lower dissolved mercury concentrations. The methyl mercury

model in Equation 3.3 attributes this difference to much lower available fraction of inorganic mercury due to high sulfide in the anaerobic incubation. Methyl mercury model results for the HO incubations are similar to the MO environment, however, the mildly reduced incubation showed much lower methyl mercury than expected. This could be attributed to either the inhibition of active sulfate reduction by the large spike of ferrous iron (although decreases in sulfate suggest active SR, Figure 3.5b), or possibly co-precipitation of mercury into FeS which changed the amount or nature of mercury available for methylation (Miller 2006). A very large amount of iron (15mM) was added to this incubation in order to reduce sulfide concentrations. Since solid-phases available for mercury-sorption were undoubtedly altered by this addition, the following calculations are performed with and without this outlier point.

The steady state model for methyl mercury (Equation 3.3) was also tested using the fraction of available mercury calculated with Model B (Table 3.6) and the results are presented in Appendix A with regression parameters. Because the predictions for available fraction were all very low, the application of the methyl mercury model with availability using Model B described very little of the variability ($R^2 = 0.22$) in % methyl mercury as opposed to >90% for model B' (89% with outlier). Since Model B' was more consistent with observations than Model B, this suggests that the underlying assumption of the model is valid and that HgS^0 does contribute to the fraction of available mercury in the biogeochemical conditions investigated here.

The range of the slope of the regression line in Figure 3.6 (+/- standard error of slope) considering all incubations is 305 – 397 (335 - 388 without outlier), and this slope represents the ratio of $k_{\text{meth-SRR}} / k_d'$. Although the parameter $k_{\text{meth-SRR}}$ is empirical, it does have some physical meaning and can be thought of as the fraction of the available mercury pool that is methylated per $\mu\text{mol/L}$ of sulfate reduced. The value of the intercept of the regression line represents the background methyl mercury expected in the absence of active sulfate reduction. Figure 3.6 shows that this value was close to zero, which suggests that the factors which were lumped into MeHg_0 do not have a great effect on methyl mercury. Additionally, the wide range of the 99% confidence interval shown in Figure 3.6 shows that little confidence can be placed on the exact value for this parameter and regressions were performed by forcing the intercept through zero. The larger slope within the LO environment alone (Figure 3.6 – triangles; slope = 900-1300) suggests that either more mercury was methylated per mole of sulfate reduced, that demethylation occurred less efficiently, or that other processes, such as inorganic mercury availability or methylation-demethylation equilibrium were different in this environment.

Two alternative regression methods were tested to reduce the influence of the large methyl mercury concentration observed in the HO suboxic incubation. The results of this analysis are presented in Appendix A. First, the value of MeHg_0 in Equation 3.3 was assumed to be zero and a log-log transformation was performed on the data. This resulted in a range of slopes between 360 and 760 (380 – 810 considering outlier) based on the standard error of the best-fit slope in linear-space. A second method using a weighted least squares analysis (see Appendix A) resulted in a similar best fit slope of 590 (520 considering outlier). The slopes of these regression analyses, which attempted to neutralize the effect of the one large point in Figure 3.6, gave ranges of slopes ~1-2 times that calculated with a simple linear regression. This suggests that although the

simple linear regression may be biased to some degree, the extra weight of the one large point does not invalidate the analysis.

The additional spike of inorganic mercury added at the close of the experiments resulted in a similar trend (Appendix A, Figure A.2) to that presented in Figure 3.6. The % methyl mercury measured 48 hours after the spike was lower than that observed pre-spike. Although the slope of the line and estimate for k_{m-SRR}/k_d' was smaller for the spiked conditions, the similar trend demonstrates that for both ambient and spiked mercury, the biogeochemical processes described by Equation 3.3 can be used to provide a quantitative estimate for methyl mercury production.

In this study, only total dissolved mercury was quantified in the aqueous phase, and one limitation of the parameters used for this modeling is that K_{D-Hg} was estimated from this total mercury which included both inorganic and methyl mercury. Due to its lower affinity for solids, methyl mercury can comprise up to 50% of total mercury in the dissolved phase (Fitzgerald et al. 2007). The estimate for K_{D-Hg} made from our total dissolved mercury measurements are likely to be biased low, especially for samples with high % methyl mercury and likely greater dissolved methyl mercury. Even with this limitation, the model successfully explains a large portion of the variability in % methyl mercury data (>90% excluding HO-mildly reduced, 76% with outlier). Additionally, the model provides a convenient and useful framework for qualitatively and quantitatively comparing the effects of different biogeochemical processes and parameters that affect methylation.

3.6 CONCLUSIONS AND IMPLICATIONS

The observations and conceptual model outlined here supports the theory that methylation occurs efficiently in a narrow redox zone defined by the transition to sulfate reduction and suggests that methylation will likely increase in (formerly) surficial sediment underlying an in-situ cap, especially for high-organic environments. Sediment at deeper depths may not experience an increase in methyl mercury since the factor limiting production; (available aqueous mercury) is not likely to change because of capping. It was also demonstrated that a model that incorporates parameters for biological methylation (SRR), aqueous speciation (fraction available), and solid phase partitioning (K_D) can be used to describe methylation and quantify the effects of individual processes and parameters in controlling methylation. Although model parameters may vary amongst environments (Figure 3.6), the results presented here show that a significant amount of variability in methyl mercury can be explained with a mechanistically-based simple, steady state model combining the effects of processes known to affect methylation. The application of this model to in-situ conditions could provide valuable information about the mercury-related effects of engineered capping as well as other engineered management solutions that change redox conditions of sediment.

Chapter 4: Modeling Mercury-Related Geochemistry in Salt Marsh Sediment

4.1 INTRODUCTION

Salt marshes are complex biogeochemical environments that accumulate heavy metals and hydrophobic organic contaminants (Huang et al. 2006, Scrimshaw and Lester 2001) due to the strong association of these contaminants with organic matter. Salt marshes have been found to be efficient areas for the production of methyl mercury (Canario et al. 2007, Kongchum et al. 2006), the form of mercury that readily accumulates in the tissue of aquatic organisms and has led to fish tissue consumption advisories in thousands of waterbodies in the US (EPA 1998). The reason for elevated levels of methyl mercury in highly organic salt marsh environments is due to the activity of sulfate reducing bacteria, which are known to efficiently methylate mercury (Compeau and Bartha 1984, Harmon, et al. 2004). The presence of high levels of sulfate and fresh, labile organic matter to drive bacterial processes in salt marsh sediments leads to high rates of sulfate reduction and steep gradients in sulfate and sulfide in surficial sediment. This vigorous sulfate reduction may lead to conducive geochemical conditions for the production of methyl mercury. However, the relationship amongst sulfate, organic carbon, and methyl mercury production is complex.

While sulfate and energy rich organic matter drive the biological processes that produce methyl mercury (Lambertsson et al. 2006), sulfide, the reduced byproduct of sulfate reduction, has been shown to inhibit methylation at high concentrations (Benoit et al. 2001b) and organic content has been found to correlate with the strength of partitioning to the solid phase (Hammerschmidt et al. 08). Methylation rates in un-vegetated salt marsh sediment appear to be highest in the surficial sediment (0-5cm)

(Langer et al. 2001, Kongchum et al. 2006) where sulfate reduction is active but sulfide concentrations are not high enough to inhibit methylation. Salt marshes represent a potential source of methyl mercury to biota within them and to connected water bodies. In addition, the biogeochemical conditions in surficial sediment contain steep gradients in processes and parameters known to control mercury methylation. Thus, a salt marsh provides an ideal environment in which to investigate the relationships amongst these processes and parameters and to explore mercury management strategies such as capping.

The objectives of this chapter are (1) to test the applicability of the steady state methyl mercury model developed in Chapter 3 to in-situ conditions in a salt marsh and (2) to identify in-situ processes and parameters that need to be more fully/accurately characterized in order to describe methyl mercury in salt marsh sediment.

4.2 MATERIALS, METHODS, AND MODELING

4.2.1 Sediment Collection and Analysis

Sediment from an un-impacted salt marsh in the ship channel of Corpus Christi Bay near Port Aransas (27°50', -97°05') was collected in August 2008. Three inch diameter, 30cm length cores were collected and transported to the lab for analysis. Overlying water in the cores was refreshed with water collected at the salt marsh and allowed to equilibrate for several hours prior to profiling. Replicate depth profiles for pH (MicroelectrodesInc) and dissolved sulfide (Diamond General) were made in cores using potentiometric microelectrodes with an external reference. Cores were then extruded, sectioned into borosilicate glass sample jars, sealed, and immediately transferred to an N₂ atmosphere for subsequent processing. Profile sections were collected at 0.5 to 1cm intervals for the top 10cm and 2 to 5cm intervals for the bottom 20cm.

Each sediment section was homogenized using a PTFE lined spatula and two aliquots (~5g each) were placed into PTFE lined borosilicate glass vials and immediately frozen for subsequent total and methyl mercury analysis. Procedures for measuring acid volatile sulfides (AVS), loss on ignition (LOI), sulfate, chloride, solid phase total and methyl mercury were described in Chapter 3.

4.2.1 Diagenetic Modeling

A 1-dimensional, unsteady, reactive transport model was used to simulate diagenetic processes in the surficial salt marsh sediments. Rates of sulfate reduction and dissolved sulfide are simulated by the diagenetic model and both of these are known to influence mercury methylation (Compeau and Bartha 1995, Warner et al. 2003, Kerin et al. 2006). Processes included in the diagenetic model are based on those presented in Jaffe et al. and are described in detail in Chapter 5. Parameters, initial conditions, and boundary conditions for the salt marsh simulation are presented in Appendix B.

4.2.2 Speciation Calculations

To help understand the factors controlling mercury methylation in aquatic sediments, speciation models are used to describe the interaction of dissolved mercury with sulfide and organic ligands (Benoit et al. 1999, Hammerschmidt et al. 2004). It is assumed that the uncharged complexes HgS^0 and $\text{Hg}(\text{SH})_2^0$ represent the fraction of dissolved mercury available for methylation (Benoit et al. 1999) since the uptake mechanism is assumed to be passive diffusion across the lipid cell membrane (Mason et al. 1996). Equilibrium calculations were performed using stability constants for mercury sulfide and organic complexes based on those presented in Drott and Skjellberg 2007, parallel to that presented in Chapter 3. The speciation model includes complexation with dissolved organic ligands (Drott and Skjellberg 2007), but does not consider the formation

of solid cinnabar as its formation has been found to be inhibited by dissolved organics in highly organic environments, such as the one studied in this research (Ravichandran et al. 1999). The constants used for calculating the speciation of dissolved mercury are presented in Table 4.1.

Table 4.1 Mercury sulfide and organic complexes and stability constants used for equilibrium speciation modeling.

Reaction	Complex stoichiometry	Log K	Source
1	$\text{Hg}^{2+} + 2\text{HS}^- = \text{Hg}(\text{SH})_2^0$	37.5	Benoit et al. 1999
2	$\text{Hg}^{2+} + 2\text{HS}^- = \text{HgS}_2\text{H}^- + \text{H}^+$	31.3	Benoit et al. 1999
3	$\text{Hg}^{2+} + 2\text{HS}^- = \text{HgS}_2^{2-} + 2\text{H}^+$	23.0	Benoit et al. 1999
4 ^b	$\text{Hg}^{2+} + \text{HS}^- = \text{HgSH}^+$	20.0	Drott et al. 2007
5 ^a	$\text{Hg}^{2+} + \text{HS}^- = \text{HgS}^0 + \text{H}^+$	24.5-26.5	Drott et al. 2007, Benoit et al. 1999
6	$\text{Hg}^{2+} + 2\text{RSH}^- = \text{Hg}(\text{RS})_2 + 2\text{H}^+$	22.1	Skyllberg et al. 2001

^aModel B – $\log K_5 = 24.5$, for model B' – $\log K_5 = 26.5$. ^bthe complex from Reaction 4 was not significant (<1%) under all conditions simulated with a log stability constant of either 20 or 30

A low (speciation Model B) and high (speciation Model B') stability constant for the formation of the uncharged, monomercury sulfide complex HgS^0 were applied to test the importance of this species in controlling the availability of mercury. Figure 4.1 illustrates the effects of the two stability constants for HgS^0 over a range of sulfide and organic ligand concentrations at pH 8.0. In Figure 4.1b, lines are also plotted to show the effect of a change in pH (to pH 6), and a change in the log stability constant for the organic complex $\text{Hg}(\text{SR})_2$ to 24.1. Analogous shifts in speciation for changes in pH and $\log K_{\text{Hg}(\text{SR})_2}$ would be observed in Model B. Vertical dashed lines show the approximate concentrations of the RSH ligands in the salt marsh environment.

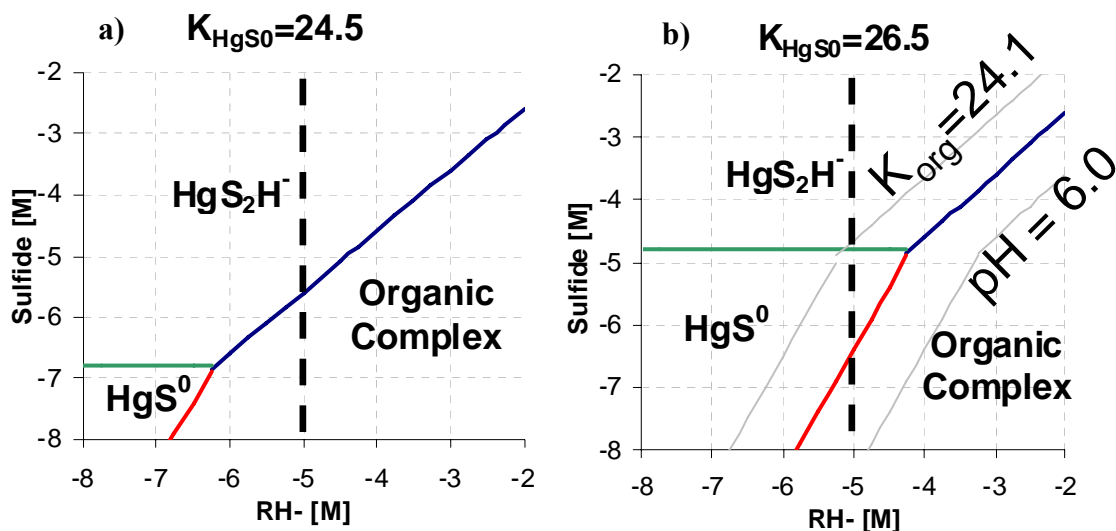


Figure 4.1 Phase diagram showing regions of predominance for two-sulfide mercury complex (upper left), single sulfide mercury complex (lower left), and organic complex (lower right) for pH 8 using (a) low formation constant for HgS^0 – Model B; and (b) high formation constant for HgS^0 – Model B'. Vertical dashed line represents organic complex concentration in the salt marsh sediment. Additional lines in (b) represent the effects of changing pH (shift right), and the stability constant for the organic complex (shift left).

For both systems, three mercury species dominate within the envelope of environmentally relevant sulfide and organic ligand concentrations. In both cases, at low organic ligand concentration the dominant species is either the neutral species HgS^0 or the negatively charged species HgS_2H^- . The particular sulfide concentration at which speciation shifts from HgS^0 (Reaction 5) to HgS_2H^- (Reaction 2) is defined by the difference between the stability constants ($\log K_2 - \log K_5$) and this concentration was $10^{-6.8}$ for Model B and $10^{-4.8}$ for Model B'. Not shown in Figure 4.1 is the effect of another uncharged mercury-sulfide complex, $\text{Hg}(\text{SH})_2^0$. At sulfide concentrations above the transition from HgS^0 to HgS_2H^- ($10^{-6.8}\text{M}$ for Model B), approximately 1% of dissolved

mercury is predicted to be present as the two-sulfide neutral complex $\text{Hg}(\text{SH})_2^0$ at pH 8. This fraction, however, is sensitive to changes in pH, and at pH 7, more than 2% of dissolved mercury is present as $\text{Hg}(\text{HS})_2^0$ at 0.5mM sulfide and at 10mM sulfide, this jumps to > 12%. At sulfide concentrations greater than 10^{-6}M , Model B predicts that $\text{Hg}(\text{SH})_2^0$ is the only relevant uncharged mercury complex in anoxic waters. Since sulfide concentrations were never below 10^{-6}M in the salt marsh, the main difference between predictions for uncharged mercury sulfide using Models B and B' is the following: for Model B', the uncharged fraction is dominated by HgS^0 at low sulfide and $\text{Hg}(\text{HS})_2^0$ at high sulfide, while for Model B, the only relevant uncharged species is $\text{Hg}(\text{HS})_2^0$. Throughout the following text, the term “available fraction” will be used to refer to the fraction of dissolved mercury (passing $0.45\mu\text{M}$ filter) calculated to be present as HgS^0 and $\text{Hg}(\text{HS})_2^0$ using speciation models B and B'.

4.2.3 Modeling Methyl Mercury Production

In Chapter 3, using sediment from the salt marsh presented above, a steady state methyl mercury model was used to describe methyl mercury concentrations as a function of geochemical processes and parameters. This model is applied here to test its ability to describe in-situ % methyl mercury observations. The equation for the steady state model is outlined in Equation 4.1, and the nomenclature used was presented in Chapter 3 (Equation 3.3).

. The parameters in the methyl mercury model, ($k_{\text{meth-SRR}} / k_d$ ’, and %MeHg₀) were developed in Chapter 3 by measuring the physical quantities sulfate reduction rate, fraction available dissolved mercury, and K_D in laboratory incubations spanning a range of geochemical conditions.

$$\%MeHg = \frac{k_{meth-SRR}}{k_d'} SRR \frac{\phi_{Hg}}{K_D} + \%MeHg_0 \quad \text{Equation 4.1}$$

In Chapter 3, the two stability constants presented above for the single sulfide complex, HgS^0 were used to calculate the fraction of available mercury for Equation 4.1. It was found that the constant which gives the most influence to HgS^0 ($\log K=26.5$) provided the best explanation for observed methyl mercury production. The slope of Equation 4.1 fit to data in Chapter 3 using high and low stability constants for HgS^0 is presented in Table 4.2.

Table 4.2 Linear regression parameters for steady state methyl mercury model developed in Chapter 3 for two different values of the HgS^0 stability constant.

	Slope	Std Error of slope	Intercept	R ²
Model parameters calculated with high K_{HgS^0} constant (26.5)	362	26.9	0.14	0.97
Model parameters calculated with low K_{HgS^0} (24.5)	2775	2190	0.33	0.2

In order to test the applicability of this steady state methyl mercury model to in-situ observations at the salt marsh site, the required inputs are (1) sulfate reduction rate (SRR), (2) fraction available mercury (uncharged complexes based on aqueous speciation), and (3) K_D , or solid phase partitioning. Figure 4.2 illustrates the process that was used to estimate steady state in-situ % methyl mercury using physical measurements, speciation calculations, and regression parameters developed in Chapter 3.

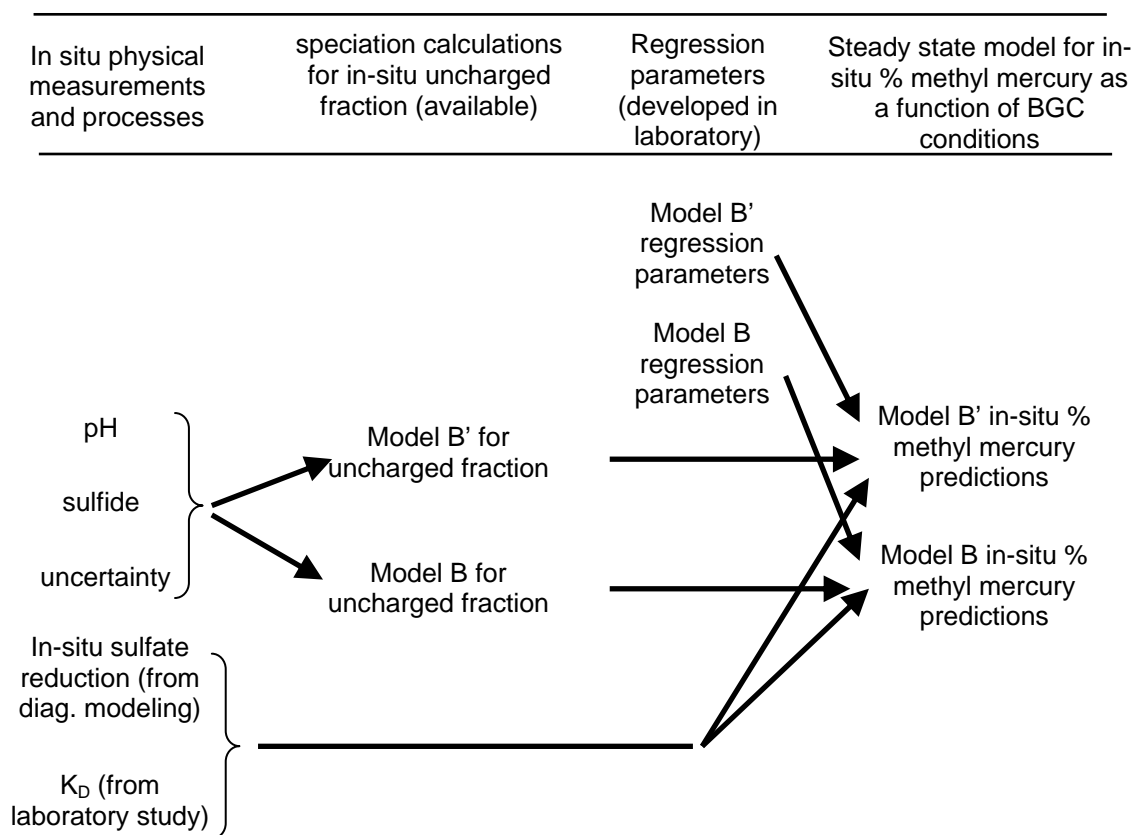


Figure 4.2 Workflow for combining physical measurements, speciation calculations, and parameters from laboratory conditions to predict in-situ % methyl mercury.

The sulfate reduction rate as a function of depth was estimated with diagenetic modeling (results below). The available fraction was calculated as a function of the observed sulfide concentration and pH (Figure 4.3a-b) using speciation Models B and B'. The partitioning of mercury to the solid phase was not explicitly measured in-situ, however $\log K_D$ of $10^{3.4} - 10^{3.6}$ was consistently measured in incubations with high sulfide (Chapter 3) in sediment from the same environment. In the absence of other information, a constant value of $10^{3.5}$ was assumed for K_{D-Hg} at all depths.

4.3 RESULTS AND DISCUSSION

4.3.1 Geochemical and Methyl Mercury Observations in Salt Marsh

Geochemical profiles made in one salt marsh core are shown in Figure 4.3 and a similar geochemical structure was observed in replicate cores taken within a ~10m radius (Appendix B, Figure B1). Observations of dissolved oxygen (not shown), pH, HS⁻, and SO₄²⁻ in the surface 5-7cm were consistent with those observed in other salt marsh environments (Langer and Fitzgerald 2001, Lord and Church 1983). A rapid depletion in sulfate was observed over the top 5cm of the sediment, and a concomitant increase in dissolved sulfide (sum of HS⁻ + H₂S) to nearly 6mM was observed (Figure 4.3a-b). pH decreased consistently from greater than 8.5 above the sediment water interface to <7.5 at 7cm depth (Figure 4.3a). Acid volatile sulfides also decreased nearly linearly between 0 and 10cm (Appendix B).

A maximum of nearly 2% methyl mercury (as a fraction of total mercury) was observed in surficial (0-0.5cm) sediment (Figure 4.3b), which is consistent with surface maximums observed in other high organic, saline environments (Langer and Fitzgerald 2001, Komchung et al. 2006, Gagnon, et al. 1996). A decrease in methyl mercury to less than 0.2% at ~3-5cm is coincident with a peak in sulfide concentration and a minimum in sulfate. Although sulfate reduction rate was not directly measured in-situ, this depth of maximum sulfide and minimum sulfate necessitates that sulfate consumption was occurring most rapidly between 3-5cm despite the minimum in solid phase methyl mercury. This rules out the possibility that high sulfide concentrations were inhibiting the activity of sulfate reducing bacteria which has been suggested as a possible reason for low methyl mercury in the presence of high sulfide (Han et al. 2007). Total mercury in

sediment has frequently been correlated with methyl mercury, and a decrease in total mercury with depth was also observed, from 45ng/g in surficial sediment to 20ng/g at 6cm depth. However, solid-phase methyl mercury decreased from 750pg/g in surficial sediment to less than 100pg/g at 6cm, and even after adjusting methyl mercury concentrations for total mercury, the % methyl mercury decreased substantially from a near-surface maximum.

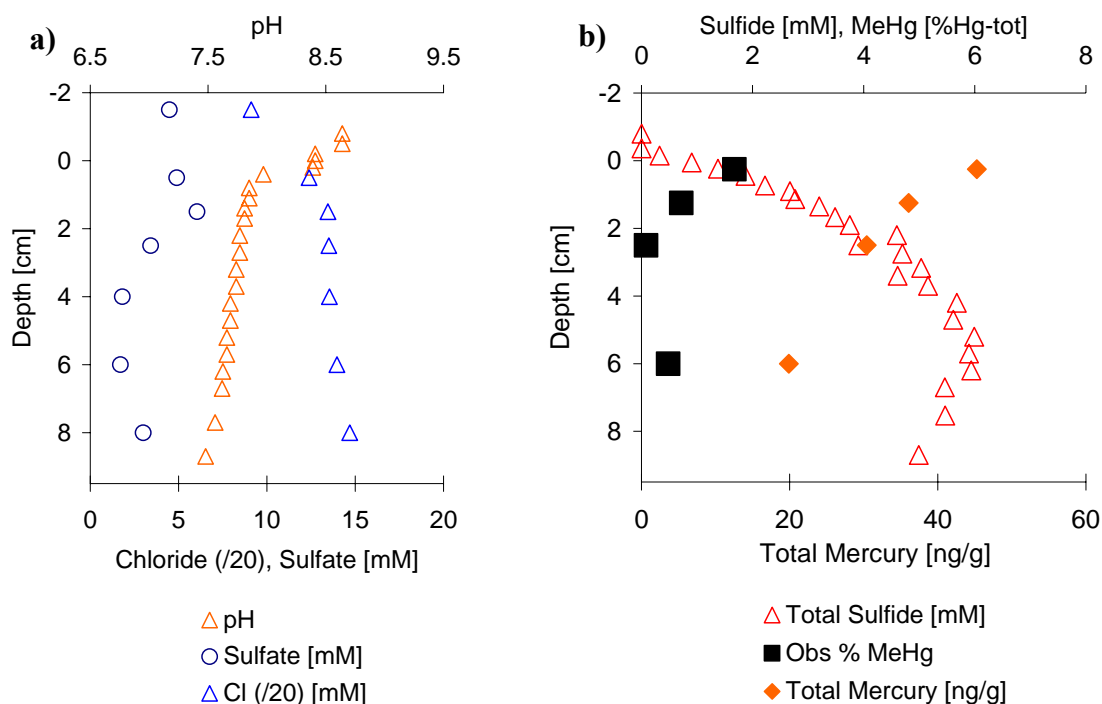


Figure 4.3 Geochemical and methyl mercury observations in surficial sediment of salt marsh. (a) porewater sulfate, pH, and chloride (/20); (b) solid phase % methyl mercury (of total mercury), total mercury, and porewater total sulfide (sum of H₂S and HS⁻). Zero depth represents sediment water interface

Two distinct zones were observed visually during coring and are also evident in geochemical observations (Figure B.2b, Appendix B). At depths below 5-10cm, a

transition from dark organic material to sandy grey material was clearly observed. This was coincident with a rapid decrease in LOI from nearly 20% to less than 10% between 7-12cm (Figure B.2). Over the same depth, percent solids increased from 40% to just over 75%. Sulfate and chloride also increased in this layer suggesting a direct connection between this relatively permeable layer and the tidal waters. Thus, modeling was limited to the top 5-7 cm, the zone assumed to be influenced by deposition of fresh organic matter and diffusion of sulfate from overlying water.

4.3.2 Diagenetic Modeling Results

In order to help understand the effects of the biogeochemical processes controlling the production of methyl mercury in salt marsh sediment, a diagenetic model was applied to observations. The diagenetic model results were used to provide an estimate for the in-situ sulfate reduction rate and the sulfate reduction rate was then used in the methyl mercury model described in chapter 3 and by Equation 4.1. Although the diagenetic model allowed for the oxidation of organic carbon by different electron acceptors, the extremely high sulfide concentrations present less than 1cm below the sediment surface suggest that sulfate reduction was the dominant carbon oxidizing pathway.

The diagenetic model assumed a constant rate of deposition of 0.5cm/year, in the range of those reported for other salt marsh environments (Hung et al. 2006, Lord and Church, 1983). The flux of labile particulate organic carbon to the sediment surface was assumed to be 50% of the total carbon deposited on the surface, or a flux of 0.9 mmol/cm²/year. The upper boundary condition for sulfate was set to 9mM based on fitting to observations of sulfate and sulfide in surficial sediment. The rate for biological

sulfate reduction was fit to the slope of the observed depletion in sulfate over the top 4cm, and set to 0.7mM/day. This rate is in the range of reported observations in other high organic saltwater environments (Lord and Church 1983) but higher than those observed in slurry incubations with sediment from the salt marsh (Chapter 3, lower temperature).

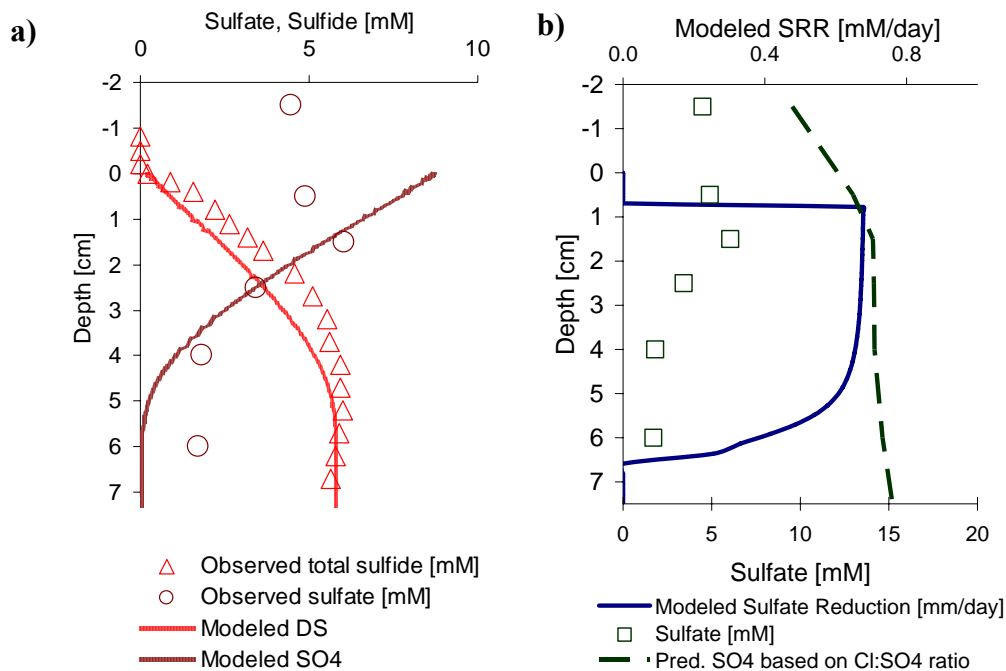


Figure 4.4 Diagenetic modeling results for surficial salt marsh sediment. (a) model fit to sulfate and sulfide concentrations. (b) simulated sulfate reduction rate, observed sulfate concentration, and sulfate concentration that would be present based on observed chloride concentration (seawater Cl:SO₄ ratio = 19.1, molar basis).

The diagenetic model was run for 20 years until steady state conditions developed. The fit to observations of decreased sulfate and increased sulfide in the top ~5 cm is shown in Figure 4.4a. The observed sulfate concentration and the concentration of sulfate that would be expected based on the chloride:sulfate ratio in seawater (in the

absence of diagenetic processes) is plotted along with modeled sulfate reduction rate in Figure 4.4b. The largest departure in observed sulfate from the chloride-predicted sulfate is coincident with the area where the diagenetic model shows sulfate reduction occurring (1-6cm depth), suggesting that the model is accurately capturing the location of sulfate reduction (Lord and Church, 1983). Although the diagenetic model predicts that methanogenesis will begin following a depletion in sulfate, observations at deeper depths (Figure B.2) show that sulfate intrusion from below likely maintains concentrations high enough to sustain sulfate reduction below 7cm in this environment.

4.3.3 Modeling Methyl Mercury Production

With in-situ estimates now for important biogeochemical processes involved in mercury methylation, including sulfate reduction rate (from diagenetic modeling, Figure 4.4b), fraction available dissolved mercury (calculated from in-situ sulfide and pH measurements using constants in Table 4.1), and an assumption of constant K_D , Equation 4.1 can be applied to test its ability to characterize in-situ methyl mercury concentrations. Research showing that methylation and demethylation processes occur more quickly than transport in aquatic sediments (Drott et al. 2007 and 2008) provides the justification for attempting to apply a steady state methyl mercury model developed in laboratory to field conditions.

Figure 4.5a and 4.5b present the range of methyl mercury model results in the top 7cm of sediment using speciation models B' and B, respectively. A detailed discussion of the method for evaluating model sensitivity and incorporating uncertainty into predictions follows in the next section. Methyl mercury model predictions using the in-situ available fraction calculated with speciation model B' and regression parameters developed for speciation model B' (Figure 4.2) are shown in Figure 4.5a. Consistent

with observations, the methyl mercury model did not predict a large increase in methyl mercury between surficial (0.5cm) and deeper (1-6cm) sediment, despite a large increase in sulfate reduction rate (Figure 4.4b). This is due to a very small available fraction calculated with both speciation models (B and B') at high sulfide concentrations. The range of methyl mercury model predictions at 1-6cm was between 0.5 and 1.5% methyl mercury, consistent with observations of less than 1%. In the top 0.5cm of sediment, a steep sulfide gradient leads to large uncertainty in the available fraction (Figure 4.6a) and also results in a wide range of model predictions for % methyl mercury. Observed methyl mercury suggest that mercury species present near the sediment water interface are more available for methylation than those at deeper depths, and this is consistent with the assumptions underlying speciation Model B'. Although a wide range is predicted in surficial sediment in Figure 4.5a, the increase (up to 2.5%), is consistent with observations of increased methyl mercury in surficial sediment. The methyl mercury model predicted range did not capture the very low methyl mercury observation made at 2.5cm. The reasons for this low value are unknown, but could be due to local variability or a transient process not captured by the steady state model.

Methyl mercury model predictions using the in-situ available fraction calculated with speciation model B and associated regression parameters (Figure 4.2) are shown in Figure 4.6b. Predicted ranges of methyl mercury are much larger than observations at depths greater than 1cm. The methyl mercury model predicts a large decrease in % methyl mercury in surficial sediment using speciation model B, which is not consistent with observations. The lower methyl mercury predictions in surficial sediment for speciation model B are due to predicted decreases in $\text{Hg}(\text{HS})_2^0$ with decreasing pH (Figure 4.6b). The fact that speciation model B predictions are inconsistent with observed increases in surficial sediment suggests that speciation calculations which

consider only $\text{Hg}(\text{SH})_2^0$ as the available fraction do not represent true availability of dissolved mercury in the system. .

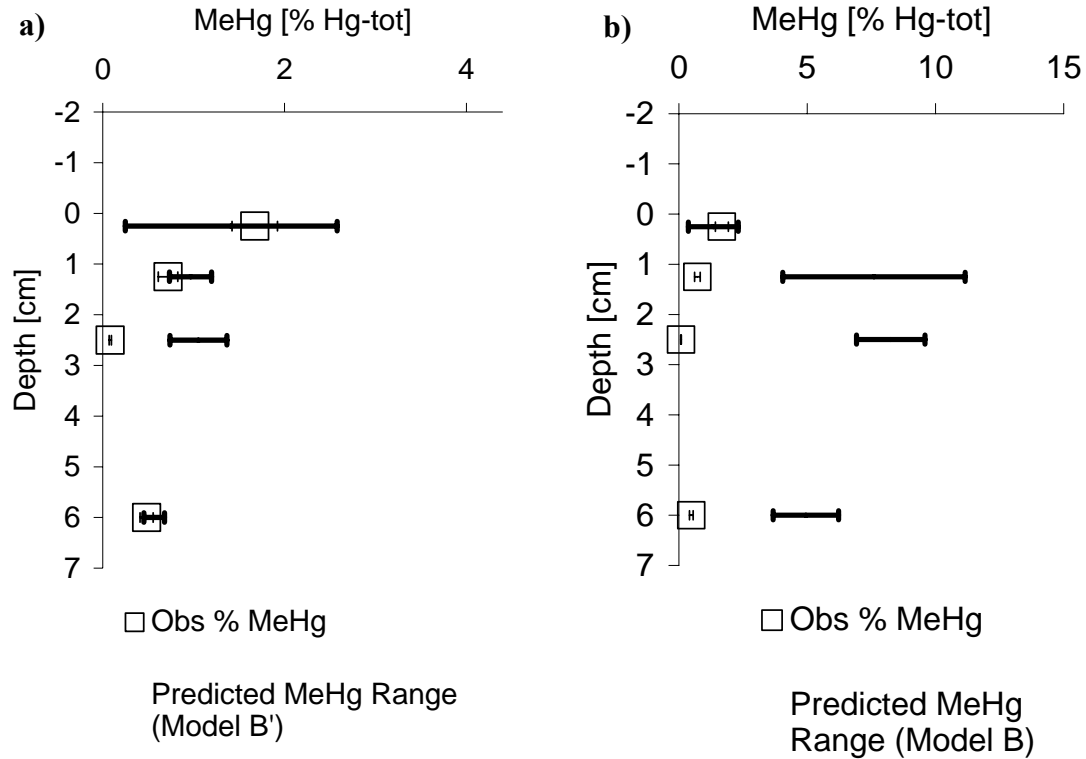


Figure 4.5 Comparison of observations with methyl mercury model predictions using (a) speciation model B' and (b) speciation model B. Range of methyl mercury model predictions represent the effects of uncertainty in both chemical measurements and location of measurement.

4.3.4 Uncertainty and Sensitivity Analysis

The sensitivity of methyl mercury model predictions to uncertainty in measurements or variability in physical quantities was investigated and used to make the range of predictions shown in Figure 4.5. Uncertainty in both the pH and sulfide concentrations (replicate profiles) and the depth of pH, sulfide, and methyl mercury

measurements was incorporated into speciation and methyl mercury modeling to provide a range of predictions. The standard deviation of total sulfide measurements from triplicate profiles in the salt marsh core are shown as horizontal error bars in Figure 4.6a. For pH (Figure 4.3a), the differences between duplicate profiles in 3 different cores were combined to calculate the pooled standard error for pH measurements (Skoog et al. 2007). This value of 0.093 pH units was used as an estimate for uncertainty in pH at all depths.

The effect of variability in pH and sulfide on calculations of the available mercury with speciation models was first investigated. The effect of uncertainty in pH on the available fraction of dissolved mercury is less complicated than that of sulfide. In investigating speciation model sensitivity to pH, it is assumed that the concentration of organic and inorganic ligand remains constant. Although pH will affect the HS^- - H_2S equilibrium, the effects of pH itself on calculations of mercury speciation (as outlined below) will outweigh effects from pH-induced ligand changes. An outline for the justification of this assumption and a more detailed presentation of the following argument is presented in Appendix B.

In all speciation calculations, a decrease in pH led to an increase in fraction available. The reason for this can be stated as follows. For all mercury complexes, the fraction of any individual species (charged or uncharged) can be written as proportional to the stability constant, a ligand raised to the power n , and divided by the hydrogen ion raised to the power m , as shown in Equation 4.2:

$$f_{\text{Hg-species}} \cong \frac{K[\text{ligand}]^n}{[\text{H}^+]^m} \quad \text{Equation 4.2}$$

At low sulfide, when HgS^0 ($m=1$) is competing with $\text{Hg}(\text{SR})_2$ ($m=2$) (Figure 4.1), $m_{\text{uncharged}} < m_{\text{charged}}$. A decrease in pH ($[\text{H}^+] + \Delta[\text{H}^+]$) will decrease the ratio on the right

hand side of Equation 4.2. This decrease will be less for HgS^0 than for Hg(RS)_2 since $m_{\text{uncharged}} < m_{\text{charged}}$. This observation can be generalized and a larger fraction for the uncharged complex at lower pH is always expected if $m_{\text{uncharged}} < m_{\text{charged}}$. At high sulfide concentrations where Hg(HS)_2^0 ($m=0$) is competing for HgS_2H^- ($m=1$) and HgS_2^{2-} ($m=2$) $m_{\text{uncharged}} < m_{\text{charged}}$, and an increase in uncharged mercury result from decreases in pH. In summary, a decrease in pH will have the effect of shifting speciation towards the uncharged species Hg(SH)_2^0 at high sulfide concentrations, and at low sulfide concentrations, a decrease in pH will shift speciation towards the uncharged species HgS^0 (from organic complex).

The effect of uncertainty in sulfide on the available fraction is more complex. In the absence of interactions with organic matter, mercury-sulfide speciation shifts from uncharged HgS^0 to HgS_2H^- at circumneutral pH, causing a decrease in the available fraction with increasing sulfide, at $10^{-4.8}$ and $10^{-6.8}$ for models B' and B, respectively (Figure 4.1). When organic ligands are considered, however, increases in sulfide concentrations below this threshold (i.e. $<10^{-4.8}$ or $10^{-6.8}$), can lead to increases in the available fraction. This can be clearly seen in Figure 4.1b for the salt marsh system. At a reduced thiol concentration of 10^{-5}M (dashed vertical line), increases in sulfide between 10^{-7} and 10^{-6}M clearly leads to a shift into the area of predominance for HgS^0 ; however, above sulfide concentrations of $\sim 10^{-5.5}$, increasing sulfide leads to a shift away from uncharged species towards HgS_2H^- . Using this understanding of the effects of pH and HS^- on the speciation of mercury, estimates for low and high available fractions were made at all depths based on the factors controlling speciation at each depth. Mean values +/- the estimated standard deviations were used for sulfide and pH.

The very soft nature of the surficial sediment (only ~20% solids in some cases) made it difficult to accurately define the location of the sediment surface for both

electrode profiles and core extrusions. It is reasonable to expect that the reference point used for these two independent measurements may have differed by as much as $\pm 0.5\text{cm}$. Additionally, it is possible that the observed sulfide concentration profile depicted in Figure 4.3b had shifted during transport to the lab or due to differences in the conditions in the overlying water. Because of this vertical uncertainty, the methyl mercury model was characterized for sensitivity to vertical shifts in observations. A reference point for each physical measurement that goes into the methyl mercury model was defined.

It was assumed that the diagenetic modeling estimates for SRR were based on the surface reference point used for % methyl mercury measurements. Furthermore, it was assumed that the reference point for sulfide and pH profiles was assumed to be the same since the free surface of the water overlying in cores was used as a reference point for both profiles. Since K_D was assumed to be constant with depth, the vertical uncertainty in the physical quantities used in the methyl mercury model of Equation 4.1, includes only the uncertainty in the surface reference points used for % methyl mercury and sulfide/pH profiles. A difference of $\pm 0.5\text{cm}$ was used as a bound on the vertical uncertainty between sulfide/pH and methyl mercury observations. This vertical uncertainty ($\pm 0.5\text{cm}$) was incorporated into methyl mercury modeling by shifting the calculations for available fraction (calculated from pH and sulfide profiles) up and down by 0.5cm relative to observed % methyl mercury to make HI (down 0.5cm) and LO (up 0.5cm) predictions.

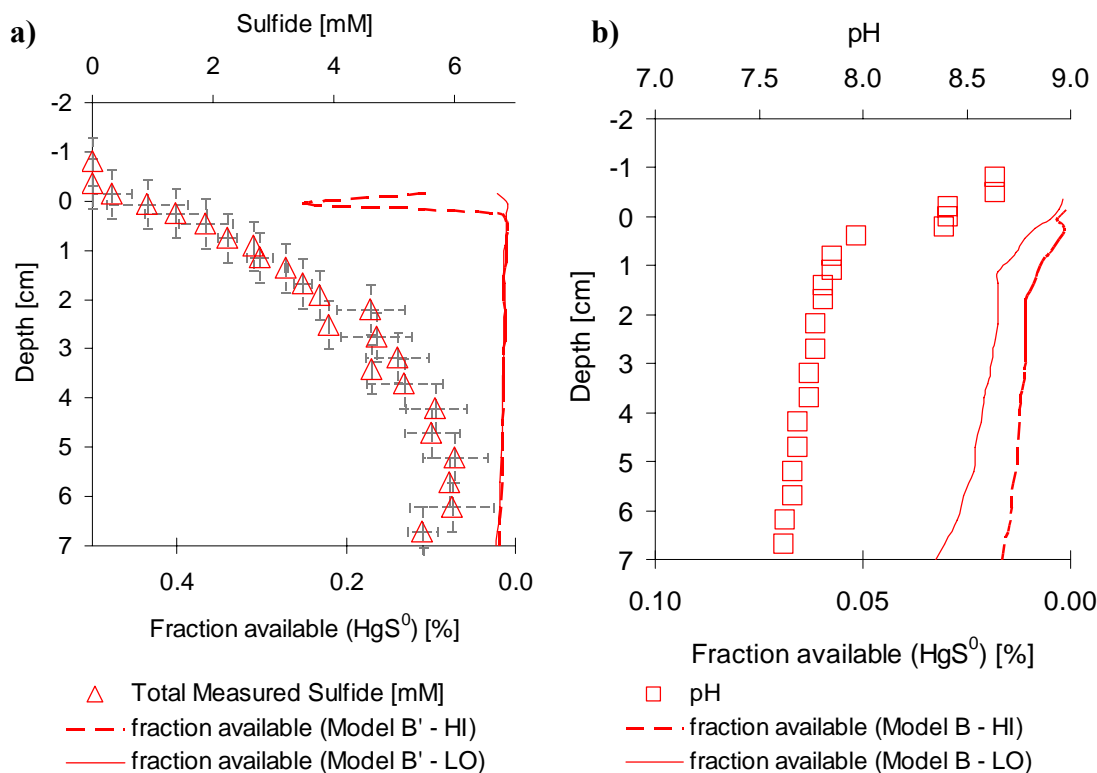


Figure 4.6 Speciation calculations for in-situ fraction available (a) uncertainty in sulfide observations associated with both concentration and measurement depth. Available fraction calculated with high stability constant for HgS^0 ($\log K=26.5$), note reversed axis direction for available fraction (b) pH profile (symbols) and available fraction calculated with low stability constant for HgS^0 ($\log K=24.5$), note reversed axis direction for available fraction

The effects of the uncertainty in pH, sulfide, and vertical reference point on calculations of available fraction are depicted in Figure 4.6a for Model B' and 4.6b for Model B. Profiles of HS^- and pH are reproduced in Figure 4.6 to illustrate their effects on speciation.

Solid and dashed lines for HI and LO calculations of fraction available (reversed axis, low availability at right) represent the available fraction at each depth calculated as a function of sulfide and pH. The HI prediction for speciation Model B' (Figure 4.6a)

shows a large increase in uncharged mercury-sulfide in the near-surface sediment where the steep sulfide gradient causes a drastic increase from less than 2% to greater than 20% HgS^0 over only 0.5cm. This near-surface maximum is responsible for the large range of methyl mercury model predictions in near surface sediment. The sensitivity of the speciation and methyl mercury models to the steep sulfide gradient suggests that the location of this gradient could be critical in defining methyl mercury in surficial sediment. Below 1cm, where sulfide concentrations are much higher, the speciation model predictions are relatively insensitive to sulfide, and the greatest contribution to methyl mercury model uncertainty is from pH measurements. This is clearly seen in Figure 4.6b for speciation Model B. Although the available fraction is low in Figure 4.6b (<2%), the difference between low and high estimates due to uncertainty in pH, is relatively large (10-20% at >2cm, and up to 50% at <2cm). Methyl mercury concentrations were much lower at deeper depths and pH gradients are not as steep as sulfide, which shows that the effect of pH in changing availability of mercury is less important than that of sulfide.

An analysis of the diagenetic effects of capping and concomitant effects on methyl mercury production in underlying sediment is presented in Appendix B. For this modeling, a cap with similar geochemical characteristics to the underlying sediment but 10x less total mercury was placed on top of a 20cm sediment column with realistic in-situ initial geochemical conditions. The model was run for 6 months and sulfate reduction rate and dissolved mercury were used with an assumed constant value for K_D to predict methyl mercury according to the steady state model presented in Equation 3.3. Results show that for a high sulfide environment like the salt marsh, the steep sulfide gradient which led to a surficial maximum in methyl mercury will quickly move from near the

sediment-cap interface into capping material, and that methylation in underlying sediment will be inhibited by high sulfide concentrations as well as limited electron acceptor (sulfate). Following cap placement, the zone of efficient methylation near the onset of sulfate reduction will occur in capping material, which, assuming this material is less contaminated than underlying sediment, will reduce the absolute concentrations of methyl mercury. Modeling was also performed for a different, hypothetical geochemical environment (similar to the LO environment in Chapter 3) with lower organic carbon and in which an excess of ferrous iron limits increases of sulfide in pore water. Results for this system showed that methyl mercury production in sediment underlying an in-situ cap will be uninhibited by sulfide and aqueous availability, and will be directly related to rates of sulfate reduction. Although the absolute magnitudes of the model predictions for methyl mercury in these hypothetical situations cannot be extended to field situations with confidence, this modeling exercise does shed light on the importance of differences in high and low organic systems and provides a starting point for evaluating processes important for evaluating mercury methylation in sediment underlying an in-situ cap.

4.3.4 Conclusions

The results presented here show that a model developed for steady state methyl mercury in laboratory simulated biogeochemical conditions predicted a range of in-situ methyl mercury concentrations consistent with observations. This included an increase in % methyl mercury in surficial sediment when stability constants for speciation modeling included the formation of HgS^0 at low sulfide concentrations (Model B'). Consistent with the results of Chapter 3, a speciation model that includes the formation of HgS^0 and its influence on availability is more consistent with observations than one that considers

only $\text{Hg}(\text{SH})_2^0$ availability. At depths greater than 1cm below the sediment-water interface, where sulfide remains consistently above the transition from HgS^0 to HgS_2H^- , the effects of pH was the most important factor controlling uncharged speciation and consequent availability. The sensitivity of methyl mercury model results to changes in the location of the sulfide gradient showed that this factor could have extreme effects on the availability of mercury to methylating microbes. The potential methyl mercury-related implications of a diurnal migration of the redox-cline across the sediment water interface were noted by Langer et al. 2001. It was suggested that supersaturated oxygen conditions can be found at the sediment water interface due to photosynthesis during the day. At night, sulfide produced by biological activity in underlying sediment can consume this oxygen and diffuse into overlying water. The steep gradients in observations near the sediment-water interface and the methyl mercury model sensitivity to sulfide concentrations revealed that the processes controlling in-situ sulfide concentrations are important to accurately predicting methyl mercury in surficial sediment due to the importance of mercury-sulfide complexes in limiting the availability of inorganic mercury to methylating bacteria. The magnitude, location, and temporal variations in steep near-surface sulfide gradients must be accurately characterized to understand methylation in surficial salt marsh sediment.

Chapter 5: Biogeochemical Changes and Mercury Methylation beneath an In-Situ Sediment Cap

5.1 INTRODUCTION

Contaminated aquatic sediments comprise almost one third of the sites listed on the EPA's Final National Priority List (EPA 2008). Metals are contaminants of concern at over half of these sites, many of which contain mercury. Aquatic sediments present a complex environment and a challenging scenario for environmental management due to a plethora of interacting biological and chemical processes that affect contaminant fate and transport. One strategy that is considered for managing the risk posed by contaminated sediments is in-situ capping (EPA 2008). In-situ capping involves the placement of a clean layer of material on the sediment surface for the purpose of reducing or eliminating the mobilization of contaminants from sediment to the overlying water and subsequent exposure pathways. The primary objective of an in-situ cap is to physically separate exposure and mass transfer processes occurring in surficial sediment from contaminated material; however, capping is also expected to alter biogeochemical processes known to affect contaminant fate and transport.

Some short-term laboratory-scale capping studies have attributed reductions in contaminant flux to both the physical separation provided by a cap and cap-induced changes in the biogeochemistry of the underlying sediment; e.g. immobilization of metals by metal-sulfide precipitation and biodegradation of chlorinated organics (Simpson et al. 2002, Himmelheber et al. 2007, Eek et al. 2008). Himmelheber et al. 2007 explicitly measured biogeochemical changes beneath a sediment cap in freshwater sediment columns in both stagnant and upflow conditions. Formerly surficial, oxic sediment was driven anaerobic, and redox zones experienced a clear upward shift as a result of cap

placement. Iron reducing conditions were observed within a cap placed over sediment from a freshwater system. It was hypothesized that these shifts in biogeochemistry, and redox profiles in particular, will influence the speciation and fate of reactive contaminants. In this work, we explore the implications of those shifts for the fate and transport of mercury, a contaminant sensitive to biogeochemical conditions.

The speciation of mercury is critical in controlling dietary exposure to humans and much effort in recent years has been devoted to understanding the biogeochemical processes affecting mercury speciation and transformations in aquatic sediments (Benoit et al. 2003). Methyl mercury, the most dangerous form of mercury, is an acute neurotoxin and readily accumulates in the tissue of organisms (Morel et al. 1998). Both laboratory (Fitzgerald et al. 2007) and field-scale (Harmon et al. 2004, Gilmour et al. 1992, Compeau and Bartha 1985) evidence has shown that sulfate reducing bacteria (SRB) play a dominant role in the production of methyl mercury; however, in freshwater systems containing limited amounts of sulfate, it has been suggested that other anaerobic bacteria, including iron reducing bacteria and methanogens, may be involved in mercury methylation (Warner et al. 2003, Kerin et al. 2006, Fleming et al. 2006). In-situ concentrations of methyl mercury represent a balance between methylation and demethylation processes (Hintelmann et al. 2000, Drott et al. 2008) and it is believed that rates of demethylation are relatively constant regardless of dominant biological populations, but that methylation rates are strongly dependent upon the activity of sulfate reducing bacteria (Warner et al. 2003, King et al. 2001).

Due to the complexities associated with mercury bioavailability and mobility, it is not immediately obvious what effect an in-situ cap will have on underlying methylation/demethylation processes. Methylating bacteria populate anaerobic environments that a cap is expected to promote; consequently, there is justifiable concern

that an increase in underlying methylation could limit the effectiveness of an in-situ cap. In order to evaluate the mercury-related effects of capping, a fundamental understanding of the underlying biogeochemical processes that control methylation must be considered. The objective of this research is to characterize changes to the location and extent of stratified biogeochemical zones beneath an in-situ cap and demonstrate the effect of these changes on underlying methyl mercury production. Toward this end, biogeochemical zones and methyl mercury were studied in laboratory microcosms following the placement of an in-situ cap. To further elucidate the coupling of mercury methylation to observed biogeochemical changes, a diagenetic model is presented to simulate relevant biogeochemical processes in surficial sediment. The conceptual framework implemented in the model explicitly considers the biological and chemical processes known to affect mercury methylation, including sulfate reduction, iron reduction, and dissolved sulfide. The modeling results are used to interpret differences in stratified biogeochemical zones and methyl mercury concentrations in capped and uncapped microcosms.

5.2 MATERIALS AND METHODS

5.2.1 Sediment Microcosms

Sediment from a mercury-contaminated estuarine environment, Lavaca Bay, TX, was used for the study (Bloom et al. 1999). Sediment was collected from the top 12" and stored at 4°C until the initiation of laboratory experiments. In order to examine in-situ biogeochemical zones, approximately one kilogram of wet sediment was homogenized and sieved under an N₂ atmosphere to maintain reduced conditions and placed into 5cm x 15cm acrylic sediment microcosms (Wang et al. 1991) to a depth of 7cm. A well-mixed, 3cm column of synthetic sea water (8ppt salinity, Instant Ocean® Sea Salt) was

continuously refreshed over the sediment with a residence time of ~1.5 hours. Though this flow rate is slower than most natural environments, it is sufficient to avoid water-side mass transfer resistances to oxygen and other species affecting the development of realistic stratified biogeochemical zones.

One microcosm that did not contain a cap was left open to the atmosphere as a control (referred to as Control). In a second treatment, a 2cm acid-washed sand cap was placed on top of the sediment and the overlying water was open to the atmosphere (referred to as Capped). A third microcosm with no cap in which the overlying water was purged with nitrogen to ensure anoxic conditions (<1 mg/L O_2 , referred to as Anoxic) was used to provide an upper boundary condition expected to be similar to an in-situ cap (reduced oxygen flux from the overlying water). For three weeks, oxic conditions (DO ~8mg/L) were maintained above all three microcosms and similar stratified biogeochemical zones were observed (Appendix C). Capped and anoxic conditions were then initiated and porewater geochemical observations verified the existence of characteristic differences in the biogeochemical zones induced by capped and anoxic conditions. A non-destructive microelectrode sampling technique allowed measurements to be made at several time points throughout the experiment. Little transient change was observed between 2 and 4 months (Appendix C) and sediment cores were extracted, sliced, and analyzed for solid phase total and methyl mercury, acid volatile sulfides (AVS), and inorganic constituents in porewater.

5.2.2 Analytical Techniques

Profiles of dissolved geochemical species in sediment porewater were obtained using voltammetric microelectrodes (Brendel and Luther 1995, Himmelheber et al. 2008) at a vertical resolution of <3 mm using a single axis automated micromanipulator

(Analytical Instrument Systems, Flemmington, NJ). Analytes included O_2 , Mn^{2+} , Fe^{2+} , and dissolved sulfide (DS). The voltammetric electrodes respond to all reduced forms of dissolved sulfide (H_2S and HS^-) and measurements do not need to be adjusted for pH. Microelectrodes were prepared in the laboratory using the method of Brendel and Luther (Brendel and Luther 1995). At the beginning of each profiling event, electrodes were calibrated for oxygen using a 2-point calibration, and the method of standard additions was used for iron, manganese, and sulfide in synthetic seawater with 2mM acetate or HEPES buffers (Acros.). Scan parameters and detection limits were the same as those reported in Brendel and Luther (Brendel and Luther 1995). Calibration checks were performed on electrodes after each profile. Triplicate scans were made at each depth and duplicate or triplicate electrodes were spaced 2-3cm apart.

Organic carbon content of bulk, homogenized soil samples was measured using a CHN elemental analyzer (Carlo Erba) after acidification (1N HCl) to remove inorganic carbon. Following microwave digestion, bulk metal concentrations (Fe, Mn, and Hg) were measured by GFAA (Perkin Elmer AAnalyst600). AVS was measured by the diffusion method (Brouwer and Murphy 1994), and the detection limit was determined to be $<0.1 \mu\text{mol/g}$ dry sediment based on the mass of sediment and the detection limit of the sulfide electrode. Chloride and sulfate were quantified using chromatography on a MetroOhm IC system (700 Series, 15cm Metrosep A Supp 5 column). At the end of the experiments, cores were extracted using a 2cm diameter polypropylene syringe, sectioned into 0.5 - 1.0cm slices under an N_2 atmosphere and homogenized with a Teflon spatula. For methyl mercury, samples from each depth were immediately frozen and sent to a commercial laboratory (BrooksRand Labs, Seattle, WA) in Teflon lined borosilicate glass vials for analysis by EPA Method 1630 (organic extraction, aqueous ethylation, purge and trap, GC separation, and CVAFS). Additional QA/QC data is included in Appendix

C. Cores were taken from adjacent locations in the microcosms, sectioned under an N₂ atmosphere, and analyzed for AVS (diffusion method, immediately) and sulfate (IC, within 8 hours).

5.3 MODEL DESCRIPTION

A 1-dimensional, unsteady, reactive transport model was developed to simulate fundamental, interrelated diagenetic processes in surficial sediments, many of which are known to affect mercury methylation (Compeau and Bartha 1995, Warner et al. 2003, Kerin et al. 2006). Processes included in the model are based on those presented in Jaffe et al. 2002 and include the biological degradation of organic matter, considering O₂, NO₃⁻, Mn⁴⁺, Fe³⁺, and SO₄²⁻ as electron acceptors as well as methanogenesis. Other oxidation/reduction, precipitation/dissolution, and sorption reactions were considered along with diffusive transport of all species. A complete model description is included in the Appendix C including parameters, reaction formulations, and boundary/initial conditions used in model simulations. The model was implemented in Fortran 90 using the Method of Lines and a standard ordinary differential equation (ODE) integration routine (Boudreau 1996). Central difference approximations were substituted for the spatial derivatives and modified for uneven grid spacing, and a standard integrator, VODE (Brown et al. 1989), was used to solve the equations.

5.4 RESULTS AND DISCUSSION

5.4.1 Model Calibration & Simulations

Bulk geochemical observations made at the initiation of the experiments were used to define initial conditions for modeling. Based on porewater measurements,

simulations began with all redox-active species in the reduced form, except for 1mM SO_4^{2-} . Organic carbon, total iron, and total manganese for the sediment were measured at 0.4%, 0.56%, 0.008% (dry mass basis), respectively. Measurements of bulk solid phase total and ferrous iron suggested that 10% of the total iron in the system was available for biological reduction. Sulfate, dissolved oxygen, and pH were measured at ~6mM, 0.26mM, and 8.2 respectively in the overlying water and these values used in a diffusive upper boundary condition ($\delta_{bl}=0.2\text{cm}$). Zero flux of all constituents was assumed at the bottom of a 7cm model domain. To simulate the initial experimental phase in which all microcosms were exposed to oxygenated overlying water, the model was run for 22 days during which the iron in a surface layer was oxidized to iron hydroxides by overlying oxygen. The model was calibrated to observations in the control microcosm (Figure 5.1a) by adjusting the rates for biological reduction of organic matter to match geochemical observations ($\text{O}_2/\text{Fe}/\text{Mn}/\text{HS}$). Published rates (Jaffe et al. 2002) were used for most other parameters (Appendix C). Subsequently, leaving all other parameters the same, boundary conditions were set to simulate capped and anoxic conditions.

Observations before the initiation of capping/anoxic conditions showed similar profiles in all 3 microcosms (0 months, Appendix C). However, differences amongst the three treatments quickly developed. Profiles taken at 1, 2, and 4 months showed consistent, characteristic, stratified redox zones in each microcosm (Appendix C). These differences amongst treatments persisted until cores were taken at ~4 months. Figure 5.1 (a, d, and g) show geochemical porewater observations 122 days after the initiation of capped/anoxic conditions and associated modeling results. Error bars for O_2 , DS and Mn^{2+} represent the standard deviation of independently calibrated triplicate electrode measurements spaced 2cm apart. Error bars for O_2 fall within the symbols. The

concentration range of duplicate electrode measurements is shown for Fe^{2+} . A single microcosm was run for each treatment, however, replicate microelectrode profiles with a separation distance to sample size ratio of approximately 20:1 (2cm:0.1mm) can be considered independent measurements for the treatment. Though our homogenized sediment resulted in a system somewhat different from a natural, depositional environment in which metals cycle and build up in surficial sediment (Katsev et al. 2006); the realistic, stratified biogeochemical zones observed in this study are analogous to a natural system and provide a dynamic change to biogeochemical zones applicable for evaluating the effects of capping on mercury methylation.

Both observations and model predictions show sulfide appearing at shallower depths in capped and anoxic conditions than in the control (uncapped) conditions. This upward shift in reducing conditions was consistent with expectations and previous observations (Himmelheber et al. 2008). After 4 months, dissolved sulfide was observed only at the bottom (>6cm) of the control microcosm (Figure 5.1a), while increases in dissolved sulfide at shallower depths (3-4cm) is clearly observed in the capped (Figure 5.1d) and anoxic (Figure 5.1g) microcosms.

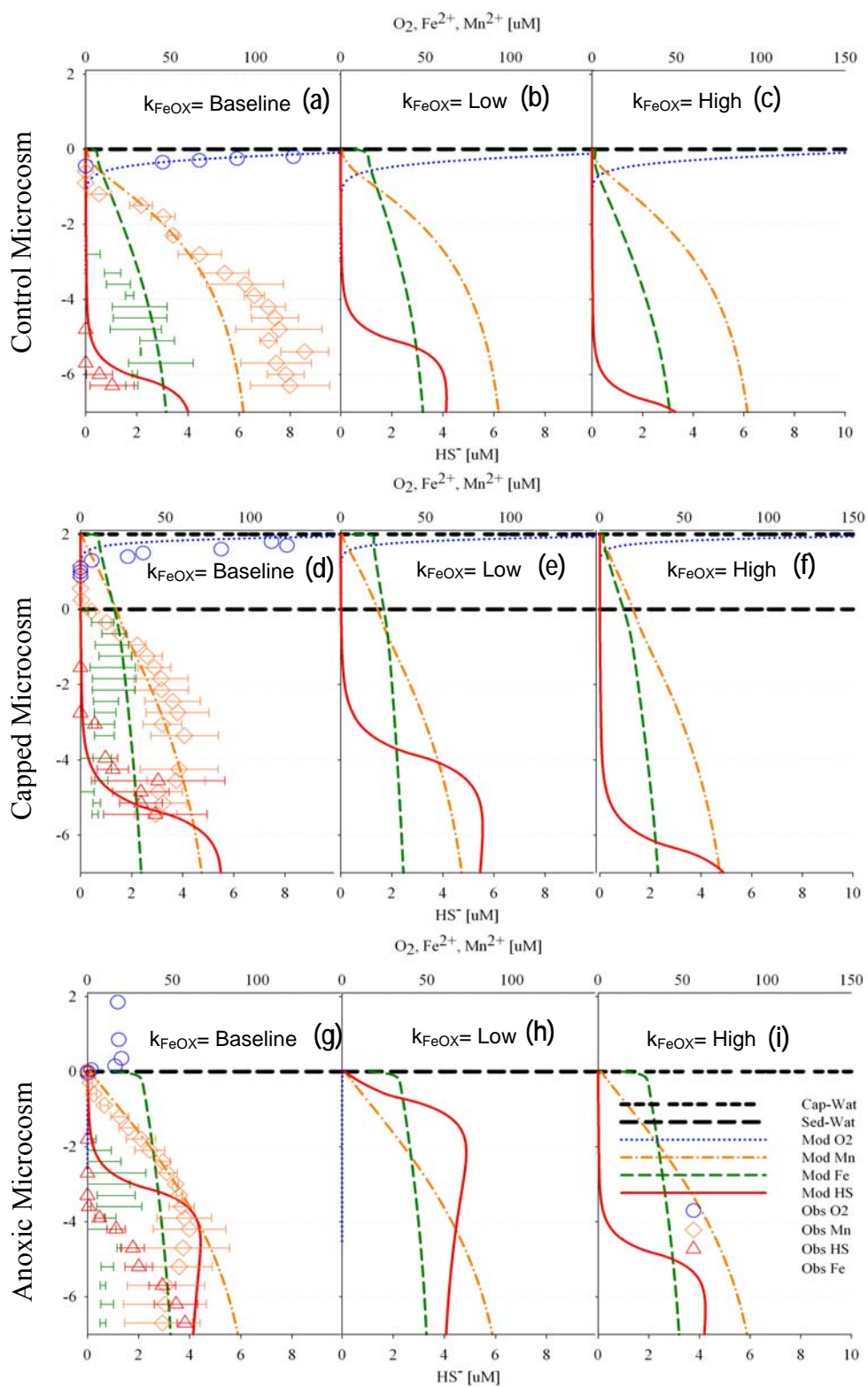


Figure 5.1. Diagenetic model calibration (a – Baseline, 10umol/cm² initial iron oxidized, $k_{FeOX}=1.6(106) \mu M\text{-}1yr\text{-}1$) and sensitivity analysis of iron oxidation rates (b–Low rate, 5umol/cm² or $k_{FeOX}=4.8(105) \mu M\text{-}1yr\text{-}1$, and c–High rate 15umol/cm² or $k_{FeOX}=1.6(107) \mu M\text{-}1yr\text{-}1$) for control microcosm. Model predictions for capped and anoxic microcosms are shown in (d) and (g) respectively, with associated iron oxidation sensitivity analysis in (e,f) and (h,i) respectively.

Anoxic conditions were expected to provide a similar upper boundary as the capped condition, and observations clearly showed evidence of increased sulfate reduction at shallower depths in both anoxic and capped microcosms. Modeling results, however, showed that the location of the transition to sulfate reduction under anoxic overlying water was strongly dependent on the mass of iron oxide present at the onset of anoxic conditions. A sensitivity analysis of iron oxidation rates that resulted in the oxidation of 5, 10, and 15umol/cm² ferric iron ($k_{FeOX}= 4.8 \times 10^5$, 1.6×10^6 , and $1.6 \times 10^7 \mu M\text{-}1year\text{-}1$, respectively) during the initial 22 day period is shown in Figure 5.1 (a-c for control, d-f for capped, g-i for anoxic). Model predictions for the depth of the onset of sulfate reduction are more sensitive to the initial mass of oxidized iron in the anoxic system (0.5cm – 4.5cm) than in the control (5cm - 6cm) or capped (4cm – 6cm) system in which oxic overlying water provides a strong oxidizing force.

Additional evidence of increased sulfate reduction in capped and anoxic microcosms included solid-phase AVS and porewater sulfate concentrations (Appendix C) as well as visual observations (Figure 5.2a-c). In the control microcosm, AVS remained low (<1μmol/g) at depths less than 6cm, and little sulfate depletion was observed. However, in capped and anoxic microcosms, AVS increased with depth, and a depletion in SO_4^{2-} was clearly observed. Both of these observations are consistent with increased sulfate reduction at depths between 2-5cm (Appendix C). This increase in

sulfate reduction at shallower depths clearly demonstrates the effects of capping on a biological process known to control methyl mercury production in many stems.

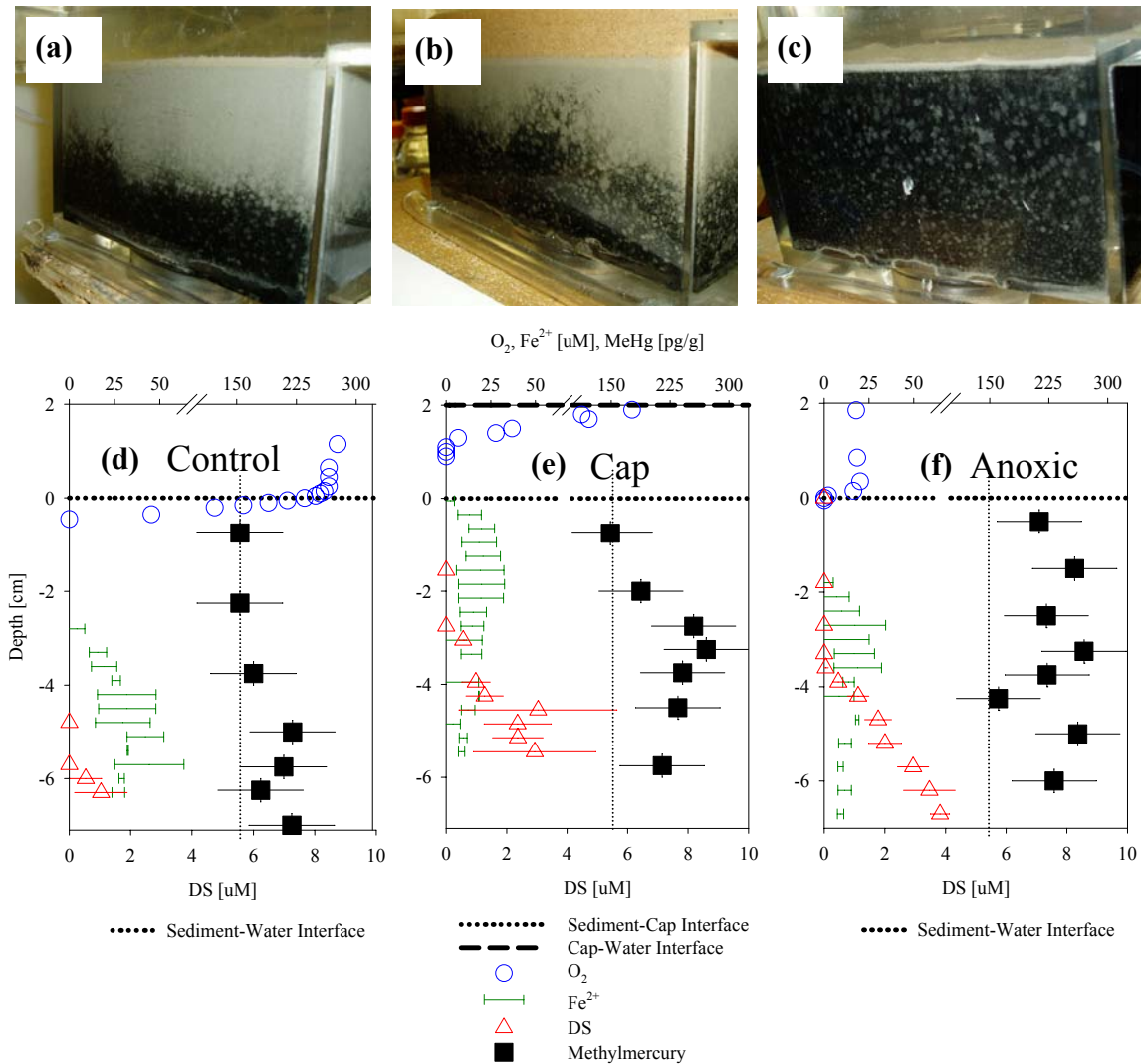


Figure 5.2 Visual observations of biogeochemical zones in (a) control, (b) capped, and (c) anoxic microcosms at 3 months. Depth profiles of methyl mercury, oxygen (O_2), dissolved iron (Fe^{2+}), and dissolved sulfide (HS^-) in (d) control, (e) capped, and (f) anoxic microcosms at 120d. Error bars for HS^- represent the standard deviation of triplicate electrodes spaced 2cm apart. The concentration range of duplicate electrode measurements is shown for Fe^{2+} . Error shown for methyl mercury was calculated using the pooled variance of duplicate analytical analyses.

5.4.2 Methyl mercury Observations

Solid-phase methyl mercury concentrations [pg/g-dry] in each of the microcosms are plotted with geochemical profiles in Figure 5.2(d-f). Methyl mercury was below detection limits in the capping material. Error bars represent the pooled variance of duplicate analytical analyses (Skoog et al. 2007). Total mercury content averaged 0.33ug/g-dry weight and showed little variability with depth (Appendix C), therefore %methyl mercury is proportional to methyl mercury concentrations. In-situ methyl mercury concentrations, which represent a balance between methylation and demethylation, were relatively constant in the control microcosm over the first 4cm at ~160 [pg/g-dry] in an area where active sulfate reduction was not occurring. Methyl mercury observations in capped and anoxic microcosms were up to 50% higher than this baseline in areas where evidence of increased sulfate reduction was observed (Figure 5.2 e-f). Methyl mercury under capped conditions showed a maximum at ~3cm, near the onset of sulfate reduction. Previous research has shown similar trends due to biological methylation and porewater speciation (Benoit et al. 2006, Merritt et al. 2008), although the dissolved sulfide observed in our study remained low and inhibition of methylation by mercury-sulfide complexes seems unlikely (Benoit et al. 1999). Observations in the anoxic microcosm showed higher methyl mercury than the control microcosm at all depths, even near the sediment-water interface. Although dissolved sulfide was not observed in surficial sediment, visual observations (Figure 5.2c) and model simulations (Figure 5.1g) suggest that sulfate reducing activity may have extended to very near the sediment-water interface.

The observed increase in in-situ methyl mercury is likely due to the extension of sulfate reduction to shallower sediment depths causing an increase in methylation without

an equal increase in demethylation. In order to quantify the cap-induced differences, it was assumed that the in-situ methyl mercury concentrations in the control microcosm between 0-4cm represent a baseline level associated with transport, methylation and demethylation in the absence of active sulfate reduction. The methyl mercury in excess of this baseline level (160pg/g) was integrated over the surficial 6 cm. Capped and anoxic microcosms had 400 and 600pg/cm², respectively, in excess of this baseline while the control microcosm had less than 100pg/cm² in excess of the baseline. Methyl mercury concentrations 0-2cm below the capping layer are similar to those observed in the surficial sediment of the control microcosm (150-190 [pg/g-dry]), while in the anoxic microcosm, surficial concentrations are greater than 200 [pg/g-dry]. The lower methyl mercury at 0-2cm depth in the capped microcosm coincides with an area of relatively high dissolved ferrous iron and visual observations showed that the surficial sediment beneath the cap was not as reduced as the surficial sediment in the anoxic treatment. Ferrous iron produced near the surface of the anoxic microcosm, could have diffused out into the overlying water and been oxidized at the surface or carried away, while in the capped microcosm, a broader oxic zone within the cap may have re-oxidized ferrous iron and prevented its loss to the overlying water. The ferrous/ferric iron cycling in the surficial sediment underlying the sediment cap may have prevented sulfate reduction from moving into the sediment at 0-2cm below the cap-sediment interface, and is a result that highlights the need to consider the geochemical effects of capping in detail during cap design and monitoring.

Results presented here demonstrate the influence of cap-induced biogeochemical changes on methyl mercury production in underlying sediment and confirm the importance of sulfate reducing bacteria in controlling mercury methylation in an in-situ system with realistic, stratified microbial communities. The methyl mercury-related

effects of changes to in-situ biogeochemical process were previously observed in the context of bioturbation intensity (Benoit et al. 2006). In Boston Harbor, the activity of bioturbating organisms forced anaerobic biogeochemical zones to deeper depths in the sediment, and a downward shift in methyl mercury profiles was observed. Analogously, beneath a sediment cap, biogeochemical zones will be shifted due to cap placement, and associated changes in methyl mercury production should be expected.

It is believed that mercury is methylated during the metabolism of sulfate reducing bacteria (Eckstrom et al. 2003), and quantitative links between methyl mercury concentrations and sulfate reduction rates have been demonstrated in studies using intact sediment cores (King et al. 2001, Gilmour et al. 1998) as well as pure culture experiments (King, et al. 2000, Benoit et al. 2001b). While observations and model simulations shown in Figure 5.1 represent byproducts of biological activity, Figure 5.3 shows the model simulated rates [$\mu\text{mol/L/day}$] of biological organic carbon utilization in control, capped, and anoxic microcosms for the baseline iron oxidation rate of $1.6 \times 10^6 \text{ uM}^{-1} \text{ yr}^{-1}$ four months after the initiation of capped and anoxic conditions.

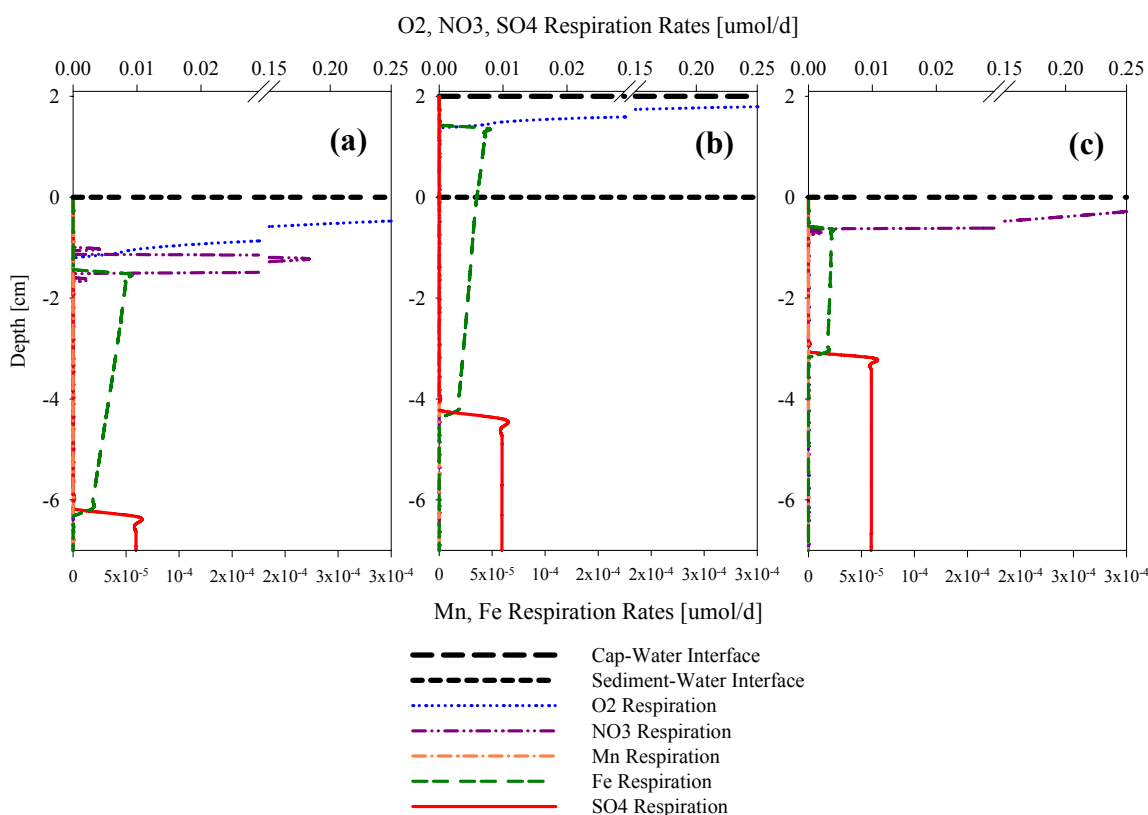


Figure 5.3 Simulated profiles of rates for biological organic carbon utilization by different electron accepting populations in (a) control, (b) capped, and (c) anoxic microcosms (iron oxidation rate = 107 $\mu\text{mol}/\text{cm}^3\text{-year}$). Rates for iron and manganese reduction are orders of magnitude smaller and shown on a separate axis

In the control microcosm, model simulations show sulfate reduction occurring at and below 6cm. Model predictions show that biological sulfate reduction begins slightly below 4cm from the sediment-cap interface and around 3 cm for the anoxic case although this is sensitive to the iron oxidation rate and initial amount of iron oxides in the sediment as shown previously. These modeling results are consistent with observed geochemical and methyl mercury concentrations (Figure 5.1 and 5.2) and suggest that increased sulfate reducing bacterial activity at 3-5cm depth contributed to increases in in-situ methyl mercury below the cap. The geochemical observations, methyl mercury observations,

and biogeochemical modeling in this short-term laboratory study suggest that the presence of an in-situ sediment cap encouraged the activity of sulfate reducing bacteria, at shallow depths beneath a cap and altered the methylation-demethylation balance to increase in-situ methyl mercury concentrations. This highlights the importance of considering fundamental biogeochemical processes when developing engineering solutions to natural systems, especially for contaminants like mercury whose transformations are sensitive to geochemical conditions.

The steady state equation calibrated in Chapter 3 (Equation 3.3) was applied to the observations made in the microcosms using the modeled sulfate reduction rates ($\sim 11 \mu\text{M}/\text{day}$) in Figure 5.3, constant K_D estimated from the batch slurry experiments in Chapter 3 with this environment ($\log K = 4.2$), and available mercury calculated using a value of 26.5 for the $\log K$ for the formation of HgS^0 and observed concentrations of HS^- ($< 5 \mu\text{M}$) and pH (7.5, from pre-spiked Chapter 3 slurries). The assumption of constant K_D is a limitation of this modeling, since solid phases appeared to change with depth (Figure 5.2a-c). The methyl mercury model in Equation 3.3 defines increases in methyl mercury as proportional to active sulfate reduction and potentially limited by aqueous availability and dissolved mercury. Low sulfide concentrations even in locations of active sulfate reduction in all three microcosms led to predictions of mostly uncharged and available dissolved mercury. Therefore, methyl mercury as described by Equation 3.3 was limited only by the rate of sulfate reduction and not by availability in this low-sulfide system. By definition then, the modeling results predicted increases in methyl mercury above background to be coincident with increases in sulfate reduction rate, which is consistent with the location of observed increases in methyl mercury in the microcosms as noted previously. The magnitude of the increase predicted by the model, however, was more than 5 times that observed in the sediment (up to 800 pg/g). Even with the limitations

imposed by the assumption of constant K_D and the discrepancy in the magnitude of model predictions, the results of this modeling are useful in that they show that for this low organic system, in which sulfide does not build up to inhibitory levels in surficial sediment, cap-induced increases in methyl mercury are likely to be related only to increases in sulfate reduction and unaffected by availability limitations.

5.4.3 Implications for Capping

In this study, the upward extension of anaerobic communities toward the sediment/cap interface was accompanied by an increase in methyl mercury production at depths consistent with the transition to sulfate reduction (Gilmour et al. 1998, Langer et al. 2001). The increase in methyl mercury observed in this study (~50%) and the 2-4 cm upward shift in the location of its generation is insufficient to substantially increase diffusive flux of methyl mercury through an intact, thick capping layer (20-1000cm). The magnitude of this increase, however, is likely a function of local geochemical conditions, and a faster shift over a larger distance scale may be expected in a system with substantially more organic carbon and larger rates for biological processes. Thin capping layers (5-15cm), are frequently considered to reduce bulk surficial sediment concentrations (EPA 2005). The results presented here suggest that in-situ methyl mercury concentrations will be altered by the placement of even a thin capping layer, and bioturbating organisms could be exposed to higher underlying methyl mercury concentrations if the cap is physically compromised. Evaluations made during cap design should consider biogeochemical changes related to mercury transformations; particularly for thin or unstable capping layers where the physical sequestration provided by a cap may be compromised and organisms exposed to higher methyl mercury concentrations in underlying sediment.

Chapter 6: Conclusions and Recommendations

6.1 SUMMARY

The purpose of this research was to develop an understanding of how the biogeochemical effects induced by in-situ sediment capping will affect the production of methyl mercury in underlying sediment. Although the motivation for this work arose from capping as a risk-reduction strategy for heavily contaminated sediment, the investigation is applicable to any situation that involves the burial of mercury-contaminated sediment either by natural deposition or through engineered capping. Fundamental biological and geochemical processes responsible for limiting mercury methylation were investigated using laboratory-scale experiments and mathematical models to evaluate the potential for cap-induced increases in the production of methyl mercury. The mercury-related processes considered include: (1) the rate of sulfate reduction, (2) the aqueous availability of inorganic mercury, and (3) the strength of partitioning to the solid phase. The combined effects of these processes in controlling methyl mercury were described quantitatively using a simple, steady-state model calibrated to observations in laboratory experiments. This model was also applied to in-situ methyl mercury observations to test its ability to predict field conditions and used to investigate sensitivity to changes or uncertainty in key processes. Finally, a lab-scale in-situ capping simulation was used to demonstrate concomitant changes in biogeochemical processes and methyl mercury production in sediment underlying an in-situ cap.

6.2 CONCLUSIONS

The first, and perhaps most obvious, conclusion that can be drawn from this research is that the production of methyl mercury in sediment underlying a cap will be

closely tied to biogeochemical conditions. Results from the in-situ capping simulation presented in Chapter 5 showed an upward translation in biogeochemical redox zones following cap placement and a concomitant shift was observed in the location of maximum methyl mercury. In the batch slurry experiment presented in Chapter 3, experimental and modeling results in a range of geochemical conditions likely to be found beneath a sediment cap showed large differences in methyl mercury concentrations. High methyl mercury concentrations were observed in some of the simulated conditions and this suggests that there is reason to be concerned about the mercury-related impacts of capping. However, other simulated conditions showed relatively low methyl mercury concentrations, suggesting that not all capping situations will lead to methyl mercury increases in underlying sediment. This leads to the question: For what scenarios should we be particularly concerned about increases in methyl mercury beneath an in-situ sediment cap? The complexity of the interrelated biogeochemical processes that affect the production of methyl mercury in sediment necessitates a site-specific evaluation of the potential effectiveness of capping mercury contaminated sediment. However, some specific conclusions from this research can be used to identify locations or conditions likely to be especially conducive to the production of methyl mercury and to characterize the potential effects of various important processes and geochemical parameters that should be considered in an evaluation.

The differences in methyl mercury observed in the laboratory experiments presented in Chapter 3 are a result of interrelated biogeochemical processes known to control methyl mercury production including sulfate reduction, aqueous speciation, and solid-phase partitioning. Experimental and modeling results showed that different

processes limited the production of methyl mercury in the variety of geochemical conditions examined. In geochemical conditions with high rates of sulfate reduction and high dissolved mercury (fully reduced MO and HO, Figure 3.5), methyl mercury production was limited by the availability of dissolved mercury to methylating microbes. In other conditions, low sulfate reduction rates and low dissolved mercury (LO, Figure 3.5) limited methyl mercury production despite dissolved mercury speciation conducive to methylation. This suggests that a conceptual model including the effects of all three of these potentially limiting processes (sulfate reduction, aqueous speciation and availability, and dissolved inorganic mercury) is necessary to effectively describe methylation.

The highest methyl mercury concentrations observed in laboratory batch slurry experiments (>3% of total mercury) were found in sediment with a very high organic carbon content (>25% LOI) that had been previously oxidized and then incubated under anoxic conditions (HO, Figure 3.2a-c). Over a period of less than 10 days, methyl mercury concentrations increased by an order of magnitude from the initial concentrations in oxidized conditions. Sediment from the same environment that had not been previously oxidized experienced almost no change in methyl mercury concentrations over the 50+ day anoxic incubation. These results suggest that in a high-organic environment, methyl mercury concentrations could increase in surficial, oxidized sediment following the elimination of oxygen by the placement of a sediment cap. However, this increase may be confined to the top few centimeters since redox conditions in deeper sediment will not be affected significantly by cap placement.

In the low organic environment used in this study (LO), relatively lower methyl mercury concentrations (<0.5% of total mercury) were observed in even the most conducive geochemical conditions. Due to the lower organic content of 3% LOI, sulfate

reduction rates were about 3 times lower than those observed in the high organic sediment (Figure 3.4). No sulfate reduction was observed in the previously oxidized sediment throughout the anoxic incubation (Figure 3.1a-c), and for the mildly and fully reduced sediment (Figure 3.1d-i), methyl mercury remained low despite the fact that 10-20% of the dissolved mercury was calculated to be available for methylation (Table 3.6). Since the sulfide concentrations observed in the LO environment were too low to inhibit methylation, differences in methyl mercury concentrations were mostly controlled by differences in sulfate reduction. The same low organic sediment was used for the in-situ capping simulation described in Chapter 5, and after 150 days, sulfide concentrations were below detection limits ($0.1\mu\text{M}$) in surficial sediment and remained less than $10\mu\text{M}$ up to 7 cm depth. These results suggest that for low organic sediment, methyl mercury concentrations will be limited by rates of sulfate reduction rather than the availability of inorganic mercury. Organic content, therefore, is an important parameter to consider when evaluating the mercury-related effects of in-situ capping. The general conclusion that can be drawn from this analysis is that in a high organic environment, in-situ capping may initiate an uninhibited strong driver for methylation in (formerly) surficial sediment, while in a low organic environment with an overall lower potential for methylation, capping can be expected to have a less dramatic effect.

Since overall heterotrophic bacterial activity is driven by the availability of labile organic carbon, another factor that could limit methylation in the long term is a cap-induced reduction in the supply of organic carbon. The physical barrier of a capping layer will reduce or eliminate the source of organic matter from the overlying water. As labile organic carbon is consumed in underlying sediment, an overall reduction in bacterial activity is expected on a timescale of a few months to years, depending on the

quality and quantity of organic matter. This reduction in bacterial activity will assumedly slow the biologically driven methylation process as well. While time constraints on experimental work prohibited an explicit study of the effects of organic carbon limitation, the effects can be indirectly inferred from the different organic contents of the environments studied in this research. The vigorous sulfate reduction observed in the high organic environment (HO) contributed to high methyl mercury concentrations in the presence of available dissolved mercury (suboxic incubation). However, over time, bacterial activity in this environment can be expected to slow as labile organic carbon is consumed and will eventually approach the slower rates observed in the low organic environment (LO). Since lower methyl mercury concentrations were observed in the LO environment, the results suggest that there is a narrow window, both geochemically and temporally, where large increases in methyl mercury can be expected: Following the placement of a sediment cap, an increase in methyl mercury can be expected as sulfate reduction moves into surficial sediment in which substantial labile organic carbon is present; however, this increase will only last until sulfide builds up to inhibitory levels, or until labile organic carbon is depleted and overall bacterial activity slows in underlying sediment.

Another conclusion about the effects of capping can be drawn about the near surface maximum in methyl mercury observed in the surficial salt marsh sediment (Chapter 4). This maximum was due to steep gradients in sulfide and consequently, dissolved mercury available for methylation. The placement of a sediment cap over sediment with a steep surficial sulfide gradient will eliminate the flux of oxygen that causes the steep gradient, allowing for the diffusion of sulfide into (formerly) surficial sediment and capping material. In highly sulfidic environments, this will cause the

speciation of dissolved mercury to be completely dominated by charged, unavailable mercury-sulfide complexes in sediment underlying a cap, which will limit the production of methyl mercury. Although a sulfide gradient will still be present somewhere in the capping material, the zone of efficient methylation surrounding this gradient will be in less contaminated material with lower inorganic mercury to drive methylation.

The assumption of a steady state balance between methylation and demethylation used in developing the model presented in Chapter 3 places some limitations on the scope of its applicability. In many in-situ conditions, research has shown that rates of methylation and demethylation are faster than rates of transport or changes in bulk geochemical conditions, and the steady state assumption is justified in these situations. However, in cases where hyporheic flow, variable groundwater discharge, or tidal pumping lead to non-steady flow in sediment porewater, the assumption of a local balance between methylation and demethylation processes is not valid. In these cases, a description of absolute rates of methylation and demethylation (rather than a net rate) as well as the effects of transport are necessary to accurately characterize methyl mercury concentrations.

This research focused primarily on the effects of sulfate reduction and aqueous speciation in limiting methylation and did not explicitly investigate the processes that led to differences in solid-phase partitioning. Rather than characterizing the factors that control solid-phase partitioning, dissolved mercury was measured directly. The factors that control dissolved mercury are important, however, since they define the inorganic mercury available for methylation and are known to be dependent on redox sensitive solid phases like iron hydroxides and iron sulfides. Since limited sample volume currently constrains the feasibility of obtaining high-resolution in-situ profiles of

dissolved mercury, further research into the mechanisms that control solid-phase partitioning could provide valuable information about its role in limiting in-situ methylation.

6.3 RECOMMENDATIONS FOR FUTURE WORK

The work presented here combined the study of both (1) the geochemical processes and parameters controlling the production of methyl mercury in conditions likely to occur beneath a sediment cap, and (2) cap-induced changes to biogeochemical conditions in underlying sediment. Future work that could further the current state of knowledge in each of these areas is outlined below.

The use of passive sampling techniques, including DGT to quantify mercury availability

The fraction of the dissolved mercury pool available for methylation is critical understanding the production of methyl mercury in sediments (Benoit et al. 2001, Drott et al. 2007, Hammerschmidt et al. 2003), and this fraction may change considerably over small distance scales in sediment (Chapter 4). In this research the available fraction was quantified using calculations from speciation models and measurements for dominant mercury ligands (Benoit et al. 1999). Although this method is currently the most sophisticated approach to defining availability of inorganic mercury to methylating microbes (Fitzgerald et al. 2007), the uncertainty associated with the nature and thermodynamic definitions of mercury-sulfide and organic complexes makes results dependent upon underlying assumptions (Drott et al. 2007). Rather than making calculations using uncertain thermodynamic data, an alternative method is to directly quantify labile, or available mercury in sediment porewater. An operationally defined

approach to estimating the labile fraction, or ‘reactive mercury’ is based on the thermodynamics of chemical reduction (Lamborg et al. 2003). This technique, however, requires large sample volumes for environmentally relevant detection limits and this restricts its applicability to measuring sediment porewater concentrations with high resolution.

A promising alternative to these approaches that has been applied in sediment is DGT (Diffusive Gradient –Thin Film). DGT uses a resin designed to efficiently bind divalent metals in order to quantify very low dissolved concentrations based on rates of diffusion through a gel layer of known thickness (Zhang and Davidson, 1995). Divis et al. 2005 applied resins with different binding efficiencies for mercury to quantify a fraction of the dissolved mercury pool associated with strong and weak ligands. Although this technique is also operationally defined, it has the advantage of pre-concentrating mercury so that low detection limits can be achieved. By changing the thickness of the diffusive gel or the properties of the mercury-binding resin, the slower rates of diffusion for mercury bound to large organic molecules could be used to quantify a shift from organic to sulfide dominated speciation. DGT has the potential to directly quantify changes in dissolved mercury speciation in sediment, and could be used to achieve high resolution information about mercury speciation near steep sulfide gradients in sulfidic sediments.

Further characterization of cap-induced biogeochemical changes in other sediment systems and with other capping material

The results presented in Chapter 5 showed an upward translation in the location of sulfate reduction that was similar in magnitude to the thickness of the capping layer. The magnitude of the transition in microbial communities present in sediment will be

dependent upon the bulk geochemistry of the natural environment as well as the bulk geochemistry of capping material. Based on a basic understanding of diagenetic processes one can assume that a capping layer in low organic, iron dominated system will not encourage the onset of sulfate reduction in underlying sediment as quickly as that observed in Chapter 3 for a high organic sulfate dominated system. An investigation of the contaminant-related effects of cap-induced biogeochemical changes at ongoing capping demonstration sites for either mercury or another contaminant, would be the next step in moving the findings of this research towards applicability in cap design and monitoring. Active capping material such as zero valent iron and activated carbon have been proposed to encourage the degradation or sequestration of organic contaminants, and the effects of these materials on biogeochemical processes in underlying sediment should be considered.

Transport/partitioning/methylation of mercury and methyl mercury in capping material

The research presented here focused on characterizing the production of methyl mercury in sediment underlying an in-situ cap and these conditions will provide a lower boundary condition for transport through a cap. If the physical integrity of a confinement capping layer remains intact, transport of mercury from underlying sediment will be limited by movement with pore fluid. Mercury's strong association with organics ($\log K_D = 3.5-5.5$, Fitzgerald et al. 2007) makes it likely that a capping material containing even a modest organic content (1-5%) would provide enough sorptive capacity to delay the flux of mercury to the overlying water for a considerable time (10s-100s of years, Thoma et al. 1993) in diffusive-dominated environments. In advective systems, however, the transport of mercury would be greatly accelerated (Liu et al. 2001) and the

partitioning characteristics of capping material may need to be tailored to more efficiently scavenge mercury from the dissolved phase. Several companies have begun manufacturing specially formulated materials to efficiently trap mercury in the aqueous phase. An investigation of the equilibrium partitioning properties and sorption capacity should be characterized with laboratory and field-scale experiments to ascertain their potential effectiveness in containing mercury.

Appendix A: Supporting Information for Chapter 3

A.1 RADIOLABELED SULFATE REDUCTION RATE ASSAY

Radiolabeled $^{35}\text{SO}_4^{2-}$ reduction rates were performed based on the method outlined in Ullrich et al. 1997. An aliquot of 4mL homogenized sediment slurry material was placed in a 125mL serum bottle along with an empty 12x27mm test tube and sealed under a N_2 atmosphere with 1cm thick butyl rubber stoppers (Bellco Glass Inc.). Using a gas-tight syringe, 300uL of $\sim 3\text{uCi/mL}$ $^{35}\text{SO}_4^{2-}$ was injected through the rubber stopper and the incubations left stationary for 48 hours. After this incubation period, fresh batches of acidic chromium and alkaline zinc acetate solutions were prepared using the method described by Burton et al. 2008. Briefly, a 50% Cr(III) solution in 32% HCl was warmed and added to a N_2 flushed bottle containing 20% (mass:volume) zinc shot (Alfa Aesar). A 20% zinc acetate solution was mixed 1:4 with 2N NaOH for the trapping solution. The alkaline zinc acetate solution (2.5mL) was injected into the inner vial through the butyl rubber stopper with a syringe and subsequently, 12mL of the acidic chromium solution was injected to the sediment slurry to halt the production of $^{35}\text{S}^{2-}$ or $^{35}\text{S}^0$ and release the reduced sulfur for trapping in the zinc acetate solution. The bottles were placed on a shaker table (150RPM) for 48 hours after which the inner vial was removed and Zn^{35}S in the trapping solution quantified by scintillation counting (Perkin Elmer Ultima Gold XR scintillation fluid).

Although substantial and consistent reductions in sulfate concentrations were observed in the incubations (Figure 3.4), the SRR assays gave minimal rates of sulfate reduction for all except the fully reduced HO and MO incubations. The results of linear regressions for sulfate observations are compared to measurements from SRR assays in Table A.1 in Appendix A. Conditions during the SRR assay were slightly different than

those present in the incubations, however, the consistently large differences observed between sulfate depletion and SRR assays (Table A.1) suggest that the assay was ineffective in characterizing sulfate reduction. A thorough analysis of the quantified sulfate reduction rate and method detection limits is presented in Figure A.1 in Appendix A.

Ullrich et al. 1997 suggest that an extended extraction period may be necessary for complete recovery of materials containing sulfur solids that are resistant to acidic chromium extraction (Ullrich et al. 1997), and it is possible that the incomplete recovery of sulfur from the SRR assays is the reason for low estimates of sulfate reduction. A thorough time-course analysis of the kinetics of release and trapping of reduced ^{35}S was not performed; however, one extraction with the MO slurries was allowed to proceed for close to 96 hours as opposed to 48 hours and consistently higher rates were found during this assay. The mildly reduced incubations for HO and MO environments were amended with high concentrations Fe^{2+} and it is possible that the Fe^{2+} interfered with the volatilization of reduced sulfide, although the 32% hydrochloric acid should have been sufficient to dissolve most FeS minerals (Poulton et al. 2005). Another possibility is that the precipitation of ZnS on the surface of the inner vial resulted in incomplete transfer to scintillation fluid, although repeated rinsing and scraping of solids from the inner vial did not increase scintillation counts and some vials were even broken and placed entirely in the scintillation counting vial with fluid. Due to the apparently biased low rates measured with the SRR assay, sulfate reduction rates for each condition were estimated directly using the decrease in sulfate concentrations over time in the sediment incubations. These results are illustrated in Figure 3.4 and summarized in Table A.1 in Appendix A.

A.2 SULFATE REDUCTION RATE SUMMARY

Table A.1 Summary of sulfate reduction rates obtained using linear regression for observed sulfate concentrations, in uM/day. Comparison with rates obtained with $^{35}\text{SO}_4^{2-}$ assays.

	SRR-Regression			SRR-Assay	
	Rate [uM/day]	Date Range	R2	Rate [uM/day]	StDev
LO- fully-red	18	1-46	0.82	2.15	1.19
LO-mild-red	30	1-64	0.94	1.17	0.76
LO- subox	5.9	1-64	0.54	-0.011	0.020
HO- fully-red	90	1-38	0.92	27.89	10.59
HO- mild-red	111	5-38	0.92	0.57	0.42
HO- subox	101	1-23	0.98	0.38	0.55
MO-fully-red	42	1-61	0.88	17.50	2.74
MO- mild-red	62	1-61	0.98	1.21	1.09
MO- subox	52	5-38	0.99	0.08	0.04

Sulfate Reduction Rate Summary

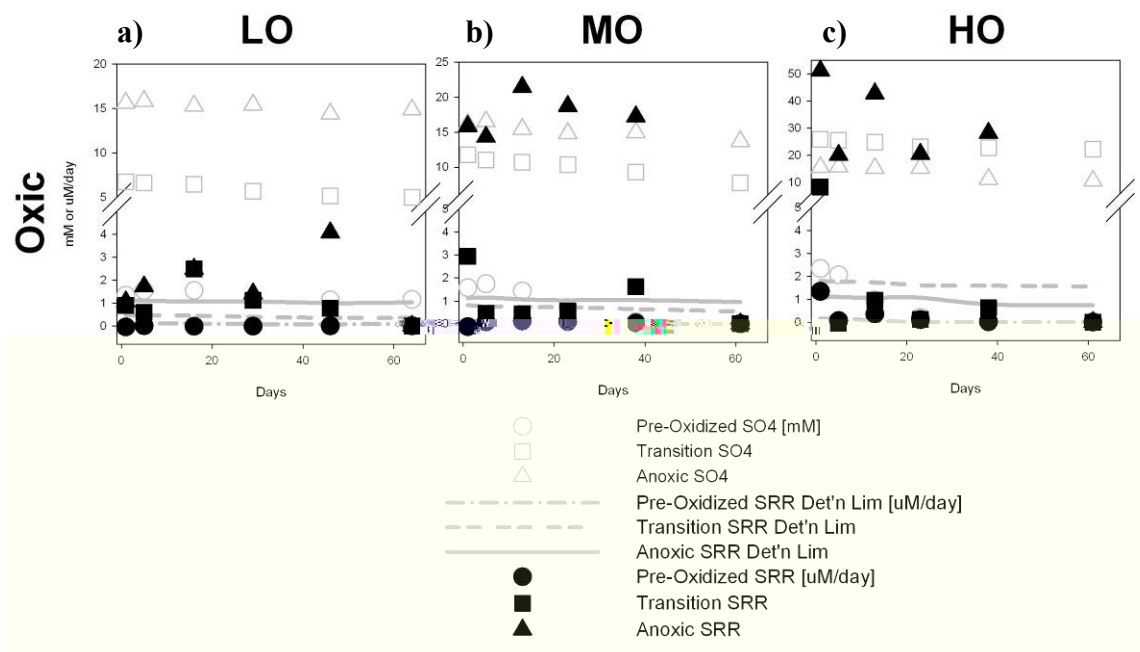


Figure A.1 Summary of sulfate reduction rate measurements with radiolabeled sulfate. measured sulfate concentration (open symbols), detection limit for sulfate reduction rate (lines, based on minimum count of 250DPM), and sulfate reduction rate (closed symbols).

A.3 ADDITIONAL SPIKED MERCURY RESULTS

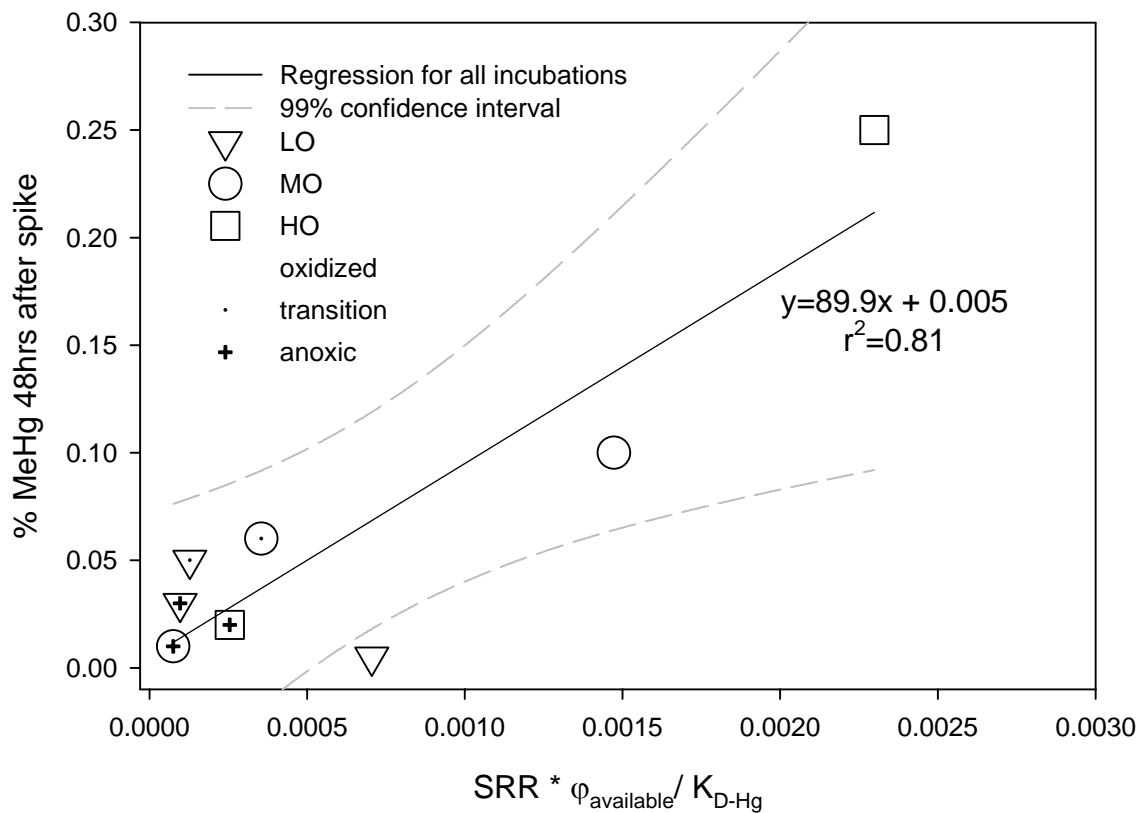


Figure A.2 Model for % methyl mercury 48 hours after additional spike considering sulfate reduction rate, available aqueous fraction (Model B'), and partitioning to the solid phase.

Table A.2 Summary of regression parameters for alternative speciation models.

		ALL	LO	MO	HO	
%MeHg vs. [SRR * φ * Hg _{diss}]	Model A	m	350	4780	-2010	-10500
		b	0.79	0.2	0.95	6.1
		r2	0.003	0.85	0.88	N/A
	Model B	m	2880	5050	-2540	-43600
		b	0.25	0.15	1.1	24.8
		r2	0.22	0.84	0.78	N/A
	Model B'	m	362	1100	154	393
		b	0.14	-0.03	0.39	0.05
		r2	0.97	0.97	0.98	N/A

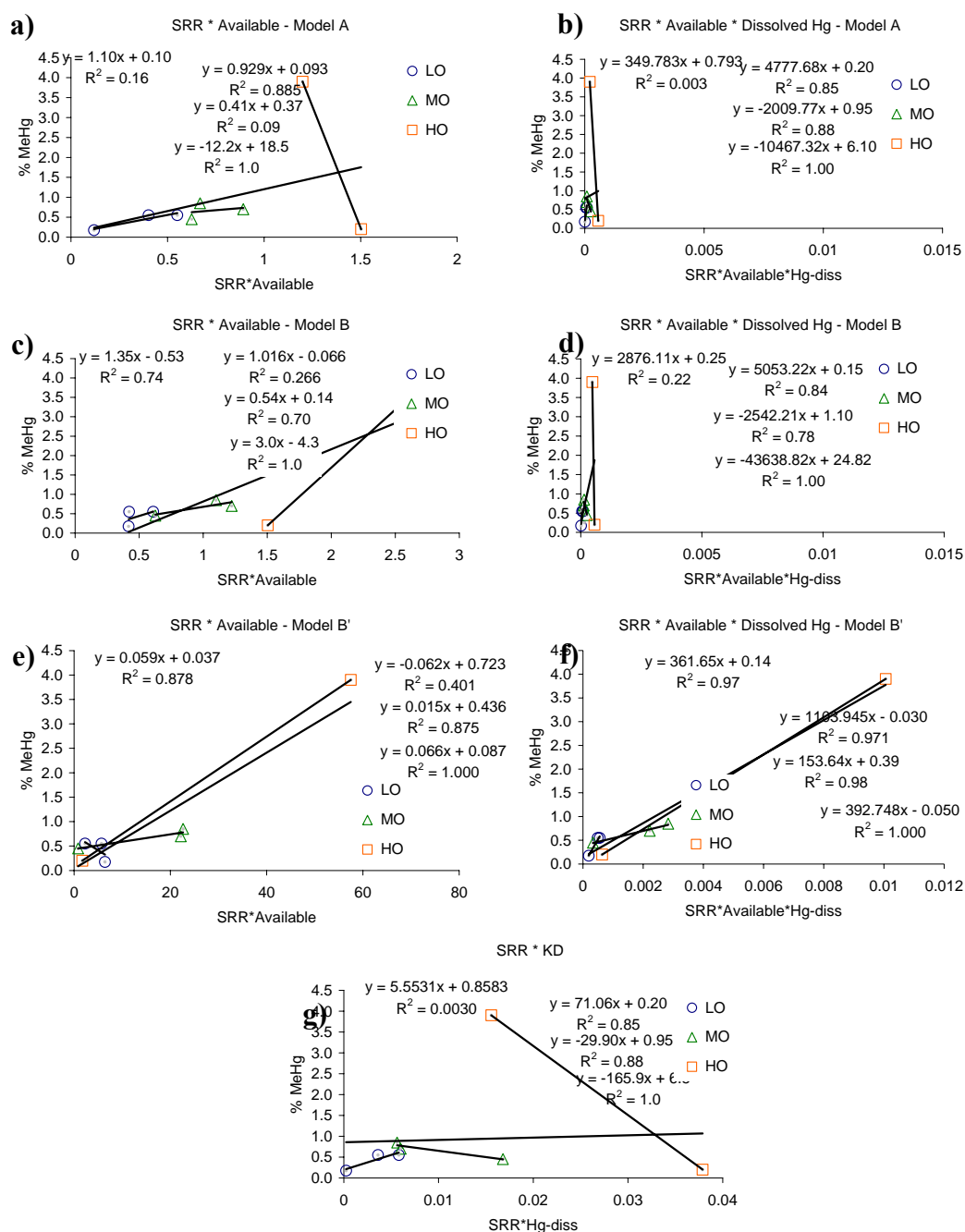


Figure A.3 Alternative models considering speciation calculated with Model A and Model B (panels b,d). Regressions with only two of the geochemical parameters from the model of Equation 4.3. SRR & availability (panels a, c, e), and SRR & Kd (panel g).

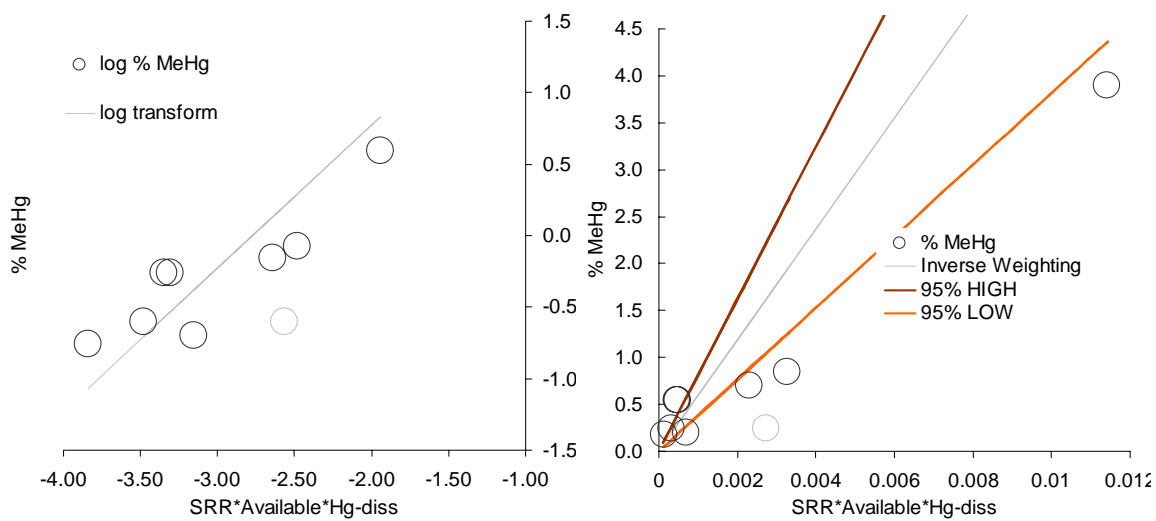


Figure A.4 Alternative weighted regressions for minimizing the weight of the large methyl mercury point. (a) log-log regression (slope = 595, 560 without outlier), (b) weighted least squares regression (slope = 590, 520 without outlier) and 90% confidence intervals. Weights were calculated using the reciprocal of the power of the independent variable which minimized the error of the dependent variable.

Appendix B: Supporting Information for Chapter 4

B.1 GEOCHEMICAL PROFILES FOR REPLICATE CORES

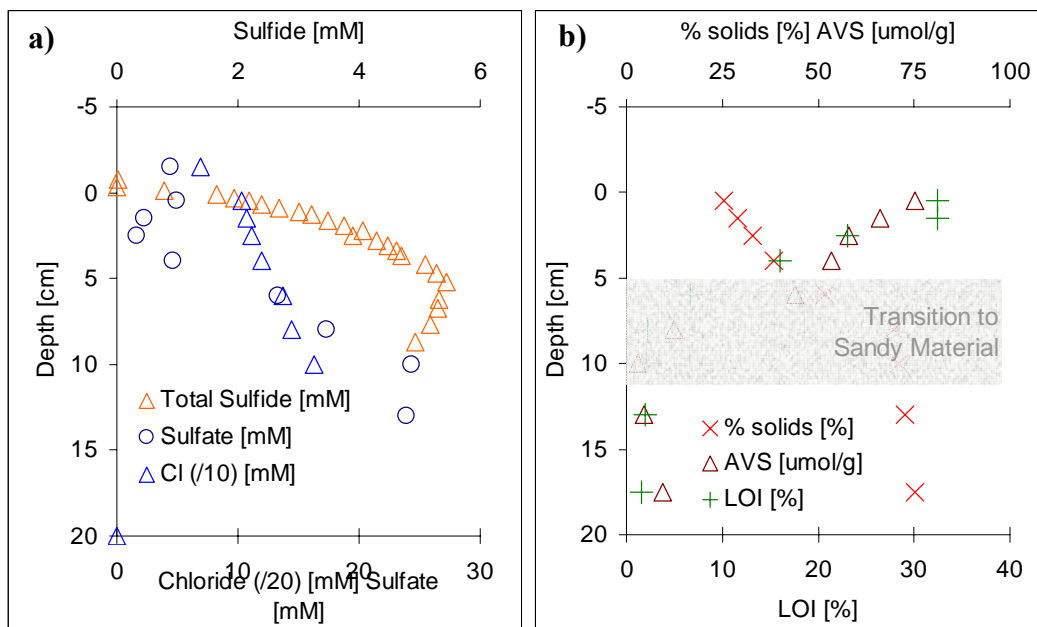


Figure B.1 Geochemical profiles for replicate core in salt marsh

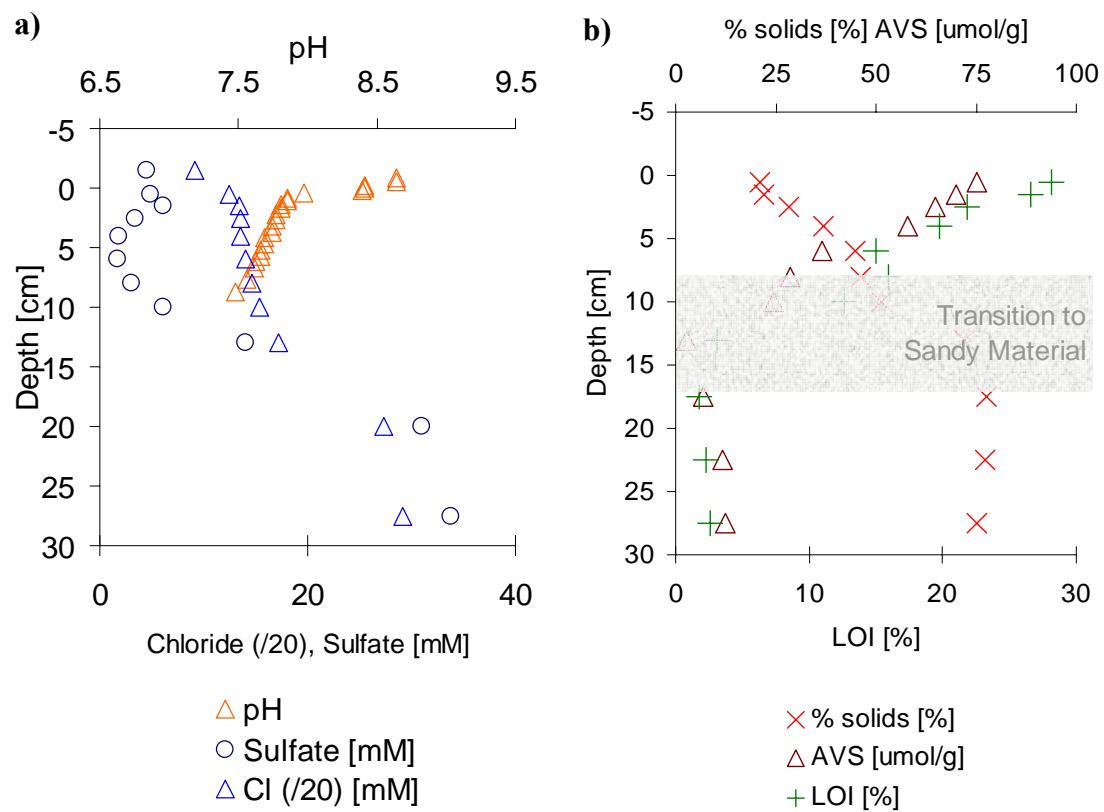


Figure B.2 Geochemical observations for full 30-cm of core described in Chapter 4.

Table B.1 Reactions, constituents, rate, and equilibrium constants included in modeling Salt Marsh sediment for Chapter 4.

DESCRIPTION	STOICHIOMETRY	RATE	UNITS	SOURCE
<i>Primary Reactions (biological organic matter degradation)</i>				
Aerobic Respiration	$O_2 + POC^a = DIC^a$	400,100,0.5 ^b	uM/yr,uM,uM	Calibrated
Nitrate Reduction	$NO_3^- + POC = DIC$	150, 20, 6	uM/yr,uM,uM	Calibrated
Manganese Reduction	$Mn^{4+} + POC = DIC + Mn^{2+}$	0.2, 1, 0.001	uM/yr, umol/g	Ref. 27
Iron Reduction	$Fe^{4+} + POC = DIC + Fe^{2+}$	0.032, 1, 0.005	uM/yr, umol/g	Ref. 27
Sulfate Reduction	$SO_4^{2-} + POC = DIC + HS^-$	250, 100, 50	uM/yr,uM,uM	Calibrated
Methanogenesis	$POC = DIC + CH_4^+$	0.05, N/A, N/A	uM/yr,-,-	
POC		N/A, 0.1, N/A	-,umol/g,-	
<i>Oxidation/Reduction Reactions</i>				
By O_2				
Mn^{2+}	$Mn^{4+} + 0.5O_2 = Mn^{2+}$	4.6	(mol/L) ⁻¹ yr ⁻¹	Ref. 27
Fe^{2+}	$Fe^{4+} + 0.25O_2 = Fe^{2+}$	6.3x10 ⁴	(mol/L) ⁻¹ yr ⁻¹	Sensitivity Analysis
HS^-	$SO_4^{2-} + 2O_2 = HS^-$	2.0x10 ⁵	(mol/L) ⁻¹ yr ⁻¹	Ref. 27
CH_4^+	$CH_4^+ + 2O_2 = DIC$	1.0x10 ¹⁰	(mol/L) ⁻¹ yr ⁻¹	
$MnS_{(s)}$	$MnS_{(s)} + 2O_2 = Mn^{2+} + HS^-$	3.0x10 ⁵	(mol/L) ⁻¹ yr ⁻¹	
$FeS_{(s)}$	$FeS_{(s)} + 2O_2 = Fe^{2+} + HS^-$	3.0x10 ⁵	(mol/L) ⁻¹ yr ⁻¹	Ref. 27
$R-Mn_{(s)}^{2+}$ ^a	$R-Mn_{(s)}^{2+} + O_2 = Mn^{2+}$	2.1x10 ⁷	(mol/L) ⁻¹ yr ⁻¹	Ref. 27
$R-Fe_{(s)}^{2+}$ ^a	$R-Fe_{(s)}^{2+} + O_2 = Fe^{2+}$	4.8x10 ⁵	(mol/L) ⁻¹ yr ⁻¹	Ref. 27
By Mn^{2+}				
Fe^{2+}	$0.5Mn^{4+} + Fe^{2+} = 0.5Mn^{2+} + Fe^{3+}$	1.0x10 ⁶	(mol/L) ⁻¹ yr ⁻¹	Ref. 27
HS^-	$4Mn^{4+} + HS^- = 4Mn^{2+} + SO_4^{2-}$	8.0x10 ⁵	(mol/L) ⁻¹ yr ⁻¹	Ref. 27
By Fe^{2+}				
HS^-	$Fe^{4+} + HS^- = Fe^{2+} + SO_4^{2-}$	1.0x10 ³	(mol/L) ⁻¹ yr ⁻¹	Ref. 27
<i>Precipitation/Dissolution</i>				
Manganese-Sulfide	$Mn^{2+} + HS^- = MnS_{(s)} + H^+$	10 ^{3.1} , 0.1 ^c	mol/L, umol/g/yr	Ref. 22, Calibrated
Iron-Sulfide	$Fe^{2+} + HS^- = FeS_{(s)} + H^+$	10 ^{-4.2} , 0.1 ^c	mol/L, umol/g/yr	Ref. 22, Calibrated
<i>Solid-phase Sorption</i>				
Manganese sorption	$Mn^{2+} = R-Mn_{(s)}^{2+}$	3.0, 150 ^d	L/kg, L/g/day	Calibrated
Iron sorption	$Fe^{2+} = R-Fe_{(s)}^{2+}$	800, 150 ^d	L/kg, L/g/day	Calibrated

^a abbreviations: POC–Particulate Organic Carbon; DIC–Dissolved Inorganic Carbon; ‘R-’–Organo & solid oxide -metal complexes

^b Maximum utilization rate[uM/day], Half saturation constant [uM or umol/g], Threshold concentration [uM or umol/g], respectively

^c K_{sp} [mol/L], Precipitation rate [umol/g/year] K_d [L/kg], Adsorption rate [L/g/day]

^d K_d [L/kg], Adsorption rate [L/g/day]

Table B.2 Initial Conditions

Primary Constituents	Control	Anoxic	Cap	Comment
POC	250 $\mu\text{mol/g}$			
O ₂	0.000 mM			
NO ₃	0.000 mM			
Mn ⁴⁺	0.000 $\mu\text{mol/g}$			
Fe ³⁺	0.00 $\mu\text{mol/g}$			
SO ₄ ²⁻	1.0 mM			
HCO ₃ ⁻	0.46 mM			
Mn ²⁺	0.08 mM			
Fe ²⁺	0.042 mM			
HS ⁻	0.0 mM			
CH ₄	0.0 mM			
MnS _(s)	0.01 $\mu\text{mol/g}$			
FeS _(s)	2.5 $\mu\text{mol/g}$			
R-Mn ²⁺	0.0 $\mu\text{mol/g}$			
R-Fe ²⁺	4.0 $\mu\text{mol/g}$			

Table B.3 Boundary Conditions

Primary Constituents	Control	Anoxic	Cap	Comments
POC	1800 $\mu\text{mol/cm}^2/\text{yr}$			
O ₂	0.13 mM			
NO ₃	0.02 mM			
Mn ⁴⁺	1.0 $\mu\text{mol/cm}^2/\text{yr}$			
Fe ³⁺	2.0 $\mu\text{mol/cm}^2/\text{yr}$			
SO ₄ ²⁻	9.0 mM			
HCO ₃ ⁻	0.46 mM			
Mn ²⁺	0.0 mM			
Fe ²⁺	0.0 mM			
HS ⁻	0.0 mM			
CH ₄	0.0 mM			
FeS _(s)	2.0 $\mu\text{mol/cm}^2/\text{yr}$			
TOTH	1.65E ⁻⁵			
R-Mn ²⁺	2.0 $\mu\text{mol/cm}^2/\text{yr}$			
R-Fe ²⁺	2.0 $\mu\text{mol/cm}^2/\text{yr}$			

Table B.4 Other Parameters

	Control	Anoxic	Cap
Deposition velocity	0.5 cm/year		
Particle diffusion	9.6cm ² /year		
Domain length	10.0 cm		
Porosity	f(depth)		
Diffusive boundary	0.2 cm		

B.2 EFFECT OF pH ON FRACTION UNCHARGED (AND CONSEQUENTLY AVAILABLE)

Assuming that only 2 competing ligands, the ratio of the uncharged ligand to charged ligand can be written:

$$\frac{f_u}{f_c} = \frac{\frac{K_u L_u^{n_u}}{H^{m_u}}}{\frac{K_c L_c^{n_c}}{H^{m_c}}} = \frac{K_u}{K_c} \frac{L_u^{n_u}}{L_c^{n_c}} \frac{H^{m_c}}{H^{m_u}}$$

An increase in this ratio for a small decrease in pH, is equivalent to an increase in fraction available. For a small change in pH, the fractions can be re-written:

$$\frac{f'_u}{f'_c} = \frac{K_u}{K_c} \frac{L_u^{n_u}}{L_c^{n_c}} \frac{(H + \Delta H)^{m_c}}{(H + \Delta H)^{m_u}}$$

Assuming that the change in pH does not affect the ligand concentrations, the new fraction can be written as a function of the old fraction and the change in pH:

$$\frac{f'_u}{f'_c} = \frac{(H + \Delta H)^{m_c}}{(H + \Delta H)^{m_u}} \frac{H^{m_u}}{H^{m_c}} \frac{f_u}{f_c}$$

or

$$\frac{f'_u}{f'_c} = \frac{\left(\frac{H}{(H + \Delta H)} \right)^{m_u}}{\left(\frac{H}{(H + \Delta H)} \right)^{m_c}} \frac{f_u}{f_c} = \frac{f_u}{f_c} \left(\frac{(H + \Delta H)}{H} \right)^{(m_c - m_u)}$$

The above equation states that the ratio of the fraction will increase with a decrease in pH $(H + \Delta H) / H > 1$ if m_u is less than m_c .

A parallel (but more complex) argument can be made when considering the pH-induced changes to ligand concentrations, but is not included here for brevity.

B.3 SIMULATION OF DIAGENETIC AND METHYL MERCURY IMPACTS OF CAPPING

The results from diagenetic simulations for the effects of in-situ capping and the concomitant effects on mercury methylation are shown in Figures B.3 and B.4 for a high organic system and a low organic system, respectively. A discussion of the results is found in the text of Chapter 4.

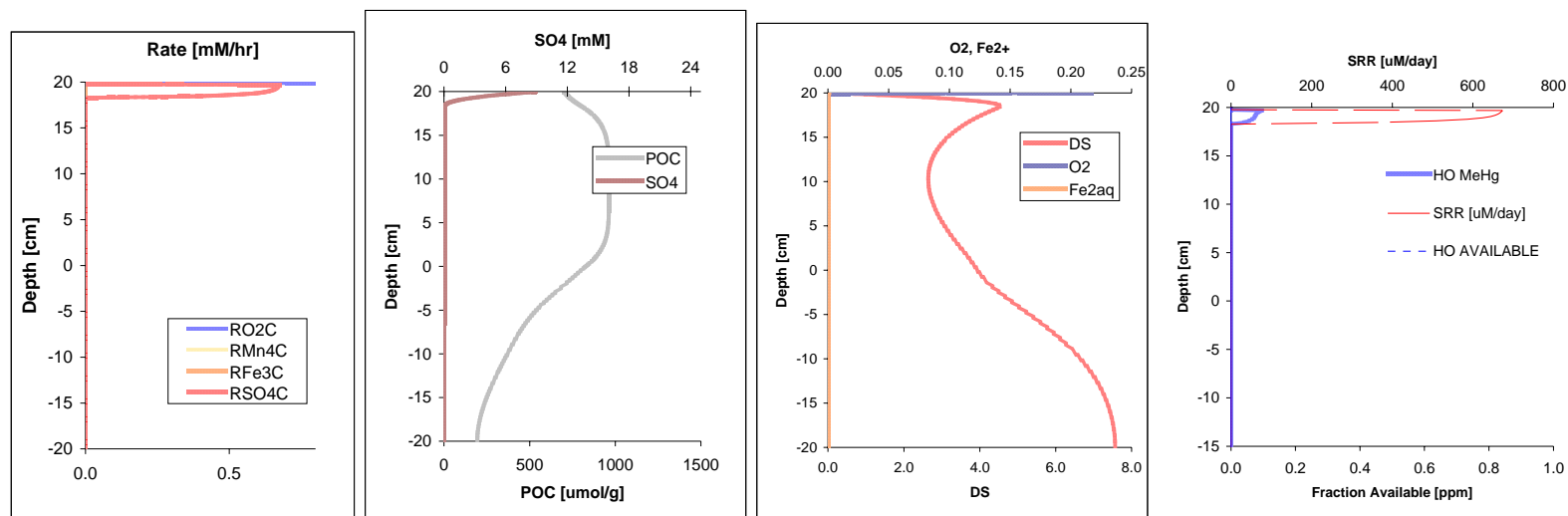


Figure B.3 Diagenetic modeling results and predicted methyl mercury according to Equation 3.3 for high organic capping simulation in high organic environment. Zero represents interface between 20cm capping layer and underlying sediment. (a) bacterial carbon oxidation rates, (b) sulfate and organic substrate concentration, (c) dissolved sulfide, oxygen and dissolved ferrous iron, (d) available mercury, predicted methyl mercury, and sulfate reduction rate.

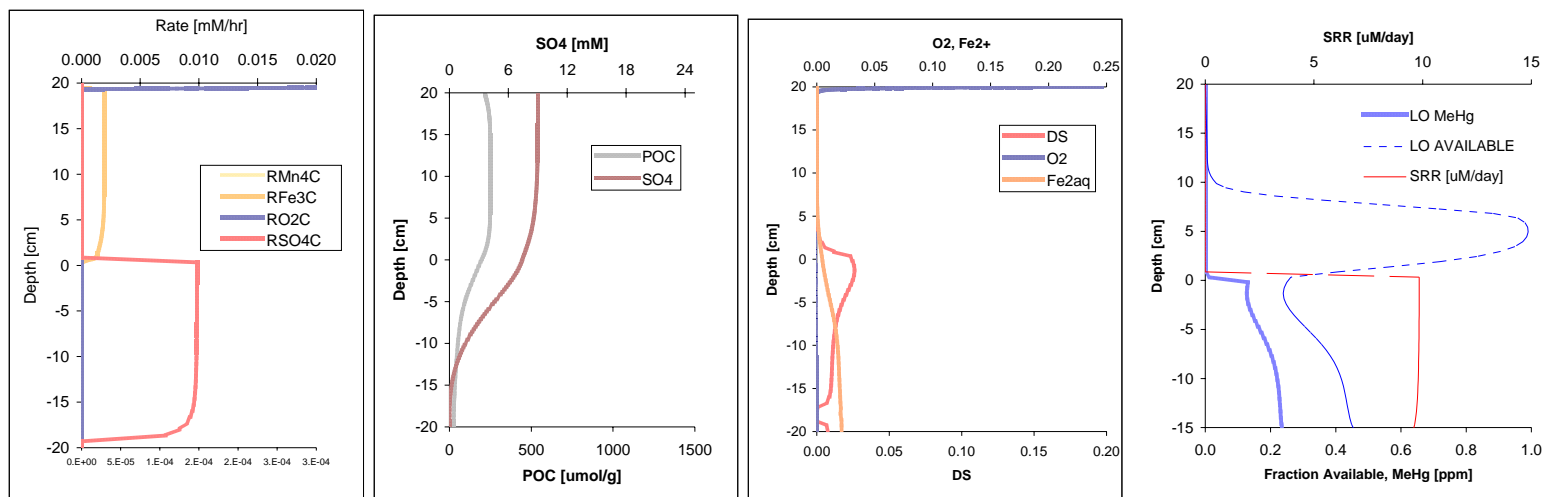


Figure B.4 Diagenetic modeling results and predicted methyl mercury according to Equation 3.3 for high organic capping simulation in low organic environment. Zero represents interface between 20cm capping layer and underlying sediment. (a) bacterial carbon oxidation rates, (b) sulfate and organic substrate concentration, (c) dissolved sulfide, oxygen and dissolved ferrous iron, (d) available mercury, predicted methyl mercury, and sulfate reduction rate.

Appendix C: Supporting Information for Chapter 5

C.1 MICROCOSM SCHEMATIC

The acrylic sediment microcosms used in this study have a bottom section to hold sediment that measures 15x5x7cm. The water column is supported by a 3cm weir and measures 25x5x6cm.

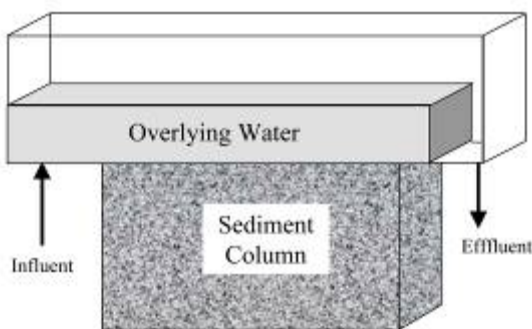


Figure C.1 Schematic of experimental microcosms. 7.5cm sediment depth with 3cm overlying water.

C.2 LABORATORY QA/QC RESULTS

Ongoing precision and recovery results fell within standard operating procedures as defined by EPA Method 1630. Although small sample mass was used, the concentration in all samples was above the method reporting limit adjusted for the use of lower sample mass. Results reported are only for analyses with our samples. Recovery of reference material (CC-580) averaged 87% during the analysis of our samples (n=3). The RPD of duplicate analyses of our samples averaged 11% (n=3), and MS/MSD recovery and RPD averaged 108% and 8% respectively (n=6,3).

C.3 TOTAL MERCURY CONCENTRATIONS

Little variability in total mercury concentration was observed in both uncapped and capped microcosms. This suggests that the observed differences in methyl mercury concentration (Figure C.2) were due to differences in methyl mercury production rather than differences in total mercury concentrations.

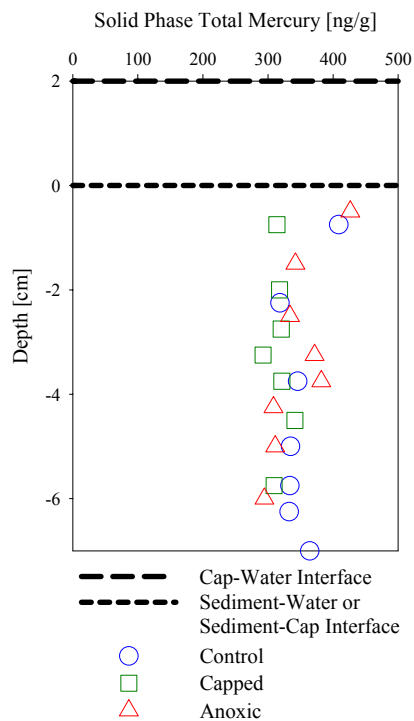


Figure C.2 Total mercury concentrations in control and capped microcosms

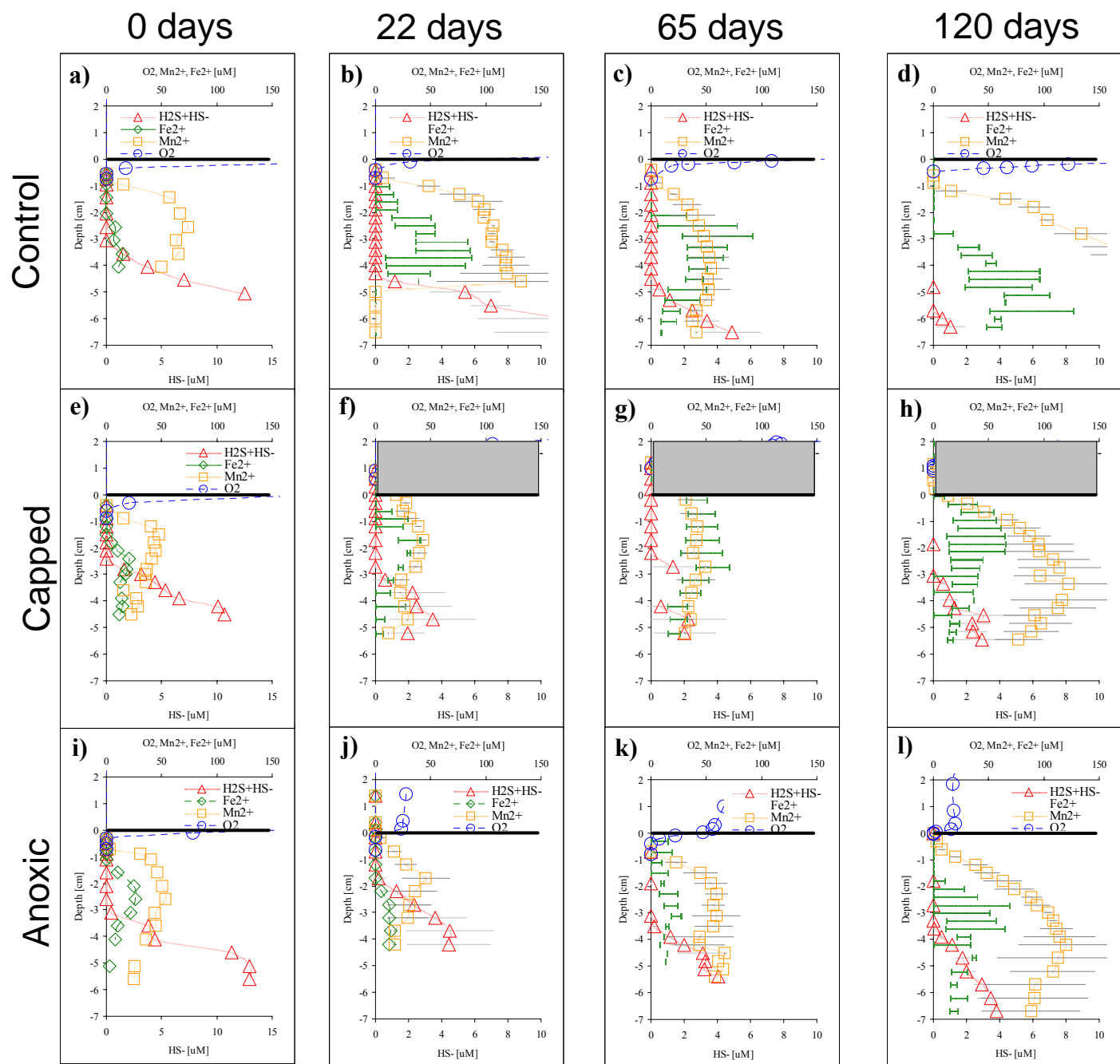


Figure C3 Timeline of development of geochemical profiles in three microcosms

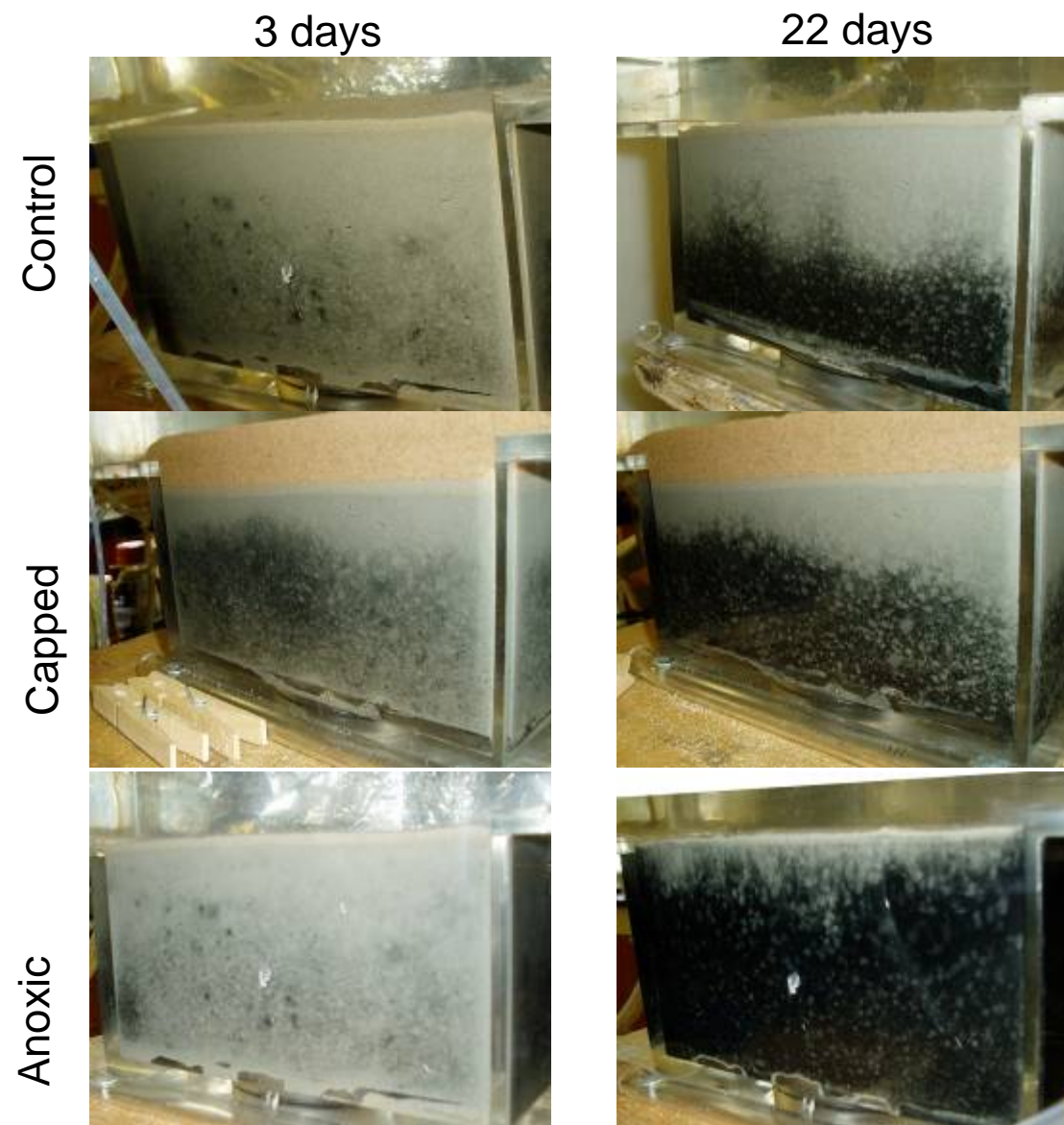


Figure C4 Visual observations of geochemical redox zones in microcosms at 3 and 22 days

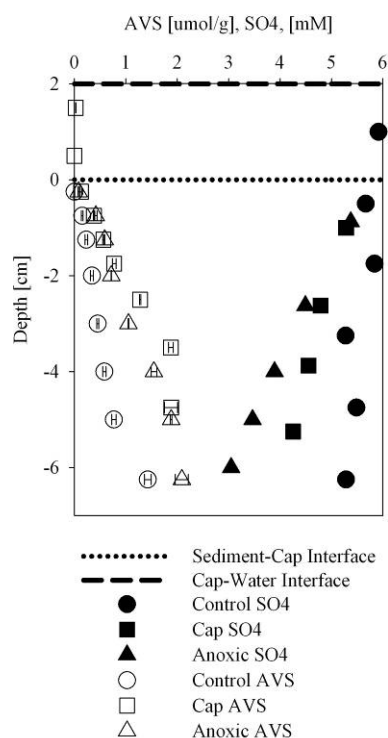


Figure C.5 Depth profiles of SO_4^{2-} and AVS concentrations in control, capped and anoxic microcosms at the close of experiments

Additional evidence of increased sulfate reduction in capped and anoxic microcosms was observed in solid-phase AVS and porewater sulfate concentrations. Figure S5 shows results from cores taken at 4 months. Error bars on AVS measurements lie within the open symbols, however, limited sample volume allowed only one SO_4^{2-} measurement to be obtained at each depth. In the control microcosm, AVS remains low ($<1 \mu\text{mol/g}$) at depths less than 6cm, and little sulfate depletion is observed. However, in both capped and anoxic microcosms, AVS and SO_4^{2-} observations are consistent with increased sulfate reduction at depths between 2-5cm. On a mole per volume basis, the increase in AVS in the capped and anoxic microcosms was greater than the reduction in sulfate (1.8 vs. $0.8 \mu\text{mol/cm}^3$; bulk density 1.2g/cm^3 , porosity: 0.5). The continued diffusion of sulfate into the sediment, driven by the observed concentration gradient, followed by biological reduction and precipitation to immobile metal sulfides typically

leads to a buildup of solid-phase sulfides in saltwater sediments. Iron concentrations observed at ~20-100µM in all microcosms are sufficient to promote iron-sulfide precipitate formation in the presence of dissolved sulfide at pH 7-8 ($\text{Fe}^{2+} + \text{HS}^- = \text{FeS}_{(s)} + \text{H}^+$; $\log K_{\text{sp}} = -4.2$ (28)). The depletion of AVS near the sediment surface in all microcosms, including the capped/anoxic microcosms, is likely due to the oxidation of metal sulfides by oxygen during the initial 3 weeks of oxic overlying water conditions before the initiation of capped/anoxic conditions.

C.4 MODEL FORMULATION

The constitutive equations for dissolved and solid constituents, as outlined by Boudreau are presented below. Specific model reactions, stoichiometry, and rates are presented in Table C.2. Initial and boundary conditions as well and other model parameters are presented in Tables C.3-5.

First order finite difference schemes for uneven grid spacing were substituted for all spatial derivatives. The Method of Lines was used to solve the resulting set of ordinary differential equations as an initial value problem.

$$\begin{aligned} \varphi \frac{\partial C}{\partial t} &= D \frac{\partial}{\partial x} \left(\frac{\varphi}{\theta^2} \frac{\partial C}{\partial x} \right) - \frac{\partial(\varphi u C)}{\partial x} + R_{xn} \\ \theta^2 &= \varphi^{-p} \\ \frac{\partial C}{\partial t} &= \frac{1}{\varphi} \left[D \frac{\partial}{\partial x} \left(\varphi^{p+1} \frac{\partial C}{\partial x} \right) - \frac{\partial(\varphi u C)}{\partial x} + R_{xn} \right] \\ \frac{\partial C}{\partial t} &= \frac{D}{\varphi} \left[\varphi^{p+1} \frac{\partial^2 C}{\partial x^2} + (p+1) \varphi^p \frac{\partial \varphi}{\partial x} \frac{\partial C}{\partial x} \right] - \frac{1}{\varphi} \left(\varphi u \frac{\partial C}{\partial x} + \varphi \frac{\partial u}{\partial x} C + \frac{\partial \varphi}{\partial x} u C \right) + \frac{1}{\varphi} (+ R_{xn}) \\ \frac{\partial C}{\partial t} &= \frac{D}{\varphi} \left[\varphi^{p+1} \frac{\partial^2 C}{\partial x^2} + \left((p+1) \varphi^p \frac{\partial \varphi}{\partial x} \right) \frac{\partial C}{\partial x} \right] - \left[u \frac{\partial C}{\partial x} + C \left(\frac{u}{\varphi} \frac{\partial \varphi}{\partial x} + \frac{\partial u}{\partial x} \right) \right] + \frac{1}{\varphi} (+ R_{xn}) \end{aligned}$$

where:

- φ = function of depth, calibrated to observations
- $p = 2.0$
- $u = 0.0$ [cm/day]
- D = molecular diffusivity of species [cm²/day]
- R_{xn} = as defined below [umol/cm³/day]

For solid-phase constituents:

$$\begin{aligned}\varphi_s \frac{\partial B}{\partial t} &= \frac{\partial}{\partial x} \left(\varphi_s D_B \frac{\partial B}{\partial x} \right) - \frac{\partial (\varphi_s w B)}{\partial x} + \varphi_s R_{xn} \\ \frac{\partial B}{\partial t} &= \frac{1}{\varphi_s} \left[\frac{\partial}{\partial x} \left(\varphi_s D_B \frac{\partial B}{\partial x} \right) - \frac{\partial (\varphi_s w B)}{\partial x} + \varphi_s R_{xn} \right] \\ \frac{\partial B}{\partial t} &= \frac{1}{\varphi_s} \left[\varphi_s D_B \frac{\partial^2 B}{\partial x^2} + \varphi_s \frac{\partial D_B}{\partial x} \Big|_x \frac{\partial B}{\partial x} + \frac{\partial \varphi_s}{\partial x} \Big|_x D_B \frac{\partial B}{\partial x} \right. \\ &\quad \left. - \left(\varphi_s w \frac{\partial B}{\partial x} + \varphi_s \frac{\partial w}{\partial x} \Big|_x B + \frac{\partial \varphi_s}{\partial x} \Big|_x w B \right) + \varphi_s R_{xn} \right] \\ \frac{\partial B}{\partial t} &= D_B \frac{\partial^2 B}{\partial x^2} + \left(\frac{\partial D_B}{\partial x} \Big|_x + \frac{D_B}{\varphi_s} \frac{\partial \varphi_s}{\partial x} \Big|_x \right) \frac{\partial B}{\partial x} - \left[w \frac{\partial B}{\partial x} + \left(\frac{w}{\varphi_s} \frac{\partial \varphi_s}{\partial x} \Big|_x + \frac{\partial w}{\partial x} \Big|_x \right) B \right] + R_{xn}\end{aligned}$$

where:

- φ_s is 1- φ [g/cm³]
- w , the particle burial velocity, was set to 0.0 [cm/day]
- D_B was set to 7.5x10⁻⁸ [cm²/day]

C.5 REACTIONS

Reactions (the term “Rxn”) should be defined on a total volume basis $\mu\text{mol}/\text{cm}^3_{\text{T}}$ /day for solid and $\text{mmol}/\text{L}_{\text{T}}/\text{day}$ for liquid. In the actual code, the RHS of the mass balance for each constituent is divided through by either ψ [$\text{L}_{\text{water}}/\text{L}_{\text{total}}$] or ψ_s [$\text{g}_{\text{sed}}/\text{cm}^3_{\text{tot}}$] and care must be taken in defining the units of reaction terms in the code. Representative equations used for each type of reaction are shown below.

PO – Primary Oxidation of organic matter

SO – Secondary oxidation/reduction reactions

PREC – precipitation of metal-sulfides

SORB – sorption of metals to solid phase

$$R_{xn} = R_{PO} + R_{SO} + R_{PREC} + R_{SORB}$$

$$R_{PO}|_{O_2} \left[\frac{mmol}{L_T - day} \right] = k_{max_{O_2}} \left[\frac{mmol}{L_T - day} \right] \left(\frac{C_{O_2}}{K_{I_{O_2}} + C_{O_2}} \right) \left(\frac{C_{POC}}{K_{I_{POC}} + C_{POC}} \right)$$

$$R_{SO}|_{FeS-O_2} \left[\frac{mmol}{L_T - day} \right] = k_{FeS-O_2} \left[\frac{L_T}{mmol - day} \right] C_{O_2} \varphi \left[\frac{mmol}{L_T} \right] C_{FeS} \varphi_s \left[\frac{umol}{cm^3_T} \right]$$

$$R_{PREC}|_{Fe-S} \left[\frac{mmol}{L_T - day} \right] = k_{prec-FeS} \left[\frac{mmol}{L_T - day} \right] (\Omega_{FeS} - 1) : \Omega_{FeS} = \frac{Fe^{2+} \left[\frac{mmol}{L_w} \right] DS \left[\frac{mmol}{L_w} \right]}{H^+ \left[\frac{mmol}{L_w} \right] K_{sp} \left[\frac{mmol}{L_w} \right]}$$

$$R_{SORB}|_{Fe2} \left[\frac{mmol}{L_T - day} \right] = k_{ads-Fe} \left[\frac{L_w}{g_s - day} \right] \varphi_s \left[\frac{g_s}{cm^3_T} \right] \left[\frac{1000cm^3_T}{L_T} \right] \left(C_{Mn2} \left[\frac{mmol}{L_w} \right] - \frac{C_{Mn2s} \left[\frac{umol}{g_s} \right] \left[\frac{1mmol}{1000umol} \right]}{K_D \left[\frac{L_w}{kg_s} \right] \left[\frac{1kg_s}{1000g_s} \right]} \right)$$

Table C.1 Reactions and constituents included in modeling

DESCRIPTION	STOICHIOMETRY	RATE	UNITS	SOURCE
<i>Primary Reactions (biological organic matter degradation)</i>				
Aerobic Respiration	$O_2 + POC^a = DIC^a$	200,100,0.5 ^b	uM/day,uM,uM	Calibrated
Nitrate Reduction	$NO_3^- + POC = DIC$	30, 20, 6	uM/day,uM,uM	Calibrated
Manganese Reduction	$Mn^{4+} + POC = DIC + Mn^{2+}$	0.2, 1, 0.001	uM/day, umol/g	Ref. 27
Iron Reduction	$Fe^{4+} + POC = DIC + Fe^{2+}$	0.032, 1, 0.005	uM/day, umol/g	Ref. 27
Sulfate Reduction	$SO_4^{2-} + POC = DIC + HS^-$	18, 10, 15	uM/day,uM,uM	Calibrated
Methanogenesis	$POC = DIC + CH_4^+$	0.05, N/A, N/A	uM/day,-,-	
POC		N/A, 0.1, N/A	-,umol/g,-	
<i>Oxidation/Reduction Reactions</i>				
By O_2				
Mn^{2+}	$Mn^{4+} + 0.5O_2 = Mn^{2+}$	4.6	(mol/L) ⁻¹ yr ⁻¹	Ref. 27
Fe^{2+}	$Fe^{4+} + 0.25O_2 = Fe^{2+}$	1.6×10^6	(mol/L) ⁻¹ yr ⁻¹	Sensitivity Analysis
HS^-	$SO_4^{2-} + 2O_2 = HS^-$	2.0×10^5	(mol/L) ⁻¹ yr ⁻¹	Ref. 27
CH_4^+	$CH_4^+ + 2O_2 = DIC$	1.0×10^{10}	(mol/L) ⁻¹ yr ⁻¹	
$MnS_{(s)}$	$MnS_{(s)} + 2O_2 = Mn^{2+} + HS^-$	3.0×10^5	(mol/L) ⁻¹ yr ⁻¹	
$FeS_{(s)}$	$FeS_{(s)} + 2O_2 = Fe^{2+} + HS^-$	3.0×10^5	(mol/L) ⁻¹ yr ⁻¹	Ref. 27
$R-Mn^{2+}_{(s)a}$	$R-Mn^{2+}_{(s)} + O_2 = Mn^{2+}$	2.1×10^7	(mol/L) ⁻¹ yr ⁻¹	Ref. 27
$R-Fe^{2+}_{(s)a}$	$R-Fe^{2+}_{(s)} + O_2 = Fe^{2+}$	1.6×10^8	(mol/L) ⁻¹ yr ⁻¹	Ref. 27
By Mn^{2+}				
Fe^{2+}	$0.5Mn^{4+} + Fe^{2+} = 0.5Mn^{2+} + Fe^{3+}$	1.0×10^4	(mol/L) ⁻¹ yr ⁻¹	Ref. 27
HS^-	$4Mn^{4+} + HS^- = 4Mn^{2+} + SO_4^{2-}$	8.0×10^5	(mol/L) ⁻¹ yr ⁻¹	Ref. 27
By Fe^{2+}				
HS^-	$Fe^{4+} + HS^- = Fe^{2+} + SO_4^{2-}$	1.0×10^3	(mol/L) ⁻¹ yr ⁻¹	Ref. 27
<i>Precipitation/Dissolution</i>				
Manganese-Sulfide	$Mn^{2+} + HS^- = MnS_{(s)} + H^+$	$10^{3.1}$, 0.1 ^c	mol/L, umol/g/yr	Ref. 22, Calibrated
Iron-Sulfide	$Fe^{2+} + HS^- = FeS_{(s)} + H^+$	$10^{-4.2}$, 0.1 ^c	mol/L, umol/g/yr	Ref. 22, Calibrated
<i>Solid-phase Sorption</i>				
Manganese sorption	$Mn^{2+} = R-Mn^{2+}_{(s)}$	3.0, 150 ^d	L/kg, L/g/day	Calibrated
Iron sorption	$Fe^{2+} = R-Fe^{2+}_{(s)}$	800, 150 ^d	L/kg, L/g/day	Calibrated

^a abbreviations: POC–Particulate Organic Carbon; DIC–Dissolved Inorganic Carbon; ‘R-’–Organo & solid oxide -metal complexes

^b Maximum utilization rate[uM/day], Half saturation constant [uM or umol/g], Threshold concentration [uM or umol/g], respectively

^c K_{sp} [mol/L], Precipitation rate [umol/g/year] K_d [L/kg], Adsorption rate [L/g/day]

^d K_d [L/kg], Adsorption rate [L/g/day]

Table C.2 Initial Conditions

Primary Constituents	Control	Anoxic	Cap	Comment
POC	250 $\mu\text{mol/g}$	250	2.5	75% of meas. OC
O ₂	0.000 mM	0.000	0.0	
NO ₃	0.000 mM	0.000	0.0	
Mn ⁴⁺	0.000 $\mu\text{mol/g}$	0.000	0.0	All reduced initially
Fe ³⁺	0.00 $\mu\text{mol/g}$	0.000	0.0	All reduced initially
SO ₄ ²⁻	1.0 mM	1.0	1.0	~80% reduced
HCO ₃ ⁻	0.46 mM	0.46	0.46	
Mn ²⁺	0.178 mM	0.158	0	~Equil. w/solid
Fe ²⁺	0.059 mM	0.059	0	~Equil. w/solid
HS ⁻	0.0 mM	0.0	0	
CH ₄	0.0 mM	0.0	0	
MnS _(s)	0.038 $\mu\text{mol/g}$	0.038	0	5% of total metal
FeS _(s)	2.5 $\mu\text{mol/g}$	2.5	0	5% of total metal
R-Mn ²⁺	0.534 $\mu\text{mol/g}$	0.564	0.75	All reduced initially
R-Fe ²⁺	47.44 $\mu\text{mol/g}$	47.44	50.0	All reduced initially

Table C.3 Boundary Conditions

Primary Constituents	Control	Anoxic	Cap	Comments
O ₂	0.26 mM	0.00026	0.26	Saturated
NO ₃	0.1 mM	0.1	0.1	25% of 5mg/L
Mn ⁴⁺	0.0 (Flux)	0.0	0.0	
Fe ³⁺	0.0 (Flux)	0.0	0.0	
SO ₄ ²⁻	6.0 mM	6.0	6.0	25% of 24mM, observe
HCO ₃ ⁻	0.46 mM	0.46	0.46	
Mn ²⁺	0.0 mM	0.0	0.0	
Fe ²⁺	0.0 mM	0.0	0.0	
HS ⁻	0.0 mM	0.0	0.0	
CH ₄	0.0 mM	0.0	0.0	
FeS _(s)	0 (Flux)	0.0	0.0	
TOTH	1.65E ⁻⁵	1.65E ⁻⁵	1.65E ⁻⁵	
R-Mn ²⁺	0.0 (Flux)	0.0	0.0	
R-Fe ²⁺	0.0 (Flux)	0.0	0.0	

Table C.4 Other Parameters

	Control	Anoxic	Cap
Particle diffusion	2.36cm ² /year	2.36 (7.5E-8 cm ² /sec)	2.36
Domain length	7.0 cm	7.0 cm	7.0cm+2cm cap = 9cm total
Porosity	f(depth)	f(depth)	0.35
Diffusive boundary	0.2 cm	0.2 cm	0.2 cm

References

- Azcue, J. M., A. J. Zeman, et al. (1998). "Assessment of sediment and porewater after one year of subaqueous capping of contaminated sediments in Hamilton Harbor, Canada." Water Science and Technology **37**(6-7): 323-329.
- Alpers, C. N. et al. (2005). "Mercury contamination from historical gold mining in California." USGS Fact Sheet. 2005-3014
- Benoit, J. M., C. C. Gilmour, et al. (1999). "Sulfide Controls on Mercury Speciation and Bioavailability to Methylating Bacteria in Sediment Pore Waters." Environmental Science and Technology **33**(6): 951-957.
- Benoit, J. M., R. P. Mason, et al. (2001). "Constants for mercury binding by dissolved organic matter isolates from the Florida Everglades." Geochimica et Cosmochimica Acta **65**(24): 4445-4451.
- Benoit, J. M., C. C. Gilmour, et al. (2001). "The Influence of Sulfide on Solid-Phase Mercury Bioavailability for Methylation by Pure Cultures of *Desulfobulbus propionicus* (1pr3)." Environmental Science and Technology **35**(1): 127-132.
- Benoit, J. M., C. C. Gilmour, et al. (2003). "Geochemical and biological controls over methylmercury production and degradation in aquatic ecosystems." ACS Symposium Series **835**(Biogeochemistry of Environmentally Important Trace Elements): 262-297.
- Benoit, J. M., D. H. Shull, et al. (2006). "Infaunal burrow densities and sediment monomethyl mercury distributions in Boston Harbor, Massachusetts." Marine Chemistry **102**(1-2): 124-133.
- Bloom, N. S., G. A. Gill, et al. (1999). "Speciation and Cycling of Mercury in Lavaca Bay, Texas, Sediments." Environmental Science and Technology **33**(1): 7-13.
- Boudreau, B. P. and Editor (1996). Diagenetic Models and their Implementation: Modeling Transport and Reactions in Aquatic Sediments. Berlin, Springer.
- Brendel, P. J. and G. W. Luther, III (1995). "Development of a Gold Amalgam Voltammetric Microelectrode for the Determination of Dissolved Fe, Mn, O₂, and S(-II) in Porewaters of Marine and Freshwater Sediments." Environmental Science and Technology **29**(3): 751-61.
- Brouwer, H. and T. P. Murphy (1994). "Diffusion method for the determination of acid-volatile sulfides (AVS) in sediment." Environmental Toxicology and Chemistry **13**(8): 1273-5.

- Burton, E. D., L. A. Sullivan, et al. (2008). "A simple and inexpensive chromium-reducible sulfur method for acid-sulfate soils." Appl. Geochem. FIELD Full Journal Title:Applied Geochemistry **23**(9): 2759-2766.
- Cabana, G. and J. B. Rasmussen (1994). "Modeling food chain structure and contaminant bioaccumulation using stable nitrogen isotopes." Nature **372**(6503): 255-7.
- Canario, J., M. C. C. Vale, et al. (2007). "Evidence for Elevated Production of Methylmercury in Salt Marshes." Environmental Science & Technology **41**(21): 7376-7382.
- Compeau, G. C. and R. Bartha (1985). "Sulfate-reducing bacteria: principal methylators of mercury in anoxic estuarine sediment." Applied and Environmental Microbiology **50**(2): 498-502.
- DiToro, D. D. (2001). Sediment Flux Modeling. New York, John Wiley & Sons, Inc.
- Drexel, R. T., M. Haitzer, et al. (2002). "Mercury(II) Sorption to Two Florida Everglades Peats: Evidence for Strong and Weak Binding and Competition by Dissolved Organic Matter Released from the Peat." Environmental Science and Technology **36**(19): 4058-4064.
- Driscoll, C. (2007). "Mercury Contamination in Forest and Freshwater Ecosystems in the Northeastern United States." Bioscience **57**(1): 17-28.
- Drott, A., L. Lambertsson, et al. (2007). "Importance of Dissolved Neutral Mercury Sulfides for Methyl Mercury Production in Contaminated Sediments." Environmental Science & Technology **41**(7): 2270-2276.
- Drott, A., L. Lambertsson, et al. (2008). "Do Potential Methylation Rates Reflect Accumulated Methyl Mercury in Contaminated Sediments?" Environmental Science & Technology **42**(1): 153-158.
- Eek, E., G. Cornelissen, et al. (2008). "Diffusion of PAH and PCB from contaminated sediments with and without mineral capping; measurement and modelling." Chemosphere **71**(9): 1629-1638.
- Ekstrom, E. B., F. M. M. Morel, et al. (2003). "Mercury methylation independent of the acetyl-coenzyme A pathway in sulfate-reducing bacteria." Applied and Environmental Microbiology **69**(9): 5414-5422.
- EPA, U. S. (1996). "Microwave assisted acid digestion of siliceous and organically based matrices." OHW, Method 3052
- EPA, U. S. (1997). "Mercury Study Report to Congress." ORD, EPA-452/R-97-003
- EPA, U. S. (1998). "EPA's Contaminated Sediment Management Strategy." O. W., EPA-823-R-98-001
- EPA, U. S. (2002). "Mercury in Water by Oxidation, Purge and Trap, and Cold Vapor Atomic Fluorescence Spectrometry." OW, EPA-821-R-02-019

- EPA, U. S. (2004). "The Incidence and Severity of Sediment Contamination in Surface Waters of the United States: National Sediment Quality Survey, Second Edition." OST, EPA-823-R-04-007
- EPA, U. S. (2005). "Contaminated Sediment Remediation Guidance for Hazardous Waste Sites." Office of Solid Waste and Emergency Response.
- EPA, U. S. (2008). National Priorities List (NPL), <http://www.epa.gov/superfund/sites/query/basic.htm>.
- Figueroa, R. A. and A. A. Mackay (2005). "Sorption of oxytetracycline to iron oxides and iron oxide-rich soils." Environmental Science & Technology **39**(17): 6664-6671.
- Fitzgerald, W. F., D. R. Engstrom, et al. (1998). "The Case for Atmospheric Mercury Contamination in Remote Areas." Environmental Science and Technology **32**(1): 1-7.
- Fitzgerald, W. F., C. H. Lamborg, et al. (2007). "Marine biogeochemical cycling of mercury." Chemical Reviews **107**(2): 641-662.
- Fleming, E. J., E. E. Mack, et al. (2006). "Mercury methylation from unexpected sources: Molybdate-inhibited freshwater sediments and an iron-reducing bacterium." Applied and Environmental Microbiology **72**(1): 457-464.
- Gagnon, C., E. Pelletier, et al. (1996). "Diagenetic behavior of methylmercury in organic-rich coastal sediments." Limnology and Oceanography **41**(3): 428-434.
- Gilmour, C. C. and E. A. Henry (1991). "Mercury methylation in aquatic systems affected by acid deposition." Environmental Pollution (Oxford, United Kingdom) **71**(2-4): 131-69.
- Gilmour, C. C., E. A. Henry, et al. (1992). "Sulfate stimulation of mercury methylation in freshwater sediments." Environmental Science and Technology **26**(11): 2281-7.
- Gilmour, C. C., G. S. Riedel, et al. (1998). "Methylmercury concentrations and production rates across a trophic gradient in the northern Everglades." Biogeochemistry **40**(2-3): 327-345.
- Hammerschmidt, C. R., W. F. Fitzgerald, et al. (2004). "Biogeochemistry of methylmercury in sediments of Long Island Sound." Marine Chemistry **90**(1-4): 31-52.
- Hammerschmidt, C. R. and W. F. Fitzgerald (2004). "Geochemical Controls on the Production and Distribution of Methylmercury in Near-Shore Marine Sediments." Environmental Science and Technology **38**(5): 1487-1495.
- Hammerschmidt, C. R., W. F. Fitzgerald, et al. (2008). "Organic matter and sulfide inhibit methylmercury production in sediments of New York/New Jersey Harbor." Marine Chemistry **109**(1-2): 165-182.

- Han, S., A. Obraztsova, et al. (2008). "Sulfide and iron control on mercury speciation in anoxic estuarine sediment slurries." Marine Chemistry **111**(3-4): 214-220.
- Harmon, S. M., J. K. King, et al. (2004). "Methylmercury Formation in a Wetland Mesocosm Amended with Sulfate." Environmental Science and Technology **38**(2): 650-656.
- Himmelheber, D. W., K. D. Pennell, et al. (2007). "Natural Attenuation Processes during In Situ Capping." Environmental Science & Technology **41**(15): 5306-5313.
- Himmelheber, D. W. (2008). "Spatial and Temporal Evolution of Biogeochemical Processes Following In Situ Capping of Contaminated Sediments." Environmental Science & Technology.
- Hintelmann, H., P. M. Welbourn, et al. (1997). "Measurement of Complexation of Methylmercury(II) Compounds by Freshwater Humic Substances Using Equilibrium Dialysis." Environmental Science and Technology **31**(2): 489-495.
- Hintelmann, H., K. Keppel-Jones, et al. (2000). "Constants of mercury methylation and demethylation rates in sediments and comparison of tracer and ambient mercury availability." Environmental Toxicology and Chemistry **19**(9): 2204-2211.
- Holliger, C., S. Gaspard, et al. (1997). "Contaminated environments in the subsurface and bioremediation: organic contaminants." FEMS Microbiol. Rev. FIELD Full Journal Title:FEMS Microbiology Reviews **20**(3-4): 517-523.
- Hsieh, Y. P., S. W. Chung, et al. (2002). "Analysis of sulfides in the presence of ferric minerals by diffusion methods." Chemical Geology **182**(2-4): 195-201.
- Hung, G. A. and G. L. Chmura (2006). "Mercury accumulation in surface sediments of salt marshes of the Bay of Fundy." Environmental Pollution (Amsterdam, Netherlands) **142**(3): 418-431.
- Hwang, H.-M., P. G. Green, et al. (2006). "Tidal salt marsh sediment in California, USA. Part 2: Occurrence and anthropogenic input of trace metals." Chemosphere **64**(11): 1899-1909.
- Jaffe, P. R., S. Wang, et al. (2002). "The dynamics of arsenic in saturated porous media: fate and transport modeling for deep aquatic sediments, wetland sediments, and groundwater environments." Special Publication - The Geochemical Society **7**(Water-Rock Interactions, Ore Deposits, and Environmental Geochemistry): 379-397.
- Johnson, N. W., Katz, Lynn. E., Reible, Danny. D. (in preparation). "Biogeochemical Changes and Mercury Methylation beneath an In-Situ Sediment Cap."
- Katsev, S., B. Sundby, et al. (2006). "Modeling vertical excursions of the redox boundary in sediments: application to deep basins of the Arctic Ocean." Limnology and Oceanography **51**(4): 1581-1593.

- Kerin, E. J., C. C. Gilmour, et al. (2006). "Mercury methylation by dissimilatory iron-reducing bacteria." Applied and Environmental Microbiology **72**(12): 7919-7921.
- Kerry, A., P. M. Welbourn, et al. (1991). "Mercury methylation by sulfate-reducing bacteria from sediments of an acid stressed lake." Water, Air, and Soil Pollution **56**: 565-75.
- King, J. K., J. E. Kostka, et al. (2001). "A Quantitative Relationship that Demonstrates Mercury Methylation Rates in Marine Sediments Are Based on the Community Composition and Activity of Sulfate-Reducing Bacteria." Environmental Science and Technology **35**(12): 2491-2496.
- Kongchum, M., I. Devai, et al. (2006). "Total mercury and methylmercury in freshwater and salt marsh soils of the Mississippi river deltaic plain." Chemosphere **63**(8): 1300-1303.
- Kraepiel, A. M. L., K. Keller, et al. (2003). "Sources and Variations of Mercury in Tuna." Environmental Science and Technology **37**(24): 5551-5558.
- Lambertsson, L. and M. Nilsson (2006). "Organic Material: The Primary Control on Mercury Methylation and Ambient Methyl Mercury Concentrations in Estuarine Sediments." Environmental Science & Technology **40**(6): 1822-1829.
- Langer, C. S., W. F. Fitzgerald, et al. (2001). "Biogeochemical cycling of methylmercury at Barn Island Salt Marsh, Stonington, CT, USA." Wetlands Ecology and Management **9**(4): 295-310.
- Le Roux, S. M., A. Turner, et al. (2001). "Partitioning of mercury onto suspended sediments in estuaries." Journal of Environmental Monitoring **3**(1): 37-42.
- Liu, C., J. A. Jay, et al. (2001). "Capping efficiency for metal-contaminated marine sediment under conditions of submarine groundwater discharge." Environmental Science and Technology **35**(11): 2334-40.
- Liu, J., D. D. Reible, et al. (2007). "Observations of mercury fate and transport beneath a sediment cap " Land Contamination & Reclamation **15**(4): 401-411.
- Lord, C. J., III and T. M. Church (1983). "The geochemistry of salt marshes: sedimentary ion diffusion, sulfate reduction, and pyritization." Geochimica et Cosmochimica Acta **47**(8): 1381-91.
- Marvin-DiPasquale, M., J. Agee, et al. (2000). "Methyl-Mercury Degradation Pathways: A Comparison among Three Mercury-Impacted Ecosystems." Environmental Science and Technology **34**(23): 4908-4916.
- Mason, R. P., W. F. Fitzgerald, et al. (1994). "The biogeochemical cycling of elemental mercury: anthropogenic influences." Geochimica et Cosmochimica Acta **58**(15): 3191-8.

- Mason, R. P., J. R. Reinfelder, et al. (1996). "Uptake, Toxicity, and Trophic Transfer of Mercury in a Coastal Diatom." Environmental Science and Technology **30**(6): 1835-45.
- Mehrotra, A. S. and D. L. Sedlak (2005). "Decrease in Net Mercury Methylation Rates Following Iron Amendment to Anoxic Wetland Sediment Slurries." Environmental Science and Technology **39**(8): 2564-2570.
- Merritt, K. A. and A. Amirbahman (2008). "Methylmercury cycling in estuarine sediment pore waters (Penobscot River estuary, Maine, USA)." Limnology and Oceanography **53**(3): 1064-1075.
- Miller, C. (2006). "The Role of Organic Matter in the Dissolved Phase Speciation and Solid Phase Partitioning of Mercury." Univ. of Maryland, Ph.D. Dissertation.
- Morel, F. M. M., A. M. L. Kraepiel, et al. (1998). "The chemical cycle and bioaccumulation of mercury." Annual Review of Ecology and Systematics **29**: 543-566.
- NRC (2000). "Toxicological Effects of Methylmercury." National Academy Press, Washington, DC.
- NRC (2007). "Sediment Dredging at Superfund Megsites: Assessing the Effectiveness." National Academy Press: Washington, DC.
- Pak, K. R. and R. Bartha (1998). "Mercury methylation and demethylation in anoxic lake sediments and by strictly anaerobic bacteria." Applied and Environmental Microbiology **64**(3): 1013-1017.
- Pak, K. R. and R. Bartha (1998). "Mercury methylation by interspecies hydrogen and acetate transfer between sulfidogens and methanogens." Applied and Environmental Microbiology **64**(6): 1987-1990.
- Palermo, M., S. Maynard, et al. (1998). "Guidance for In-Situ Subaqueous Capping of Contaminated Sediments." EPA 905-B96-004(Great Lakes National Program Office, Chicago, IL).
- Phillips, E. J. P. and D. R. Lovley (1987). "Determination of iron(III) and iron(II) in oxalate extracts of sediment." Soil Science Society of America Journal **51**(4): 938-41.
- Poulton, S. W. and D. E. Canfield (2005). "Development of a sequential extraction procedure for iron: implications for iron partitioning in continentally derived particulates." Chemical Geology **214**(3-4): 209-221.
- Ravichandran, M., G. R. Aiken, et al. (1999). "Inhibition of Precipitation and Aggregation of Metacinnabar (Mercuric Sulfide) by Dissolved Organic Matter Isolated from the Florida Everglades." Environmental Science and Technology **33**(9): 1418-1423.

- Schwarzenbach, G. and M. Widmer (1963). "Solubility of metal sulfides. I. Mercuric sulfides." Helvetica Chimica Acta **46**(7): 2613-28.
- Scrimshaw, M. D. and J. N. Lester (2001). "Multivariate analysis of U.K. salt marsh sediment contaminant data with reference to the significance of PCB contamination." Environmental Science and Technology **35**(13): 2676-2681.
- Sellers, P., C. A. Kelly, et al. (1996). "Photodegradation of methylmercury in lakes." Nature (London) **380**(6576): 694-7.
- Simpson, S. L., I. D. Pryor, et al. (2002). "Considerations for Capping Metal-Contaminated Sediments in Dynamic Estuarine Environments." Environmental Science and Technology **36**(17): 3772-3778.
- Skoog, D. A., D. M. West, et al. (2007). Fundamentals of Analytical Chemistry, Eight Edition
- Stumm, W., J. Morgan, J., et al. (1996). "Aquatic Chemistry: Chemical Equilibria and Rates in Natural Waters." John Wiley & Sons, Inc.: 1022.
- Sunderland, E. M., F. A. P. C. Gobas, et al. (2004). "Speciation and bioavailability of mercury in well-mixed estuarine sediments." Marine Chemistry **90**(1-4): 91-105.
- Sunderland, E. M., F. A. P. C. Gobas, et al. (2006). "Environmental controls on the speciation and distribution of mercury in coastal sediments." Marine Chemistry **102**(1-2): 111-123.
- Thoma, G. J., D. D. Reible, et al. (1993). "Efficiency of capping contaminated sediments in situ. 2. Mathematics of diffusion-adsorption in the capping layer." Environmental Science and Technology **27**(12): 2412-19.
- Tipping, E. (1998). "Humic ion-binding model VI. An improved description of the interactions of protons and metal ions with humic substances." Aquatic Geochemistry **4**(1): 3-48.
- Ulrich, G. A., L. R. Krumholz, et al. (1997). "A rapid and simple method for estimating sulfate reduction activity and quantifying inorganic sulfides." Appl. Environ. Microbiol. FIELD Full Journal Title: Applied and Environmental Microbiology **63**(4): 1627-1630.
- USGS (2004). "Methods for the Preparation and Analysis of Solids and Suspended Solids for Methylmercury." L. Analysis, Techniques and Methods 5 A-7
- Van Cappellen, P. and Y. Wang (1996). "Cycling of iron and manganese in surface sediments: a general theory for the coupled transport and reaction of carbon, oxygen, nitrogen, sulfur, iron, and manganese." American Journal of Science **296**(3): 197-243.

- Wang, X. Q., L. J. Thibodeaux, et al. (1991). "Efficiency of capping contaminated bed sediments in situ. 1. Laboratory-scale experiments on diffusion-adsorption in the capping layer." Environmental Science and Technology **25**(9): 1578-84.
- Warner, K. A., E. E. Roden, et al. (2003). "Microbial Mercury Transformation in Anoxic Freshwater Sediments under Iron-Reducing and Other Electron-Accepting Conditions." Environmental Science and Technology **37**(10): 2159-2165.
- Xia, K., U. L. Skyllberg, et al. (1999). "X-ray Absorption Spectroscopic Evidence for the Complexation of Hg(II) by Reduced Sulfur in Soil Humic Substances." Environmental Science and Technology **33**(2): 257-261.

Vita

Nathan William Johnson was born in Minnesota in 1980, the son of Owen and Nancy Johnson. After completing his work at Pine River/Backus High School, he enrolled at Princeton University in Princeton, NJ. He received his Bachelor of Science in Engineering degree in Civil and Environmental Engineering in June, 2003. In September, 2003 he began graduate studies at The University of Texas at Austin in the Environmental and Water Resources Engineering program. He received his Masters degree in August, 2005 and chose to continue school in pursuit of a PhD. During the summer of 2006, he married Rebekah Ann Wagner and they are expecting their first child (Baby J) at the time of this publication. Nathan accepted a faculty position at the University of Minnesota-Duluth following the completion of his work at UT.

Permanent address: 6730 Silbaugh Drive, Pine River, MN 56474

This manuscript was typed by the author.